CHARACTERISTICS OF SKARNS RELATED TO GOLD MINERALIZATION AT GOLD ACRES, NEVADA

by

Michaela Nicole Young

A Thesis Submitted to the Faculty of the

DEPARTMENT OF GEOSCIENCES

In Partial Fulfillment of the Requirements
For the Degree of

MASTER OF SCIENCE

In the Graduate College

THE UNIVERSITY OF ARIZONA

1 9 9 3

STATEMENT BY THE AUTHOR

This thesis has been submitted in partial fulfillment of requirements for the Master of Science degree at the University of Arizona and is deposited in the Antevs Reading Room to be made available to borrowers under rules of the Library.

Brief quotations from this thesis are allowable without special permission, provided that accurate acknowledgement of source is made. Requests for permission for extended quotation from or reproduction of this manuscript in whole or in part may be granted by the head of the department, or the graduate program coordinator, when in their judgment the proposed use of the material is in the interests of scholarship. In all other instances, however, permission must be obtained from the author.

SIGNED: Michaela N. Young

APPROVAL BY RESEARCH ADVISORY COMMITTEE

As members of the Advisory/Research Committee, we recommend that this thesis be accepted as fulfilling the research requirement for the degree of Master of Science.

Spencer R. Titley — April 23, 1993
Major Advisor (Dr. Spencer R. Titley) — Date

(Dr. Joaquin Ruiz) — April 26, 1993
Date

Mark D. Barton — April 26, 1993
(Dr. Mark Barton) — Date

ACKNOWLEDGEMENTS

Fieldwork, analytical work (trace element analyses, microprobe, X-ray diffraction), and petrographic slides for this thesis were funded by Cortez Gold Mines. I am indebted to the geologic staff at Cortez for this research opportunity. Stan Foo and Bob Hays are largely responsible for recognizing the stratigraphy, structure, and zoning patterns at Gold Acres, and I thank them for their assistance. John McCormack is acknowledged for his advice and encouragement. I am grateful to Dr. Spencer R. Titley and my other professors who provided me with the necessary background to resolve the problems at Gold Acres. And thanks to Carl, who pushed me when I needed it (but not too hard).

TABLE OF CONTENTS

TABLE OF CONTENTS-*continued*

LIST OF ILLUSTRATIONS

LIST OF ILLUSTRATIONS-*continued*

LIST OF TABLES

ABSTRACT

Gold mineralization at the Gold Acres disseminated deposit is spatially associated with two distinct skarn units. The stratigraphic sequence at the mine, from the surface down, comprises the Roberts Mountains allochthon bounded below by the Roberts Mountains thrust fault, an upper skarn unit (altered from Devonian Wenban Limestone and a felsic sill), an imbricated thrust zone (ITZ) which hosts gold mineralization, a lower skarn unit (altered from Silurian Roberts Mountains Formation), and a granitic stock. Mineralogic and metallogenic zoning indicate the upper and lower skarns are genetically related to the stock which intruded about 100-92 Ma. Late Cretaceous compression produced the ITZ which cuts skarn mineralization. Normal faulting followed compression. The normal faults served as conduits for gold-bearing solutions which permeated the ITZ and deposited the gold ore.

INTRODUCTION

The Gold Acres mine is a sediment-hosted, disseminated gold deposit located on the east flank of the northern Shoshone Range in north-central Nevada (Fig. 1). Gold Acres was one of the earliest of the Carlin-type gold deposits to be developed, having been in operation before the recognition of the Carlin trend deposits. Gold Acres lies within the Battle Mountain - Eureka trend of gold occurrences, originally delineated as the Shoshone - Eureka belt by Roberts (1960). The Battle Mountain - Eureka trend is similar to the well-known Carlin trend, though not as well constrained. The gold deposits that make up these trends are shown in Figure 2.

The gold ore at Gold Acres is hosted by the Silurian Roberts Mountains Formation (Srm) in a window of the Roberts Mountains thrust fault, a common occurrence at many of the Carlin-type deposits in the Great Basin. However, at Gold Acres the host rock is an intensely sheared, fault-bounded zone of carbonaceous, silicified limestone with disseminated pyrite. In fault contact both above and below the shallow-dipping shear zone are two skarn occurrences, presumably related genetically to a granitic stock below the lower skarn unit.

The skarn units at Gold Acres have received very little attention in the past (as skarn mineralization has proved to be sub-economic). Recent studies of gold deposits associated with skarns and porphyry systems (Einaudi, 1982; Sillitoe and Bonham, 1990; Wotruba and others, 1988; Atkinson and Einaudi, 1976) indicate that there may be a genetic link between some gold deposits and magmatic systems which produce skarn alteration. The spatial association of skarn mineralization with gold ore at Gold Acres has become a subject of much speculation by mine geologists. The focus of research for this thesis concerns the occurrence, description, and paragenetic relationships in the skarns associated with gold ore. Combining the structural data with petrographic

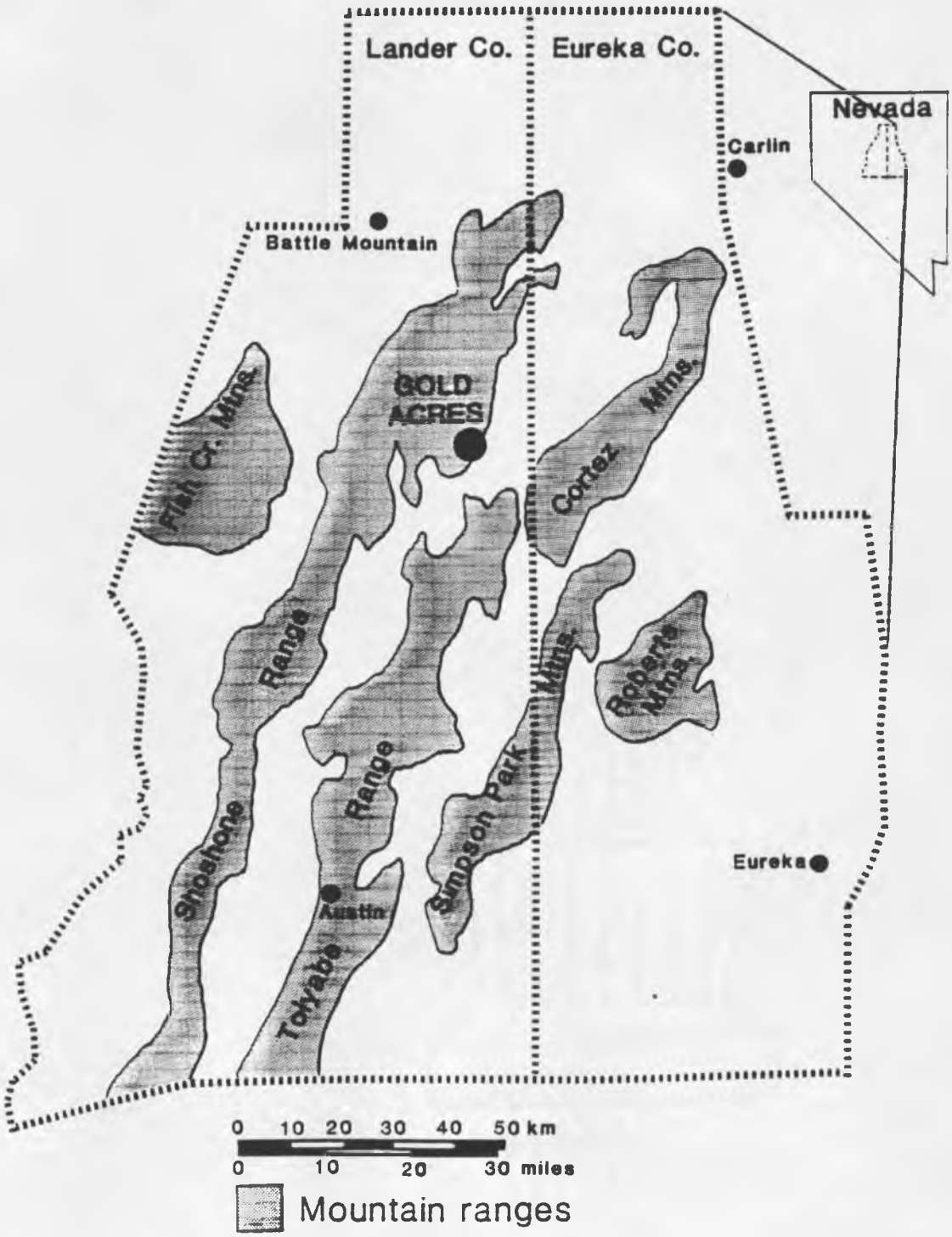

Figure 1. Location map of the Gold Acres deposit.

Figure 2. Trends of gold occurrences in northern Nevada.

observations and trace element geochemical analyses allows the interpretation of a sequence of tectonism, magmatism, and hydrothermal activity which produced the skarn units and gold deposit at Gold Acres.

HISTORY

The Gold Acres mine is currently operated by Cortez Gold Mines for Placer-Dome, US, as a joint venture with Kennecott. Gold Acres was originally discovered in 1922, although it was not mined until 1935. Near-surface oxidized ore was initially mined by underground methods until 1942, then by open-cast methods (in spite of World War II). The northern pit was mined primarily during the 1940's and 1950's (Wrucke and Armbrustmacher, 1975). Prospecting and development in the area by the Cortez Joint Venture began in 1969 and resulted in the discovery of additional oxide mineralization southeast of the original northern pit, as well as a resource of refractory mineralization south of the pit. The southeastern oxide ore body was mined from 1973 to 1976, and pods of oxide ore remaining in the original pit were sporadically removed during the 1980s. The refractory gold ore body (in the sheared zone of carbonaceous limestone) represents the unoxidized down-dip extension of the near-surface ore body initially discovered and mined. The carbonaceous gold ore body has been mined since 1989.

PREVIOUS WORK

Previous geologic investigations in the Gold Acres area were done in the 1960s and 1970s by the U.S. Geological Survey. Their work included mapping of lithology, stratigraphy, alteration, tectonics, and structure, as well as intensive trace element geochemical analyses and base-metal and precious-metal distribution plots. The tectonic setting and regional geology of the northern Shoshone Range and Gold Acres area

were described by Gilluly and Gates (1965), including a short section on the mine by Ketner (1965). More detailed mapping of structure, alteration, and geochemistry of the Gold Acres deposit in particular is presented by Wrucke and others (1968) and Wrucke and Armbrustmacher (1975).

Nash (1972) reported fluid inclusion data from the Gold Acres deposit as part of a study on Carlin-type gold deposits in Nevada. Six fluid inclusions yielded homogenization temperatures of 160°C-185°C. A separate sample homogenized at 265°C. Freezing measurements for four fluid inclusions indicate salinities of 5.4-7.3 wt.% NaCl. The inclusions were in vein quartz of uncertain affinity with gold mineralization.

Silberman and McKee (1971) obtained K-Ar age dates from altered biotite in the stock and from sericite in a shallower sill. Their results indicate minimum Cretaceous ages of the stock (98.8±2 Ma) and of alteration in the sill (94.3±1.9 Ma).

The USGS also conducted regional geophysical surveys in the area in the 1960s. Gravity and aeromagnetic data near Gold Acres are discussed by Mabey (1965). The most striking geophysical feature at Gold Acres is a large magnetic high trending west-northwest and centered south of the mine.

The mine staff has obtained data from geochemical surveys (soil and outcrop trace element geochemistry) and geophysical surveys (induced polarization, resistivity, self-potential, very-low-frequency electromagnetics (VLF), seismic refraction, and ground and aeromagnetics) as part of exploration and development plans. Data from a detailed aeromagnetic survey over the Shoshones, Crescent Valley, and Cortez Mountains was acquired in 1987. The aeromagnetic data have helped guide exploration at Gold Acres, as well as provide lateral constraints on the underlying stock and the associated skarn. Continued mapping and sampling by mine geologists in the immediate vicinity of the Gold Acres mine and in the pit have contributed much toward the understanding of the

geology and mineralization at Gold Acres. As drilling and mining in the pit continued, mine geologists were able to revise the general geologic picture in the immediate mine area (see Hays and Foo, 1991).

Previous studies of the Gold Acres deposit have dealt almost exclusively with the gold ore. Wrucke and others (1968) and Wrucke and Armbrustmacher (1975) briefly describe tactite mineralization at Gold Acres. Ketner (1965) describes a highly altered quartz latite sill in the Gold Acres mine, which is the felsite sill dated by Silberman and McKee (1971). This sill is not recognized in current exposures of the mine (Stan Foo, personal communication, 1993). Hays and Foo (1991) published a summary paper updating the stratigraphy, structural geology, and geochemistry at the mine. They recognized the upper skarn unit as such and identified the lower skarn unit. For the first time, the structural aspects of skarn associated with gold mineralization at Gold Acres was documented.

SKARN DEPOSITS

A general review of skarn deposits is appropriate at this point. The following discussion describes the origins and characteristics of skarn deposits and summarizes skarn classification schemes.

Skarns are bodies of calc-silicate-bearing rock derived from the addition of Si, Al, Fe, Mg, and/or Mn to dominantly carbonate rocks or from the addition of Ca to silicate (igneous) rocks. Development of skarn involves reaction of calcite and dolomite with metasomatic fluid to produce one or more of garnet (usually grossular to andradite), clinopyroxene (hedenbergite to diopside), wollastonite, epidote, amphibole (tremolite to actinolite), chlorite, serpentine, idocrase, and scapolite, among others. Pure limestones are replaced by Ca-rich silicate minerals (calcic skarn), whereas replacement of dolomite results in a more Mg-rich assemblage (magnesian skarn).

As skarn deposits received more attention from explorationists as targets for base metals and precious metals, more studies on skarns appeared in the literature. An excellent review of skarn deposits is given by Einaudi and others (1981). A special issue of *Economic Geology* (Vol. 77, No. 4) is devoted to skarn deposits. Therein skarn terminology and classification are reviewed by Einaudi and Burt (1982), and many skarn deposits are described. Descriptions and general features of skarns associated with porphyry copper deposits are presented by Einaudi (1982a,b). Johnson and Norton (1985) modeled hydrothermal activity in skarns associated with porphyry copper plutons.

The development of skarn involves an influx of hot siliceous fluid and consequent heating of carbonate host rock or wall rock, producing a dominantly monomineralic or bimineralic anhydrous calc-silicate assemblage of garnet and/or pyroxene. As alteration progresses, anhydrous phases are replaced by hydrous calc-silicates, sulfides, oxides, and carbonates. In the case of an intruding stock, a recrystallization front may expand out from the stock into the carbonate to produce a marble zone. Except for occasional needles of wollastonite or tremolite, there is little evidence for significant addition of new components in the marble zone. The anhydrous skarn advances simultaneously behind the marble front, and hydrous skarn follows behind anhydrous skarn. Permeability and fracture density increase, allowing more rigorous hydrothermal flow through the system. The ensuing assemblage is thereby more complex than the early anhydrous skarn. Metals are typically introduced to the skarns during hydrous alteration as sulfide and oxide replacements of garnet and pyroxene or in veins with quartz and/or calcite.

Skarns are commonly associated with intrusive stocks or dikes, which provide heat, fluids, and metal components. However, igneous activity is not a prerequisite for skarn mineralization (Titley, 1961). Structure may further complicate the

distribution of skarn assemblages. A silica-bearing hydrothermal fluid which migrates along fractures and faults may encounter carbonate lithologies several kilometers from its source, thus producing a skarn assemblage with no observable link to igneous activity. Lead-zinc skarns are commonly distal to known intrusions, whereas copper and molybdenum bearing skarns are more proximal to intrusions.

In the context of this work, skarn refers to the metasomatic replacement of carbonates by calc-silicate minerals in response to hydrothermal activity which may or may not be related to the intrusion of the Gold Acres stock. A genetic relationship between the lower skarn and the stock can be inferred, since the lower skarn is in intrusive contact with the Gold Acres stock. The upper skarn is more distal to the stock and structurally separated from the lower skarn, thus the relation of the upper skarn to the stock is uncertain.

SKARN CLASSIFICATION

Skarns may be classified on the basis of the host rock that was replaced by calc-silicate minerals. When a carbonate succession is intruded by a stock, replacement of alumino-silicates in the stock produces endoskarn. Exoskarn refers to replacement of the intruded carbonates. The application of the term endoskarn may be expanded to include calc-silicate replacement of any aluminous rock, including shales and volcanics. Endoskarn at Gold Acres refers strictly to the calc-silicate replacement of intrusive igneous rock near its contact with the altered carbonates. Mineral zoning patterns in endoskarns reflect the addition of Ca, presumably derived from the intruded carbonates. Exoskarn mineralogies indicate addition of SiO_2 with Fe + Al $\pm$ Mg $\pm$ Mn and concomitant removal of CO_2. The dominance of Ca or Mg in exoskarn minerals forms the basis of distinction between calcic and magnesian skarn. Calcic skarns are more common, and most economic skarn mineralization occurs in calcic exoskarn.

Einaudi and others (1981) have classified skarns according to the dominant metal extracted from the skarn (Fe, W, Cu, Pb-Zn, Mo, and Sn). The metal-skarn classes display distinct metal associations and mineralogies which reflect the compositions of the host rock, intruding magma, and metasomatic fluid, as well as the environment of fluid infiltration. In particular, certain garnet and pyroxene compositions are typical of the various base- and precious-metal skarn deposits (Einaudi and others, 1981; Einaudi and Burt, 1982). These variables are in turn influenced by the tectonic setting. Although gold is a by-product for some of the skarn classes listed above, many skarns have recently been targeted for their gold content alone, giving rise to a new class of Au-skarns, with its own distinctive mineralogic, petrologic, and geochemical associations (Meinert, 1989). Copper and zinc-lead skarns are the most useful as a basis for comparison with the Gold Acres skarn units.

RESEARCH OBJECTIVES

A detailed description of the mineralogy, petrography, geochemistry, and paragenesis of skarn units at Gold Acres is still lacking. The aim of this thesis is to characterize the skarn units and determine their origin in relation to the gold mineralization. Descriptions of skarns and other lithologies at Gold Acres were accomplished dominantly by petrographic study and geochemical trace-element analysis. Other analytical techniques employed included X-ray diffractometer and electron microprobe. Information on the structural controls to mineralization, lateral extent of the hydrothermal/magmatic system, and potential distribution of skarn mineralization and gold ore was obtained from pit mapping, mapping of lithology and alteration in the vicinity of the mine, drill core and rotary drill log data, and geophysical data (aeromagnetic and ground magnetic surveys). Combining all the data allows a reasonable deduction of the paragenetic history of skarn formation at Gold Acres. The results

indicate a sequence of events involving tectonic, magmatic, and hydrothermal activity, which caused the spatial association of differing styles of mineralization at the Gold Acres Mine.

REGIONAL GEOLOGY AND TECTONICS

The Gold Acres mine is located in the Gold Acres window of the Roberts Mountains thrust fault. The western part of the Gold Acres window is exposed on the low eastern foothills of the northern Shoshone Range. The eastern boundary of the exposed window is marked by Quaternary alluvium which fills Crescent Valley, the basin east of the northern Shoshones (Fig. 3). The Gold Acres window extends under the alluvial fill and may be contiguous with the Cortez window on the other side of the basin, 13 km away (Gilluly and Gates, 1965).

The rocks in the Gold Acres window represent the autochthonous (or parautochthonous) lower plate of the Roberts Mountains thrust fault (RMT). Lower plate lithology is dominated by shelf carbonate units, with terrigenous contributions of shale, siltstone, and sandstone (now quartzite). These rock types are representative of a passive margin environment (miogeocline) in which sedimentation occurred on the shallow-water (less than 100m) shelf of a passive continental margin during the early Paleozoic. The lower plate assemblage is known as the eastern, or carbonate, facies (Stewart, 1980). In the area surrounding Gold Acres, the lower plate comprises Silurian Roberts Mountains (Srm) Formation (a platy, impure limestone), Devonian Wenban (Dw) Limestone (thick-bedded, crystalline limestone), and Devonian Pilot (Dp) Shale.

The allochthonous upper plate of the RMT is known as the western, or siliceous, assemblage (Stewart, 1980). Coeval with the miogeoclinal deposition recorded in the lower plate units, deeper marine sediments and volcanics were deposited, possibly on a continental slope and rise west of the continental shelf. Such a depositional environment for the rocks of the Roberts Mountains allochthon is surmised on the basis of dominantly siliceous facies (chert, shale, argillite, siltstone, quartzite) and the occurrence of

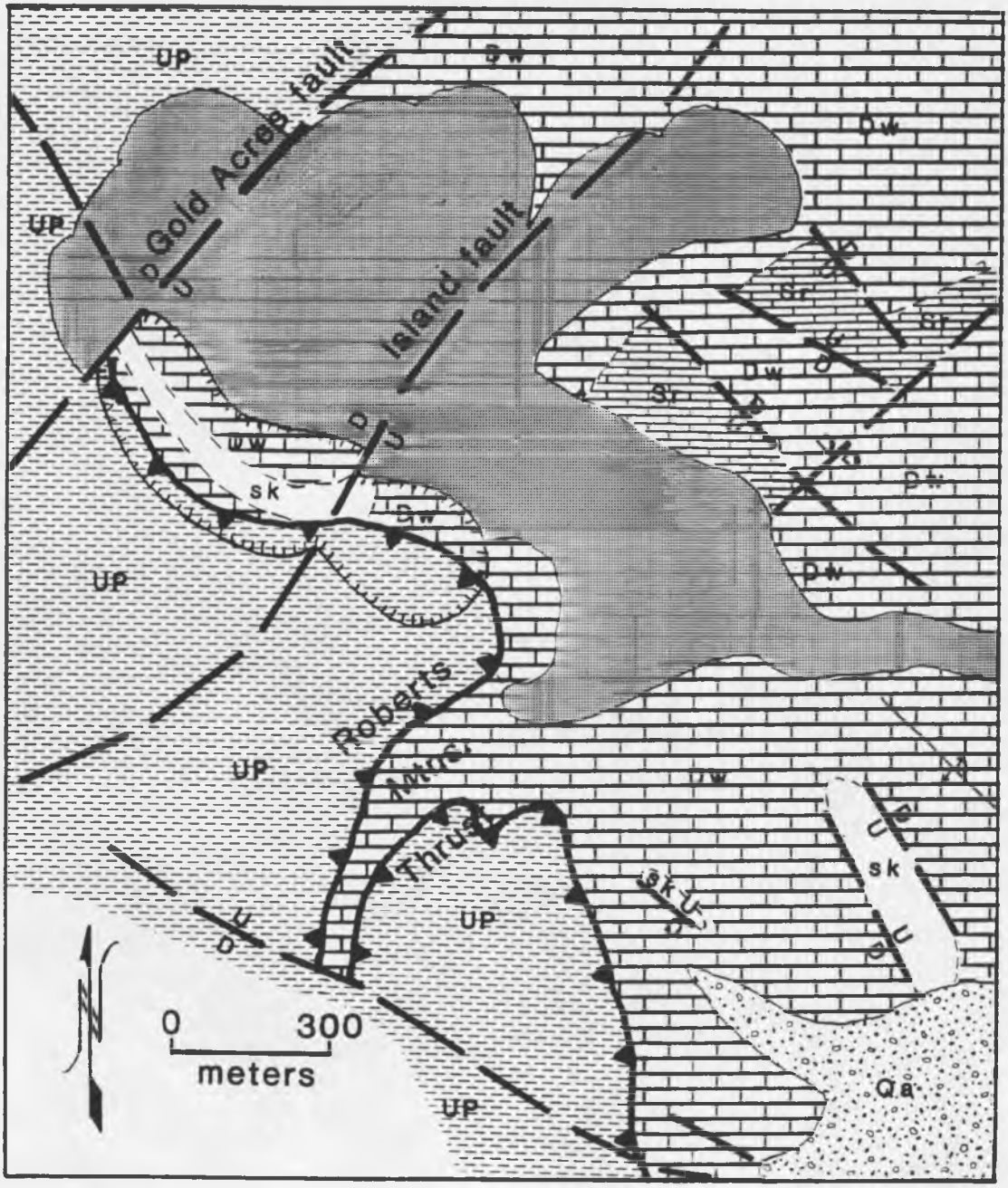

Figure 3. Simplified geology at Gold Acres.

basaltic rocks (now greenstones). In the area adjacent to the Gold Acres pits, the Roberts Mountains allochthon is represented by Ordovician Valmy formation (Ov), comprising dominantly thin-bedded chert and siltstone with lesser quartzite and greenstone, and Devonian Slaven Chert (Ds), comprising dominantly thin-bedded, contorted gray and tan cherts.

The upper- and lower-plate rocks of the RMT were originally deposited along the passive continental margin of western North America in the Early Paleozoic. The passive margin was formed by an inferred rifting event during the late Proterozoic (Stewart and Poole, 1974; Stewart and Suzcek, 1977; Stewart, 1980; Stewart, 1991). The passive margin environment persisted along the western North American continent throughout most of the Paleozoic, disrupted only briefly by the Antler and Sonoma orogenies.

In late Devonian to early Mississippian time, a change in relative plate motions caused the deeper marine siliceous assemblage to be thrust eastward over the coeval shelf carbonate assemblage along the RMT. The deformational event responsible for the thrust is known as the Antler orogeny (Merriam and Anderson, 1948; Stewart, 1980). Displacement along the RMT is about 100 km, if Cenozoic extension is removed (Burchfiel and Royden, 1991). The RMT is the predominant structural signature of the Antler orogeny and, in the strictest sense, defines the Antler orogeny (Snyder and others, 1991). Thrusting produced a topographic high, called the Antler Highland, which extended from southern Idaho to south-central Nevada, a strike length of about 200 kilometers. The literature abounds with plate tectonic models and mechanisms for the Antler orogeny, most of which involve some type of convergence between an offshore island arc and the North American craton (Burchfiel and Davis, 1972, 1976; Burchfiel and Royden, 1991; Churkin, 1974; Dickinson, 1977; Dickinson and others, 1983;

Johnson and Pendergast, 1981; Oldow, 1984; Stewart and Poole, 1974; Stewart, 1980; Speed and Sleep, 1982; Speed and others, 1988).

Compressional deformation probably continued after the Antler orogeny through the Sonoma orogeny (a Permo-Triassic tectonic event similar to the Antler orogeny and exemplified by the Golconda thrust fault). Snyder and others (1991) refer to a period of "subdued tectonism" following the Antler orogeny, with a lesser degree of deformation and thrusting than during orogenic events. Structures attributed to the Antler orogeny were partially reactivated by the unrelenting compressive stresses.

Although late Paleozoic strata are not preserved in the Gold Acres area, continued deposition on a passive continental margin in the late Paleozoic is indicated in other areas of the Great Basin. The Antler Highland was eroding and shedding debris into the foredeep basin east of the toe of the Roberts Mountains thrust. Cobbles and pebbles of both upper plate siliceous rocks and lower plate carbonate rocks are present in the Mississippian Battle Formation, a distinct overlap assemblage which constrains the timing of the Roberts Mountains thrust fault to no later than Early Mississippian (Gilluly and Gates, 1965). Rocks of the overlap assemblage are not present in the Gold Acres region.

From mid-Mesozoic to Eocene time, the Great Basin was subjected to an extended period of continental contraction related to arc-collision and subduction in response to convergence between the Farallon and North American plates (Engebretson and others, 1985). Spatially and temporally discrete phases of compressional deformation, magmatism, contact metamorphism, and regional mid-crustal metamorphism in the Cordillera between eastern California and Utah (*e.g.,* Nevada, Elko, Eureka, and Sevier orogenies) are reflections of continuous tectonic processes at the western continental margin (Nolan, 1974; Burchfiel and Davis, 1975; Speed, 1983; Thorman and others, 1991). Mapping and sedimentologic studies of the past two decades have revealed

abundant evidence for east-vergent thrusting and folding in the Great Basin during Late Jurassic and Cretaceous time (Ketner and Smith, 1974, 1982; Bartley and others, 1987; Schmitt and Vandervoort, 1987; Bartley and Gleason, 1988; Guth, 1988; Armstrong and Bartley, 1989; Bartley, 1990; Chamberlain and Chamberlain, 1990; Schmitt, 1992). Late Cretaceous thrusting in eastern and central Nevada has been referred to as the Central Nevada thrust belt (Geological Society of America, 1993).

Mesozoic magmatism which affected the Gold Acres area occurred in the Cretaceous. A granitic stock intruded the lower plate carbonate units below the current level of the mine. Silberman and McKee (1971) reported K-Ar dates on chlorite-altered biotite (98.8 ± 2.0 Ma.) from the stock and on sericite (92.8 ± 1.9 Ma.) from an altered felsite sill. The biotite age is a minimum age for the stock, since alteration may have reset K-Ar radiometrics in the biotite, which has a relatively low blocking temperature. The sericite age was interpreted to be the age of gold mineralization, assuming sericite alteration occurred with gold precipitation. Older Jurassic stocks of granodiorite, quartz-monzonite, or alaskite composition occur elsewhere in the Shoshone and Cortez Ranges.

Differing styles of Cretaceous magmatism and metallogeny in the eastern Great Basin indicate a pattern of increasing felsic composition and increasing crustal component with time (Barton, 1990). Early Cretaceous plutons are low-silica metaluminous quartz monzonites and quartz diorites associated with Cu±Mo±Au±Zn±Pb mineralization. Mid-Cretaceous (110-90 Ma) plutons are dominantly metaluminous to weakly peraluminous biotite ± hornblende granodiorites with associated mineralization of Mo±Cu+W+Zn+Pb+Au+Ag±F. Late Cretaceous (90-70 Ma) plutons tend to be strongly peraluminous granodiorites and monzodiorites accompanied by lithophile-element mineralization (Be, F, W, Mo, Sn, Zn).

Cenozoic volcanism in central Nevada was active in pulses, or waves (Stewart and

others, 1977). Each wave appears to have swept southward in a roughly east-west belt, followed by the next pulse with a similar distribution as the preceding one. Tertiary magmatic activity in the area surrounding Gold Acres is evident by the widespread occurrence of Caetano Tuffs and compositionally similar quartz porphyry dikes, dated at 34.3 Ma by K-Ar methods (Wells and others, 1971). A caldera-like volcanic trough extended from the northern end of the Toiyabe Range (immediately southwest of the Cortez Range) westward across the Shoshone Range and on to the Fish Creek Mountains southwest of Battle Mountain (Stewart and others, 1977). The tuffs are not present in the vicinity of the Gold Acres mine. Tertiary quartz porphyry dikes have been reported in the pit (Silberman and McKee, 1971; Ketner, 1965), but mine geologists contend that alteration and gouge along high angle structures through the ore zone may have been misinterpreted (R. C. Hays, personal communication, 1990).

The onset of bimodal volcanism at 17 Ma is presumably contiguous with the advent of Basin and Range extension in Nevada (Stewart, 1980). In the northern Shoshone Range, north of Gold Acres, Tertiary (7-5 Ma) basaltic andesites form a cuesta dipping 5° southeastward under the Quaternary gravels filling Crescent Valley. The Shoshone Range is a tilted fault block mountain range in which uplift occurred along Basin and Range normal listric faults on the west side of the range. The basaltic andesite which caps the Shoshones also occurs on the crest of the Cortez Range, to the east across Crescent Valley. By projecting the dip of the flows in the Shoshones, over 3000 meters of offset is estimated on the Crescent Valley Fault, which bounds the range front on the west side of the Cortez Range (Gilluly and Gates, 1965; Gilluly and Masursky, 1965). Basin and range tectonism may have reactivated earlier structures in the Gold Acres area (Hays and Foo, 1991).

With the development of Basin and Range tectonics, debris shed from the eroding Shoshone and Cortez ranges filled the intervening basin (Crescent Valley) with thick

accumulations of Tertiary and Quaternary gravels and alluvium. These unconsolidated deposits onlap the east flank of the Shoshone Range and cover the eastward extension of the Gold Acres window.

GEOLOGY OF THE GOLD ACRES MINE AND VICINITY

An updated description of the geology, structure, and stratigraphy of the Gold Acres deposit is presented by Hays and Foo (1991). Additional mapping from the pit walls, surrounding outcrops, and from drill holes was done as part of the fieldwork for this study, and the results are included in the discussion below.

The stratigraphy at Gold Acres is relatively simple (Fig. 4). Adjacent to the mine area, allochthonous siliceous rocks are separated from autochthonous (or parautochthonous) carbonate rocks by the Roberts Mountains thrust fault (RMT). Stratigraphic relations of allochthonous units are obscured by thrusting and deformation, but autochthonous units are in normal depositional contact. Deformation in autochthonous rocks is characterized by broad folding and tilting. Stratigraphic relations are more complicated within the pit, where carbonate units have been altered to skarn, and brecciation and shearing have modified the lower plate stratigraphic sequence.

Adjacent to the mine, south and west of the pit, the Roberts Mountains allochthon comprises Ordovician Valmy Formation and Devonian Slaven Chert. These units occur as thrust slices in mechanical contact with each other. Upper plate units are highly sheared and contorted as a result of deformation presumably incurred during Antler orogenic activity. Later events (Sonoma, Sevier, Laramide orogenies) may have contributed to the observed deformation (see Snyder and others, 1991).

North and east of the Gold Acres pits, the lower plate of the RMT comprises Devonian Wenban Limestone and Silurian Roberts Mountain Formation (Fig. 3). The Wenban Limestone (Dw) is a medium- to thick-bedded, gray, fossiliferous, crystalline limestone at least 50 meters thick. The upper contact of Dw is the RMT. The base of Dw

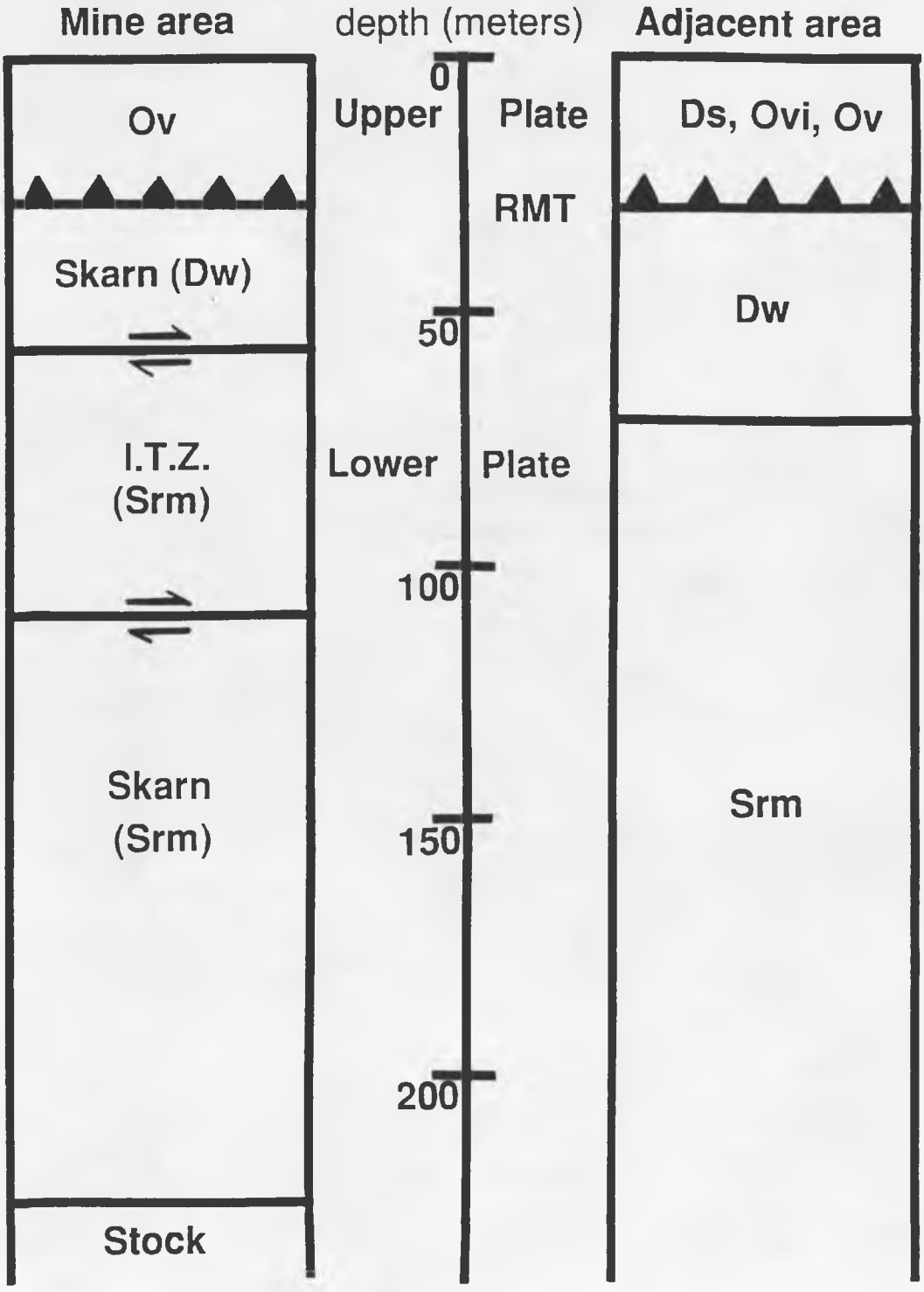

Figure 4. Stratigraphy of the Gold Acres mine and adjacent area. For descriptions of rock units, see text.

is in conformable, gradational contact with Silurian Roberts Mountains formation (Srm). The Roberts Mountains Formation (Srm) is the dominant host to gold mineralization at Gold Acres. The Srm is a thin- to medium-bedded, gray and pink, dolomitic, silty limestone to limey siltstone. The base of the unit is not exposed in the Gold Acres area, but its thickness exceeds 200 meters in drill holes. Internal deformation of the autochthonous units outside the mine area is much less intense than in the allochthonous units.

The RMT is a significant geologic structure at the Gold Acres mine. The RMT is apparently an important control on gold mineralization, as oxide gold ore is hosted in both allochthonous and autochthonous units adjacent to the thrust. The RMT is therefore well-exposed in the pit highwalls. Lithology, particularly the occurrence of greenstone above the RMT, suggests that gold mineralization in the upper plate is hosted by the Valmy Formation. Hays and Foo (1991) report that Devonian fossils from mineralized allochthonous rocks in the mine were identified by C. Wrucke. This indicates that Slaven Chert may be the primary host to gold mineralization in the allochthon at Gold Acres. Because of the high degree of sheared and interleaved thrust slices in the Roberts Mountains allochthon, it is likely that both Valmy and Slaven are present in the mine, and both could host gold mineralization.

In the mine itself, the lower plate stratigraphy is complicated by low-angle faulting and contact metasomatism (Figure 5). Below the RMT, Wenban limestone has been partially to completely replaced by skarn. This is the upper skarn unit, approximately 30-40 meters thick. The upper skarn unit encompasses a highly altered felsic sill, described by Ketner (1965) and dated by Silberman and McKee (1972). The base of the upper skarn is a low-angle shear surface dipping ≈20° to the southwest, sympathetic to the Roberts Mountains thrust. Because of the low-angle faulting, the original extent of the skarn is not known. Below the upper skarn is an imbricate thrust

Figure 5. Stratigraphy at Gold Acres exposed in the mine. The dark unit at the base of the highwall is the ITZ. The thrust contact between the ITZ and the upper skarn is sharply exposed. The RMT is near the upper part of the highwall, above which the Ordovician Valmy formation is exposed. The catch benches are 60 feet apart.

Figure 5.

zone (ITZ) consisting of highly altered and sheared Srm that hosts refractory gold mineralization. Drill data indicate the total thickness of the ITZ is approximately 50 meters, of which ≈30 meters are mineralized with gold. The ITZ is separated from the next unit below, the lower skarn, by another low-angle shear, also with an attitude sympathetic to the RMT. Limited drill data indicate the average thickness of the lower skarn is approximately 100 meters. A granitic stock lies below the lower skarn, but the contact is obscured by endoskarn alteration.

STRUCTURAL GEOLOGY

The attitudes of lithologic units at the mine are determined by low-angle faults which dip ≈20° to the southwest. Thus, the ore enclosed in the ITZ is progressively deeper to the south and west of the existing pit. Also, the ore zone thins downdip, although the ITZ and other stratigraphic units maintain a relatively constant thickness. Local bedding attitudes within lithologic units is variable.

The low-angle shears which separate the ITZ from the upper and lower skarns may be related to Antler orogenic activity. The sympathetic attitude of the low-angle shears to the RMT is the best evidence for their concurrence with Antler deformation, implying that they are also thrust faults with eastward vergence. However, if compression continued from Antler to Sonoma time and during much of the Mesozoic, displacement along the low-angle faults (thrusts) may be later than Early Mississippian, when the Antler orogeny ended. Reactivation along the faults may be as recent as late Mesozoic, as a result of compression during the Cretaceous related to the Central Nevada thrust belt or the Sevier orogeny.

The entire stratigraphic sequence, at least from the lower skarn through the RMT, has been structurally offset by a northeast-trending set of normal faults. The average dip on the normal faults is 50° to the northwest. The two faults with the

greatest amount of offset are the Gold Acres and Island faults (Fig. 3). Displacement on these structures is on the order of thirty to fifty meters. Several other faults of the same orientation exist between the Island and Gold Acres faults, but displacement along these is less than ten meters. The lower skarn is definitely offset by the normal faults, as seen both in the pit and from drill hole data. Movement on the NE-trending faults postdates ITZ deformation and skarn formation. It is not known how deeply the northeasterly normal faults penetrate, but they are assumed to offset the upper surface of the stock as well. Trace element geochemistry of rock adjacent to the normal faults indicate hydrothermal fluids migrated along the faults (Hays and Foo, 1991). These faults are the only physical connection observed between the two skarn units.

The stratigraphy in the mine has been progressively uplifted to the southeast by the set of NE-trending normal faults. The greatest uplift observed is in the southeastern pit in the footwall of the Island fault. Hays and Foo (1991) suggest that uplift was initiated by intrusion of the stock below, and the faults were later reactivated by Basin and Range extension. Topographic elevations decrease southeast of the mine. Assuming topographic lows correlate with structural lows, it is further proposed that southeast of the mine, the stratigraphic sequence has been successively down-dropped by southeast-dipping normal faults (R.C. Hays, personal communication, 1990). Physical evidence for these faults is obscured by alluvial cover east of the mine.

Skarn mineralization has not been observed northeast of the northwest-trending pit, although thermal effects have been mapped northeast and southeast of the mine (Fig. 6). Roberts Mountains formation has been mapped at the surface at elevations of 1500 to 1700 meters in the hills northeast of the pits, 60 meters higher than the level of Srm in the pit. The autochthonous carbonate units (Dw and Srm) northeast of the pit are in normal depositional contact and do not show evidence of the large low-angle shears

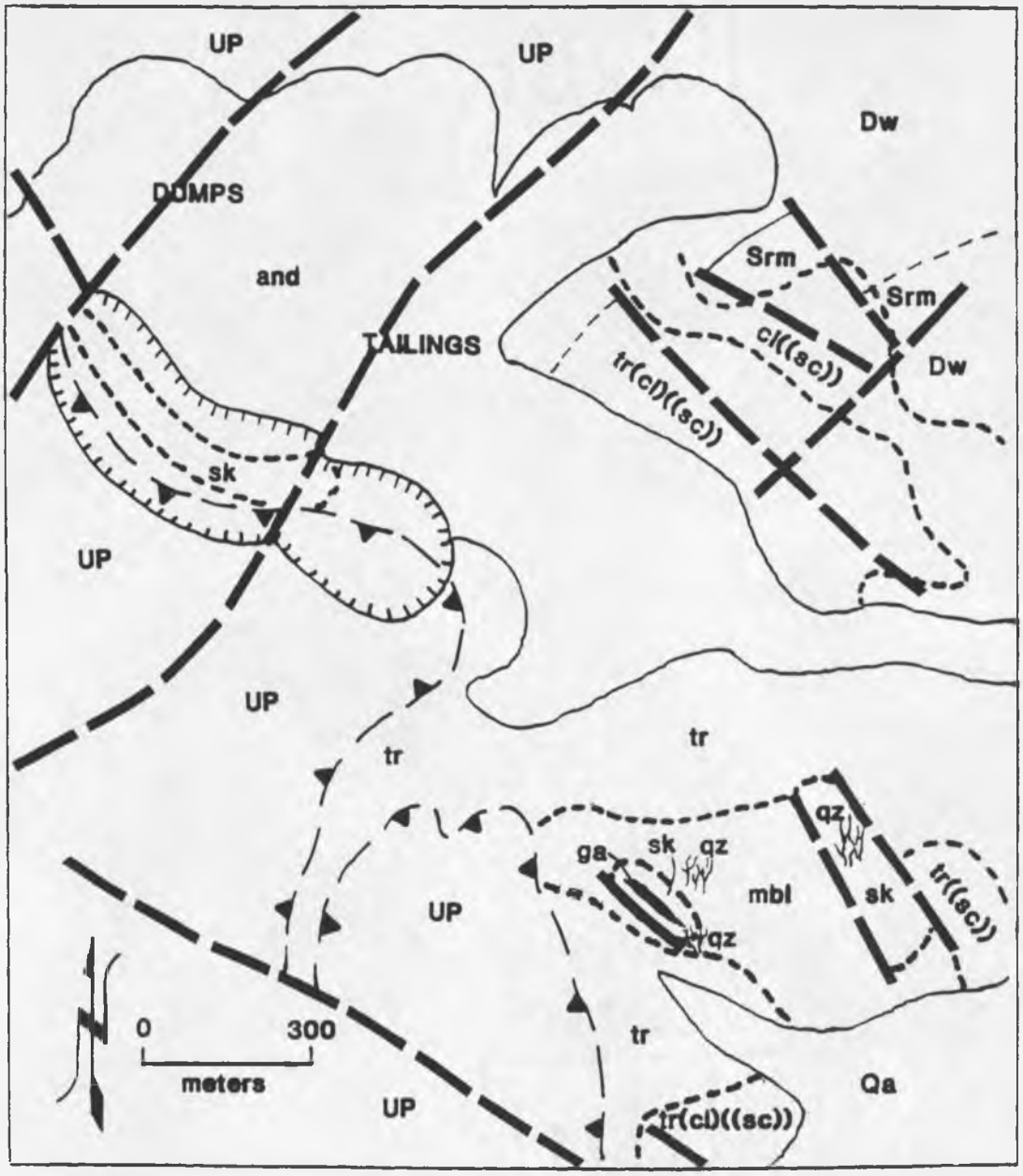

Figure 6. Thermal alteration in carbonate rocks distal to the Gold Acres mine. Geologic base and symbols taken from Figure 3.

seen in the pit (ITZ). It appears that a northwest-trending structure marks a boundary to skarn and gold mineralization northeast of the pit. Although this structure is not well-exposed in the pit nor at the surface, a northwesterly structure mapped by VLF and extending from the northern wall of the pit (Fig. 3) may represent the northwest extension of the proposed bounding structure.

Other geophysical evidence supports the existence of a northwest-trending bounding structure northeast of the Gold Acres pit. Aeromagnetic data indicate an abrupt northeastern edge of the body which produces the large positive magnetic anomaly at Gold Acres (Fig. 7, Plate I). The Gold Acres magnetic anomaly trends northwest, and has a high gradient on the northeast side, indicating a high contrast in magnetic susceptibility across the boundary. The magnetic high is caused by pyrrhotite in the lower skarn.

A magnetic susceptibility study of all rock types in the region was conducted to help constrain modeling of the magnetic data (Table I). Magnetic susceptibilities for unaltered sedimentary rocks and felsic igneous rocks in the region are very low. The felsic igneous rocks include Tertiary rhyolites, tuffs, quartz porphyry dikes, and the Jurassic Mill Canyon stock, all of which occur in the Cortez Mountains. Accurate measurements of magnetic susceptibility for the Gold Acres stock could not be made from drill cuttings. Its composition is comparable to the other felsic rocks, therefore the unaltered Gold Acres stock probably has a low magnetic susceptibility as well. Abundant pyrrhotite in the lower skarn makes it by far the most magnetic unit in the region, while the upper skarn is slightly, but significantly, more magnetic than the sedimentary units. The susceptibility of rocks in the ITZ is comparable to that of unaltered sedimentary rocks. The low magnetic nature of the ITZ rocks indicates two possibilities: (1) the carbonate rocks of the ITZ have not experienced contact metasomatism which might have produced a skarn assemblage which includes magnetic minerals, or (2) any pyrrhotite that may have been present in the ITZ was altered to pyrite.

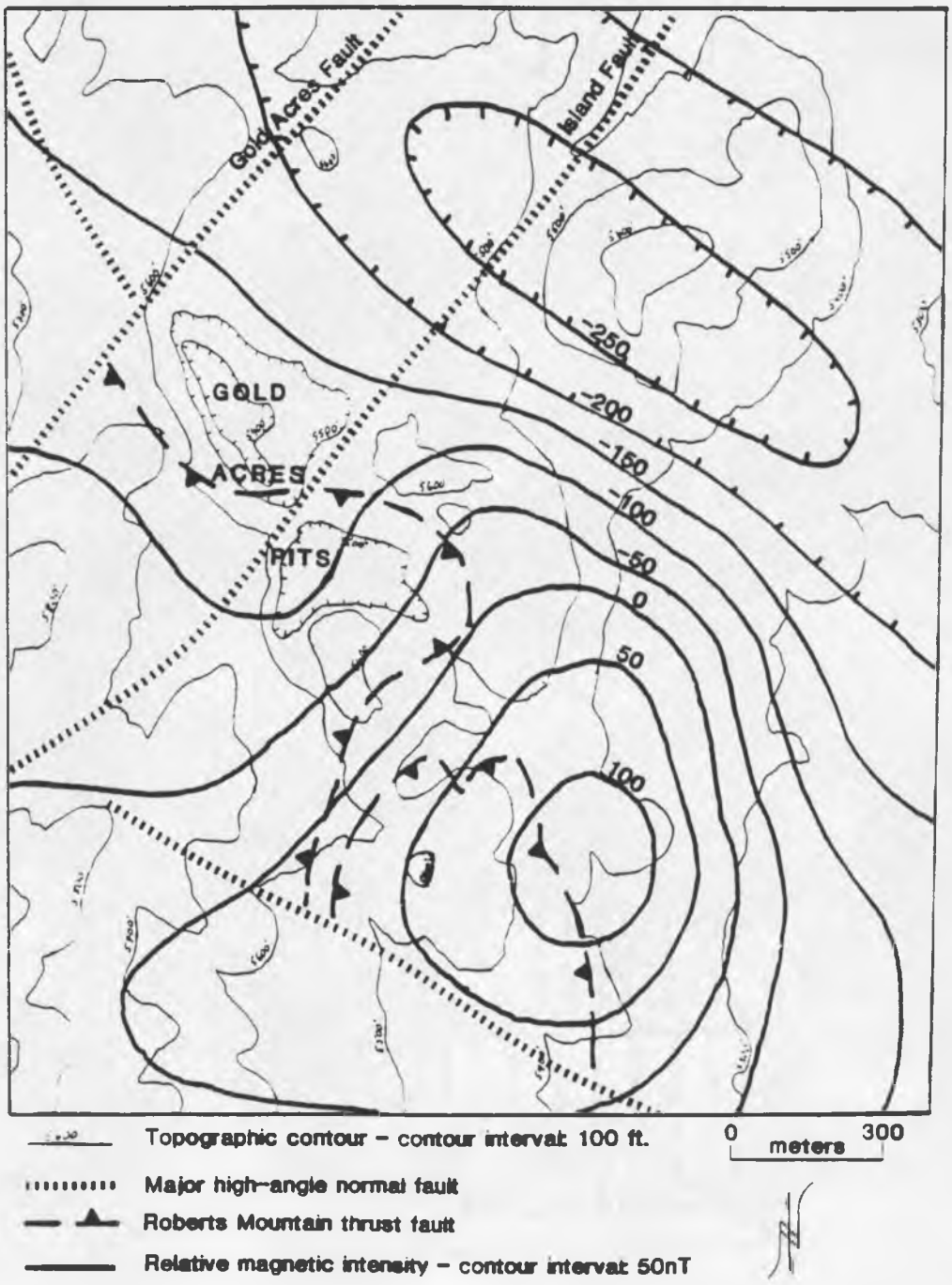

Figure 7. Aeromagnetic data at Gold Acres. Topographic base from USGS Tenabo and Corez Canyon 7.5' Quadrangles. Geology modified from Figure 3.

Table 1. Magnetic susceptibilities ($x10^{-3}$ Si units) of rock units at Gold Acres.

Unit	Lithology	Average	Range
Valmy	greenstone	0.50	0.46 - 0.58
Valmy	siltstone	0.10	0.1
Slaven	chert	0.04	0.04 - 0.05
Wenban	marble	0.16	0.07 - 0.25
Upper Skarn	px-trem skarn	0.50	0.02 - 1.3
I.T.Z.	carb. sil'd lms	0.03	0.01 - 0.06
Lower Skarn	pyrrhotite skarn	39.80	5.35-76.2

Relative intensity of the Gold Acres magnetic anomaly decreases gradually to the northwest and south. The decrease is apparently caused by increased thickness of intervening non-magnetic material as a result of down-faulting away from the center of the system and down-dip of the skarns to the southwest.

Sufficient evidence has been presented to support the existence of a major northwest-trending structure which borders the skarn and gold mineralization along the northeast side of the Gold Acres mine. Mapping of the upper contact of Srm in the pit and in the hills northeast of the pit suggest the northeastern block moved up relative to the southwestern block which contains the deposit. This must be considered an apparent motion, since there may well have been lateral displacement along the structure. There are few constraints on the timing of the northwesterly bounding structure. The NE-trending faults (Gold Acres and Island faults) are not offset across the proposed structure, so NE faulting occurred after NW faulting. Thermal alteration of carbonate rocks north of the bounding structure suggests the northern block was moved about the same time as emplacement of the Gold Acres stock.

DISTRIBUTION OF SKARN

The shape and size of the Gold Acres magnetic anomaly is an indication of the distribution of lower skarn below the surface. The Gold Acres magnetic anomaly extends eastward from the mine for ≈2000 meters, and west-northwestward under the Roberts Mountains allochthon for over 3000 meters. Calc-silicate mineralization similar to that of the lower skarn is known in drill holes northwest of Gold Acres and through the alluvium east of Gold Acres (Fig. 8). The minimum known distribution of the pyrrhotite-bearing lower skarn extends at least 3000 meters in a WNW to ESE direction and over 1000 meters from SW to NE. The actual lateral extent of lower skarn is at least five kilometers by two kilometers. The lateral distribution of the stock is probably less than that of the lower skarn. The subsurface distribution of the ITZ cannot be directly mapped from the magnetic data.

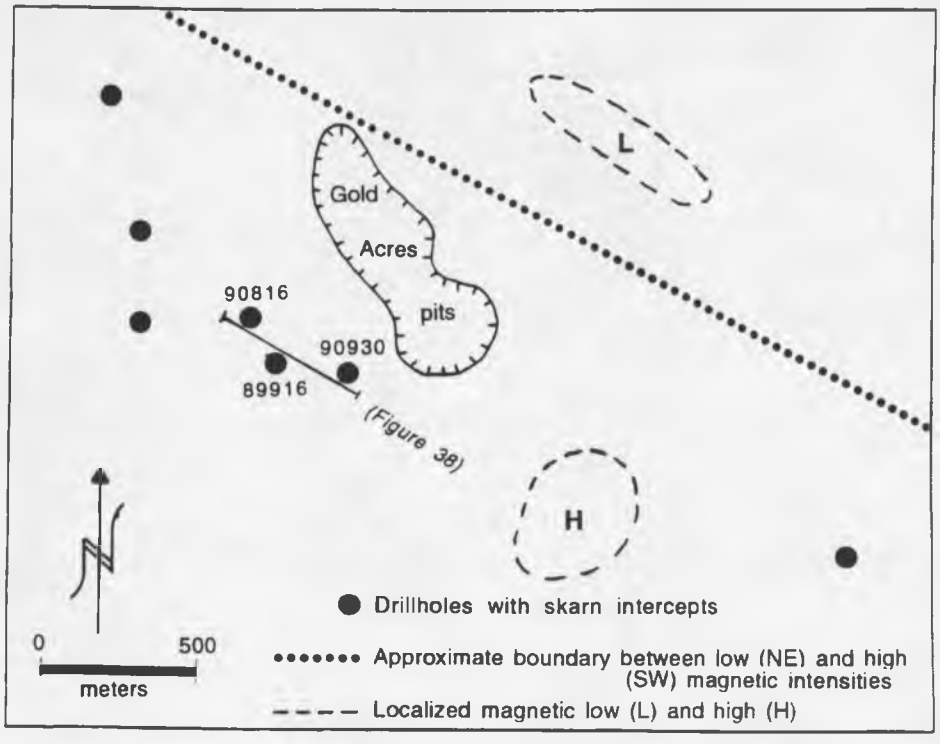

Figure 8. Lateral distribution of skarn at Gold Acres. Labeled drillholes are shown in cross section of Figure 38. Magnetic data summarized from Figure 7.

The magnetic anomaly is centered at a point 500 meters south of the Gold Acres pit (Figs. 7, 8). The highest magnetic values indicate the position where the magnetic body (lower skarn) either is closest to the surface or contains the highest concentration of magnetic material (pyrrhotite). It is likely a combination of both, since skarn alteration of Srm would have been most intense where the fluid flux was concentrated at the structural high caused by doming when the stock was emplaced.

DISCUSSION

The occurrence of a gold-bearing, imbricated thrust zone between two distinct skarn units is intriguing. Timing of the low angle faults is relevant to determining when and where the skarns were formed in relation to the stock and to the gold-bearing ITZ. If the low-angle shears are related to the Antler orogeny, and the ITZ was already emplaced between the pre-skarn units (Hays and Foo, 1991), how did the ITZ escape significant calc-silicate alteration? Otherwise, if low-angle faulting occurred after intrusion of the stock and subsequent skarn alteration (Cretaceous), what post-intrusive tectonic event could have caused the observed deformation in the ITZ and the separation of the skarns (if they were ever contiguous)? Mineralogic and metallogenic zoning patterns in the lower and upper skarn units (discussed in the following section) suggest the skarns are genetically related to one contact metasomatic system. Thus, it is most likely that low-angle faulting of the ITZ occurred after intrusion of the stock, as a result of Late Cretaceous contraction related to the Central Nevada thrust belt or the Sevier orogeny.

Evidence indicates gold mineralization occurred after displacement of the thrusts (*i.e.*, an existing gold ore body was not transported along the faults and emplaced against the skarn bodies). The NE-trending, high-angle normal faults exposed in the mine are mineralized with respect to gold and the epithermal trace element suite (Au, As, Sb, Hg, Ag, Tl). The faults cross-cut the lower skarn, which has a very low epithermal gold

geochemical signature. Therefore, the faults may have served as conduits to gold-bearing hydrothermal solutions (Hays and Foo, 1991). Precipitation of gold in the ITZ was favored because of the relatively reactive host lithology (reduced organic carbon and pyrite in silty limestone) and the high permeability of the thrusted, brecciated zone. The ITZ was more suitable for gold deposition than the skarn units which possess relatively impermeable and unreactive silicate mineralogies (Hays and Foo, 1991).

MINERALOGY, PETROGRAPHY, AND GEOCHEMISTRY

Mineralogy and petrography of the Gold Acres stratigraphic units were determined from field observations, descriptions of pit samples, drill chips and core, and thin section study. Descriptions presented below emphasize the role of mineralogy, geochemistry, and structural textures in working out the tectonic and metallogenic history at Gold Acres. Because characteristics of the upper skarn have been obscured by more intense retrograde alteration, it was possible to study the lower skarn in more detail than the upper skarn. Descriptions of the upper skarn have also appeared in earlier literature (Wrucke and Armbrustmacher, 1975; Wrucke and others, 1968).

GOLD ACRES STOCK

The Gold Acres stock is nowhere exposed at the surface nor in the pit, but its existence was suspected since 1965 on the basis of a large positive aeromagnetic anomaly (Mabey, 1965). The stock was intercepted in a core hole collared at the bottom of the Gold Acres pit. Later rotary reverse-circulation drilling south of the pit encountered the stock at 800 feet depth. Thin sections from a core sample (595-602) and from composites of rotary cuttings (Drill hole 90930) at selected intervals were examined under the petrographic microscope. In general, the Gold Acres stock is comparable to other Middle Cretaceous (110-90 Ma) plutons in the eastern Great Basin (Barton, 1990).

Hand lens study of the Gold Acres stock reveals a medium-grained, slightly porphyritic granitic rock. It contains no hornblende, and the plagioclase is Na-rich. The biotites have been extensively altered to chlorite, and K-feldspars to sericite. Other minerals are quartz, muscovite, and iron-oxides. Secondary sulfide minerals observed in the stock are pyrite, chalcopyrite, and molybdenite. Sulfides account for less than

2% of total composition. The upper contact of the stock is obscured by endoskarn development. Feldspars and micas are increasingly replaced by garnet and pyroxene, as well as chlorite, tremolite-actinolite, and epidote. Sulfide minerals, including pyrite, pyrrhotite, molybdenite, sphalerite, and chalcopyrite, increase in variety and amount. The mineralogical gradation from the stock to endoskarn to the lower skarn suggests skarn mineralization is caused by contact metasomatism related to the stock.

Thin section study reveals that the average mineral composition consists of quartz (≈30%), orthoclase (≈30%), plagioclase (≈30%), biotite (≈9%), and muscovite (≈1%). The Gold Acres stock is best classified as a granite, according to the I.U.G.S. ternary classification scheme, though the range in composition extends into the granodiorite and quartz monzonite fields (Fig. 9). The existence of primary biotite and muscovite would indicate a peraluminous composition. As will be discussed, convincing evidence for primary muscovite in the Gold Acres stock is rare, therefore a peraluminous composition for the Gold Acres stock is not inferred.

Plagioclase composition of the Gold Acres stock is estimated to be Ab_{62}-An_{38} (andesine) by measurement of extinction angles of albite twins, combined Carlsbad and albite twins, and pericline twins in rhombic sections (001) of the plagioclase crystals. Many plagioclase crystals displayed growth zoning, with Ca-rich cores and Na-rich rims, indicating disequilibrium possibly during accelerated cooling of the melt as it was being emplaced (Fig. 10). No pyroxenes or amphiboles were observed in the stock. The following accessory minerals were identified: apatite, magnetite, ilmenite, molybdenite, pyrite, calcite, rutile, leucoxene, calcite, and epidote. Of these accessories, molybdenite, pyrite, calcite, rutile, leucoxene, calcite, and epidote are considered secondary minerals.

Examination of igneous textures in the Gold Acres stock indicate the granite is equigranular to porphyritic. The average grain size of quartz and feldspar crystals in

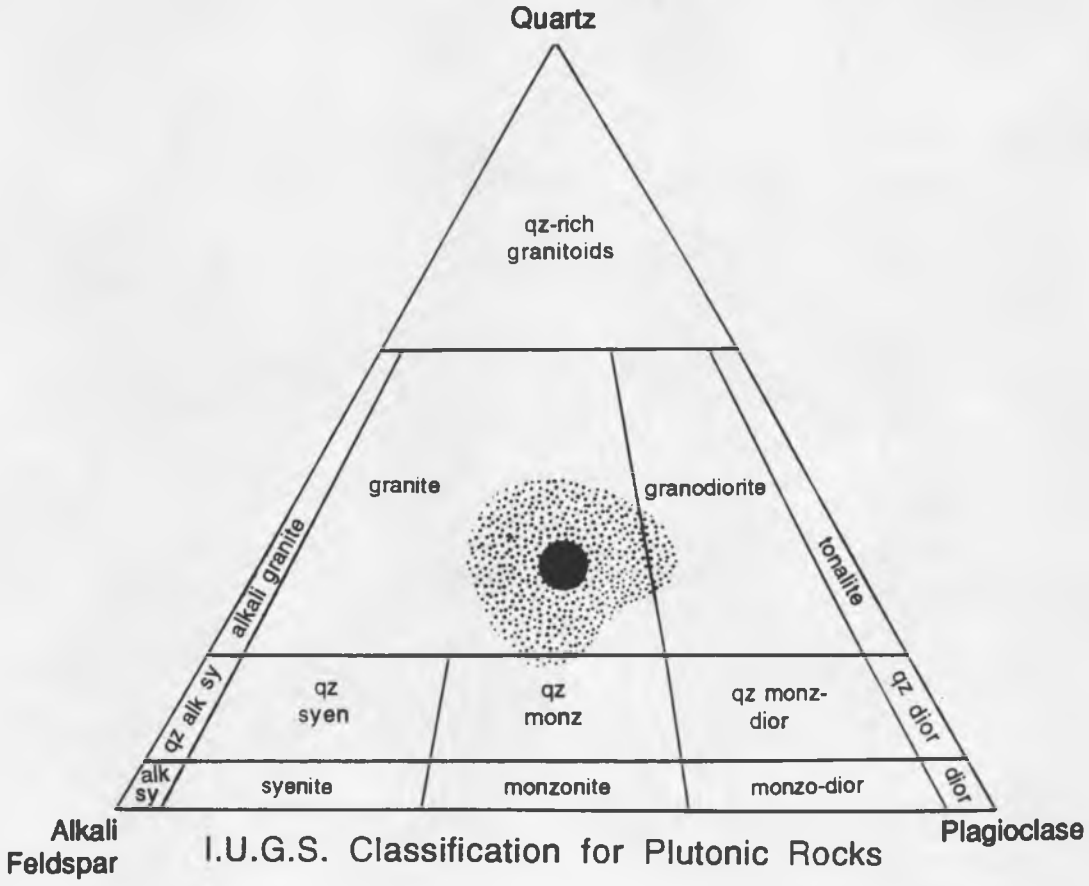

Figure 9. I.U.G.S. classification of the Gold Acres stock. The dot represents the average composition of the granite, and the stippled area represents the range of compositions. Abbreviations: qz=quartz, alk=alkali, sy=syenite, monz=monzonite, dior=diorite.

Figure 10. Typical appearance of the Gold Acres stock, with zoned and altered feldspars. (a) plane light and (b) crossed polarizers. Field of view is 2.5 mm long for each.

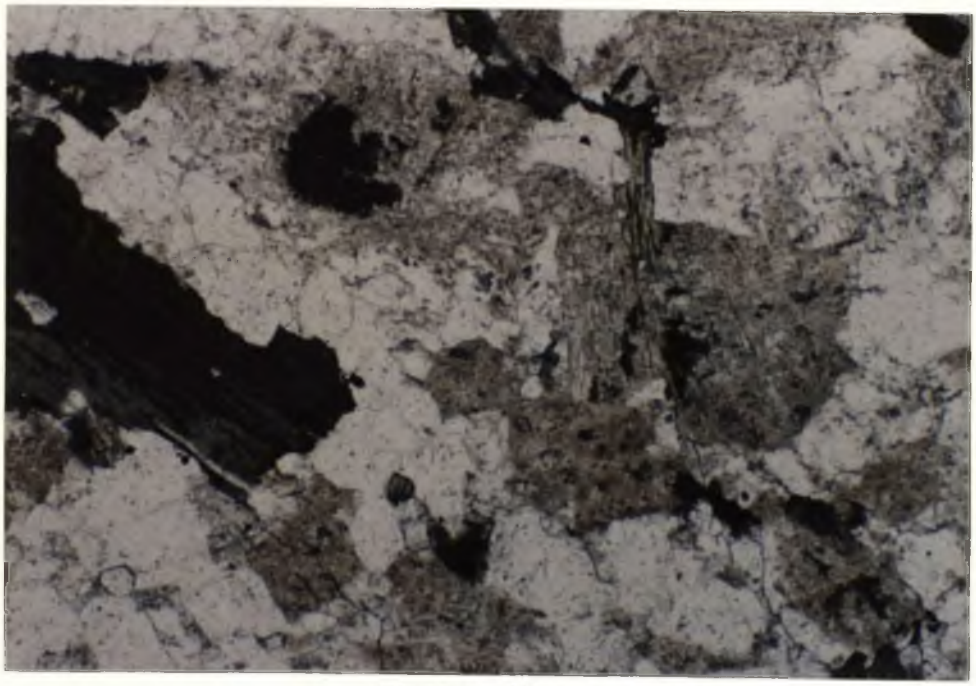

Figure 10a.

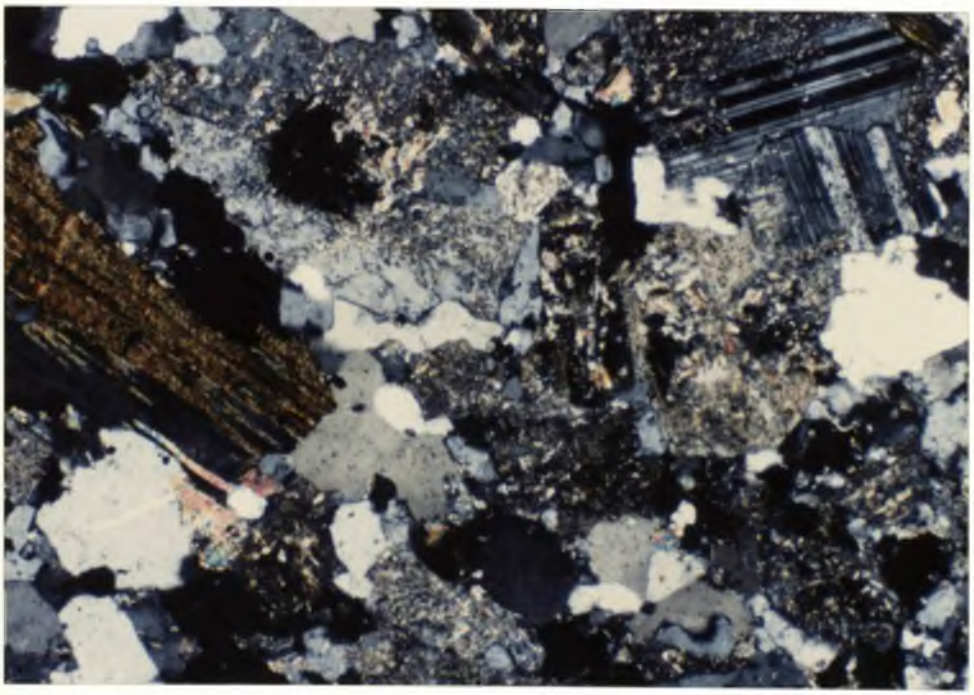

Figure 10b.

the deeper parts of the stock (more than 200 feet below the contact with the lower skarn) is 1.5 mm with a range of 0.4 mm to 4.8 mm. Most grains are between one and two millimeters in diameter. Quartz is characterized by undulose extinction, particularly in the larger grains. Phenocrysts of biotite occur in books which are up to four millimeters in diameter. The overall grain size decreases with decreasing depth, suggesting accelerated cooling closer to the contact (chill zone). In addition, the abundance of fractures and veins increases upward. Shallower parts of the stock (less than 200 feet below the contact with the lower skarn) display more prominent porphyritic texture, with approximately equal proportions of phenocrysts and groundmass. The average grain size of crystals in the groundmass is 0.1 mm (range of 0.03-0.5 mm), while phenocrysts of quartz and feldspar range up to three millimeters across.

Alteration of the Gold Acres stock is evident in all thin sections studied. The most apparent alteration is sericitic alteration of the feldspars (Fig. 11). Much of the feldspar is so completely altered that only a prismatic outline remains as an identifiable characteristic, making distinction between K-feldspar and plagioclase difficult. Hence, the I.U.G.S. classification of the Gold Acres stock as granite is an approximation. As the upper contact of the stock is approached, the feldspars are more intensely altered than feldspars in deeper portions. Altered orthoclase is probably replaced by sericite, but plagioclase may be replaced by montmorillonite or paragonite (both of which have optical properties similar to sericite). The distinction between sericite or montmorillonite in plagioclase could not be made by petrographic observation. Minor amounts of secondary calcite are also associated with altered plagioclase.

Plagioclase is more extensively altered than orthoclase. Much of the plagioclase could only be identified by ghosts of albite twinning. The degree of plagioclase alteration has a range of 20-100%. Replacement of orthoclase varies from 5% to 80%. Some of

Figure 11. Sericitic alteration of feldspars in the Gold Acres stock (plane light, field of view is 2.5 mm long).

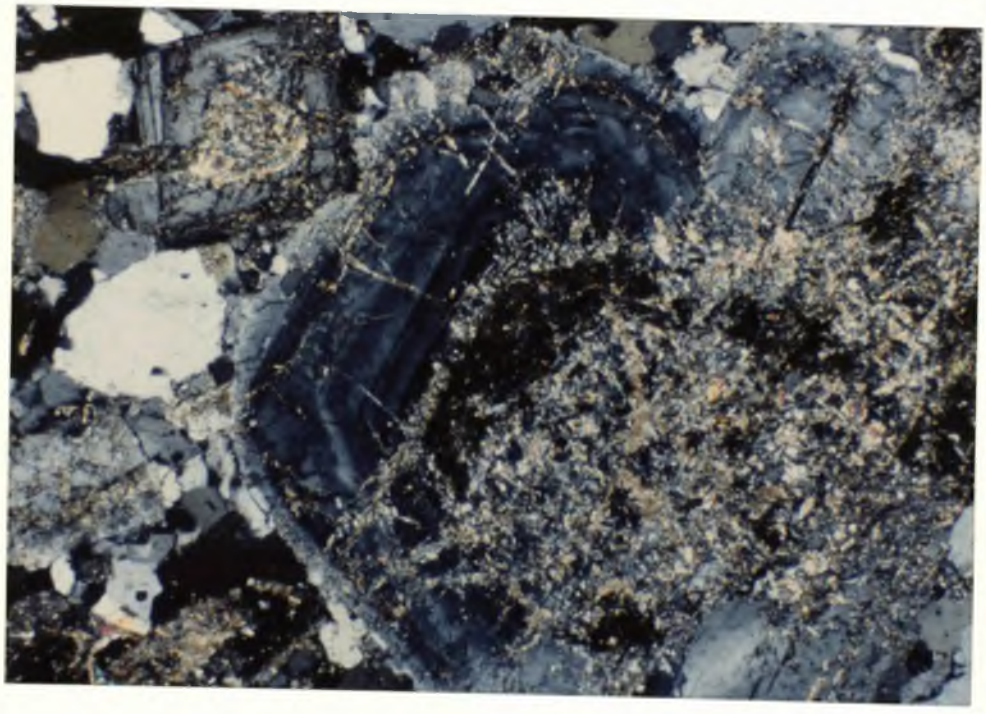

Figure 11.

the larger feldspars displayed preferential alteration of Ca-rich cores. Growth zoning is apparent in the unaltered rims.

Muscovite is abundant in the Gold Acres stock, but it is almost all secondary. Sericitization of feldspars occurred to an extreme such that recrystallization and secondary growth to relatively coarse-grained muscovite is pervasive (Fig. 12). Regions of shreddy, high-birefringent mica imply extensive sericitization and recrystallization to muscovite. Muscovite also replaces biotite. Occasional quartz veins are associated with muscovite. Two size populations of muscovite are seen in the granite: the fine-grained, shreddy type which is obviously secondary, and a coarser (2-3 mm) group with a book-like habit. Two examples suggest muscovite may occur as a primary phase. In one example, coarse muscovite appears to be intergrown against orthoclase (Fig. 13), and in another, muscovite is juxtaposed at an angle to chorite-altered biotite. Although there is possible evidence for primary muscovite in the stock, the widespread occurrence of secondary muscovite and sericite argues for a dominantly secondary origin for the questionable cases as well.

Alteration of biotite is widespread in the Gold Acres stock. As with the feldspars, alteration of biotite increases as the upper contact of the stock is approached. Although a few biotite grains were unaltered, most were partly to completely replaced by chlorite (Fig. 14). Muscovite commonly replaces biotite, resulting in a striped appearance of transparent mica with opaque hematite, ilmenite, rutile, and leucoxene (Fig. 15). Secondary green biotite replacing brown biotite was also observed, but it is not common. Chlorite is usually associated with secondary biotite and muscovite that replaced primary biotite. Epidote almost always accompanies chlorite. Most of the opaque accessory minerals associated with chlorite and secondary micas are hematite and ilmenite. Apparently the biotite included traces of titanium. Minor leucoxene and rutile are associated with the titanium minerals. Secondary sulfide mineralization, consisting

Figure 12. Coarse-grained secondary muscovite, Gold Acres stock (crossed polars, field of view is 2.5 mm long).

Figure 13. Possible primary muscovite grown against primary orthoclase (crossed polars, field of view is 2.5 mm long).

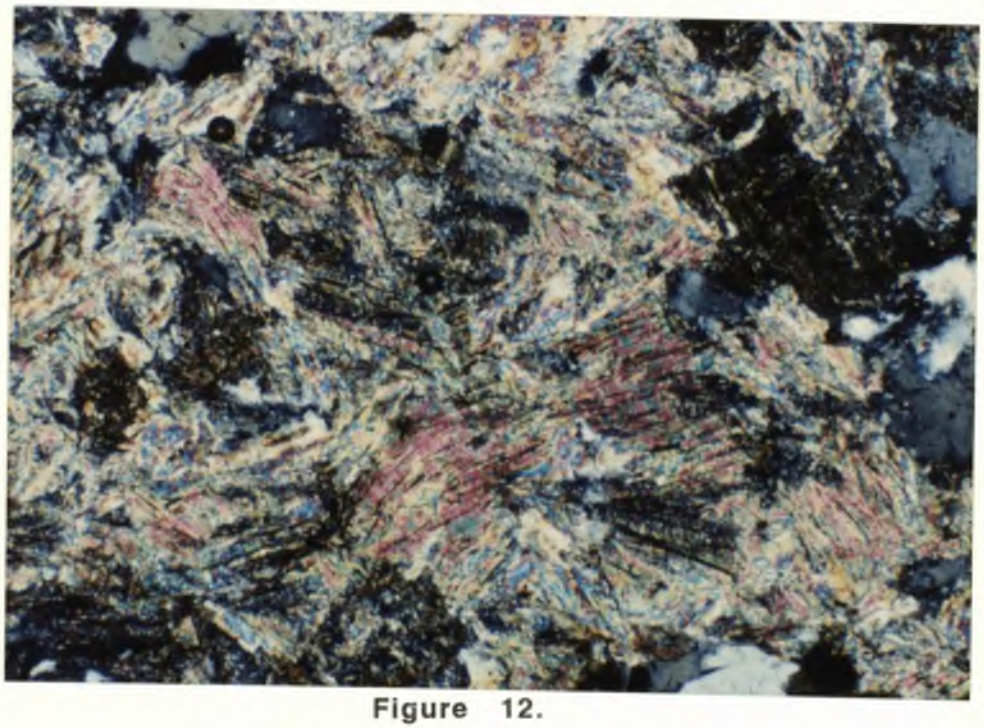

Figure 12.

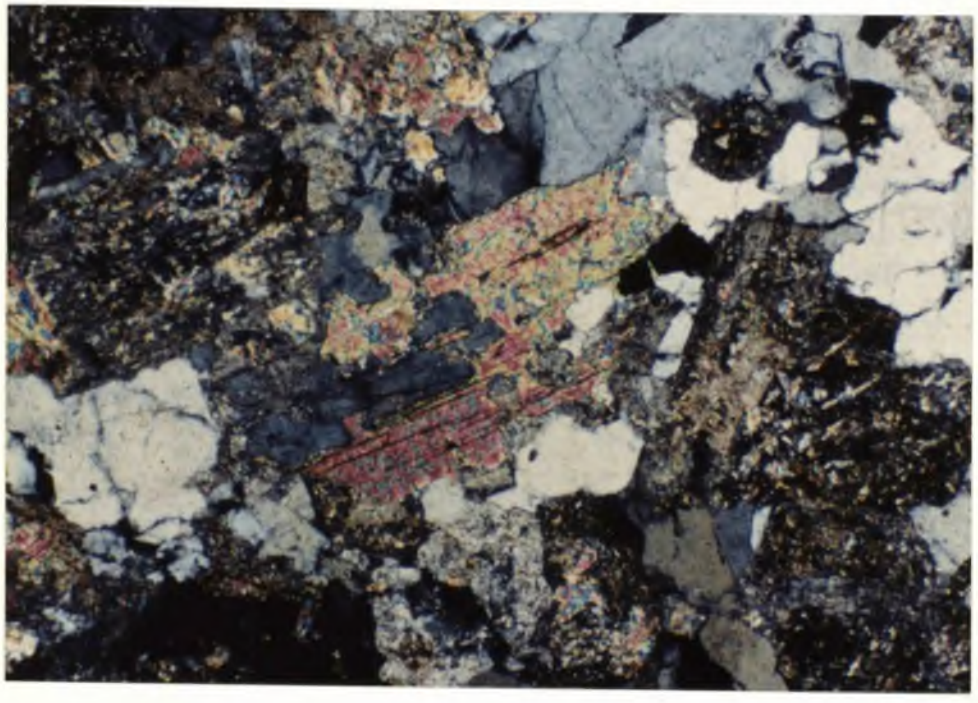

Figure 13.

Figure 14. Chloritic alteration (green) of biotite (brown), Gold Acres stock (plane light, field of view is 1.2 mm long).

Figure 15. Alteration of biotite to clear muscovite and opaque Fe-Ti oxides (plane light, field of view is 2.5 mm long).

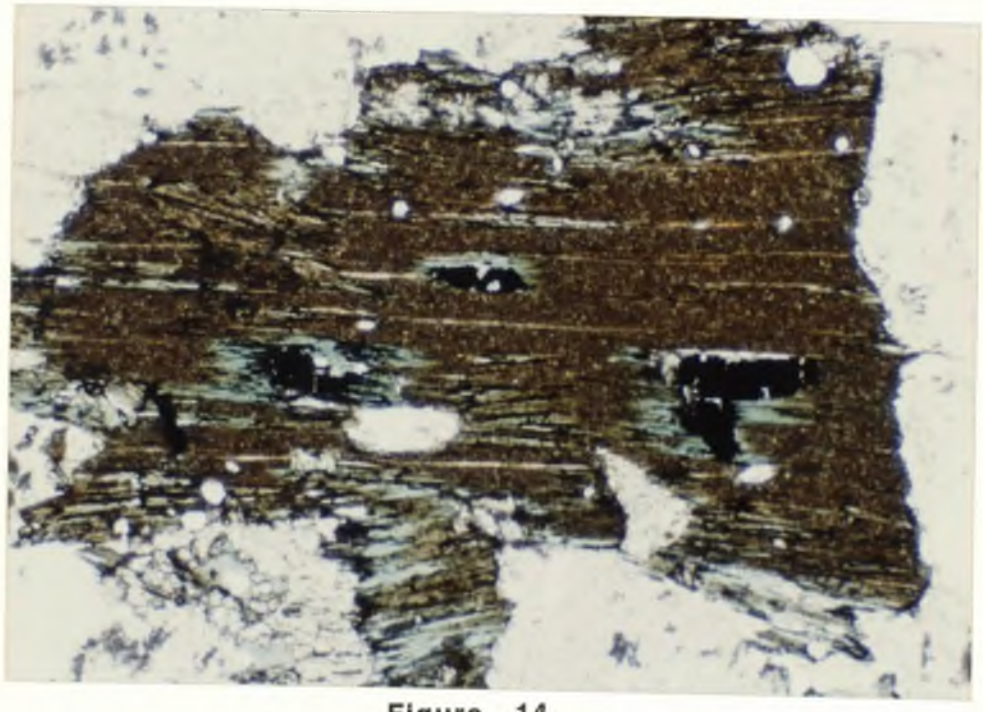

Figure 14.

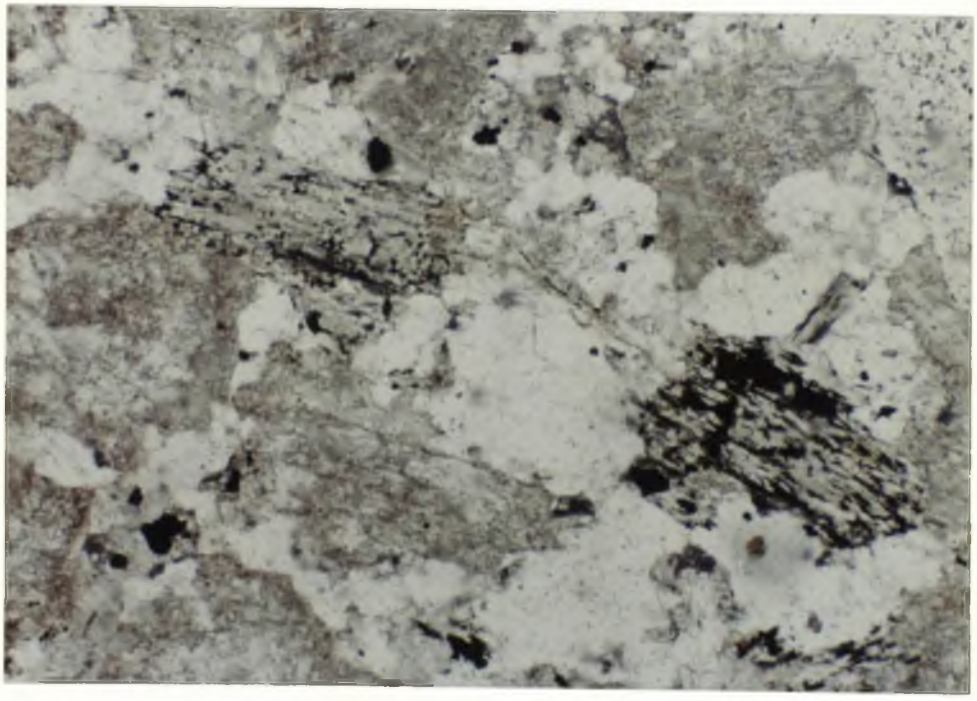

Figure 15.

of pyrite, molybdenite, and chalcopyrite, represents late magmatic or hydrothermal alteration of the Gold Acres stock.

Paragenesis of the Gold Acres stock is summarized in Figure 16. The earliest paragenetic stage consists of primary igneous mineralization: biotite, feldspars, quartz, and possibly muscovite. Secondary mineralization comprises the alteration products of the primary phases: sericite, muscovite, chlorite, epidote, hydrothermal biotite, and calcite. The endoskarn stage only occurs within the upper 200 feet of the stock. Skarn minerals include calc-silicate and sulfide phases.

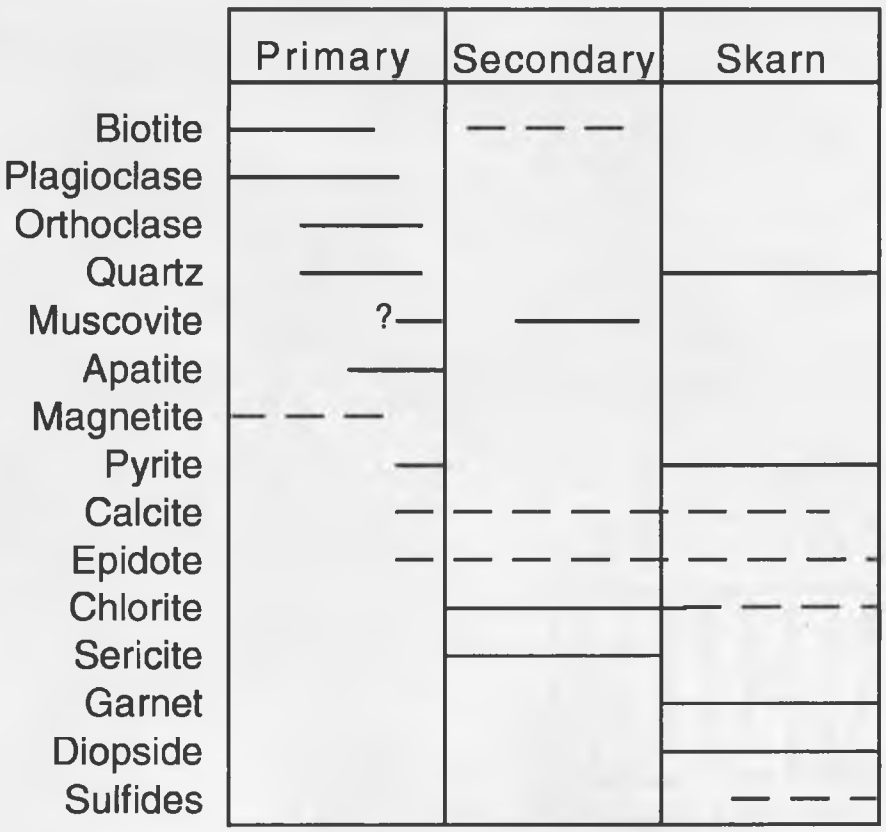

Figure 16. Paragenesis of the Gold Acres stock.

The alteration assemblage of the Gold Acres stock provides constraints on fluid evolution as alteration progressed. Mineral assemblages are determined by pressure, temperature, volatile content, and activities of aqueous species in the solutions with which the minerals equilibrated. Figure 17 is an activity diagram showing the phase relations of biotite, chlorite, orthoclase, muscovite, and quartz at 350°C and 0.5 kbar. The phases are compatible with conditions typical of porphyry copper plutons. At increased temperatures, biotite is stable with muscovite in the presence of either orthoclase or chlorite (dashed lines on Figure 17).

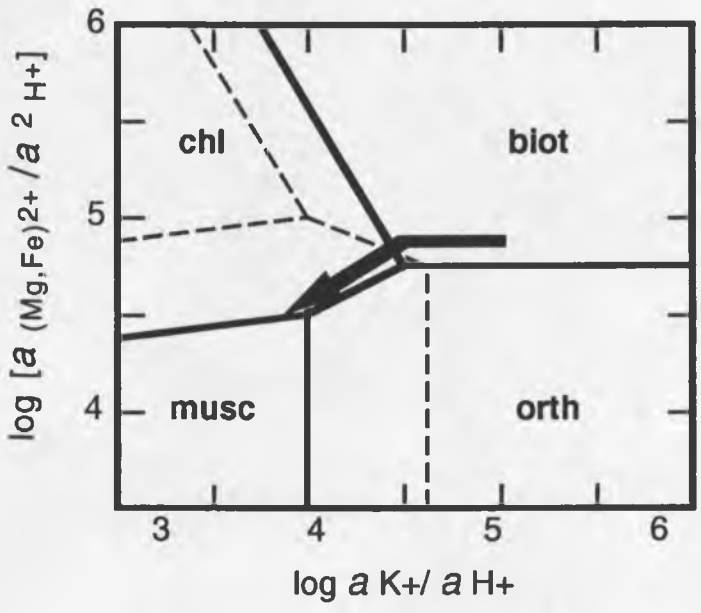

Figure 17. Phase relations of biotite, orthoclase, chlorite, and muscovite at 350°C, 0.5 kbar. Biotite field is calculated for typical porphyry copper composition, $K(Fe_{0.35},Mg_{0.65})AlSi_3O_{10}$. Chlorite field is estimated on the basis of compatibility with orthoclase at 350°C and $(Fe/Mg)_{chl} \approx (Fe/Mg)_{biot} \approx 1.5\text{-}3.0$. Dashed lines show approximate phase relations at higher temperature. Approximate path of evolving fluid indicated by arrow. Diagram modified from Beane and Titley, 1981.

Since biotite in the Gold Acres stock is altered to both muscovite and chlorite, 350°C is a lower temperature limit for the biotite and orthoclase alteration seen in the stock. The arrow indicates the path of the evolving fluid as the stock was altered. The activity ratios of (a_{K+}/a_{H+}) and (a_{Mg2+}/a^{2}_{H+}) were apparently decreasing, presumably by increase in a_{H+}. The composition of the reacted fluid as it left the stock was $(a_{Mg2+}/a^{2}_{H+}) \approx 4.5\text{-}5.0$.

LOWER SKARN

The lower skarn (exoskarn) is distinguished from endoskarn of the Gold Acres stock by a decrease in feldspars and micas and an increase in calc-silicates, carbonate, and sulfides. In hand specimen, brown andraditic garnet and green diopsidic pyroxene predominate, with chlorite and serpentine also present. Other silicate minerals are quartz, tremolite-actinolite, wollastonite, and epidote. Calcite commonly occurs in the interstices of garnet and pyroxene, as later replacement of prograde skarn minerals, and as late-stage veins. Sulfide minerals occur as disseminations, veins, and locally massive replacements up to 30 cm across. Quartz veins are commonly pyritic. Sulfide minerals observed in the lower skarn are pyrite, pyrrhotite, sphalerite, molybdenite, chalcopyrite, galena, and bornite. Fracture-controlled oxidation has affected the lower skarn assemblage, forming late-stage supergene minerals (limonite, jarosite, hematite, goethite, azurite, malachite, and anhydrite).

Several stages of alteration are observed in the lower skarn. Anhydrous calc-silicate mineralization is followed by a series of quartz/calcite/sulfide vein stages accompanied by actinolite/tremolite/chlorite/serpentine. The mineral assemblages of each stage will be described separately.

Early garnet in the lower skarn is euhedral to subhedral, indicating intergrowth during crystallization (Fig. 18). Garnet color is pale yellowish brown in thin-section.

Figure 18, Photomicrographs of early garnet-pyroxene calc-silicates of the lower skarn, (a) plane light, (b) crossed polars. Garnet is pale yellow-brown in plane light, isotropic under crossed polars. Diopside is pale yellow-green in plane light, highly birefringent under crossed polars. Field of view is 2.5 mm long.

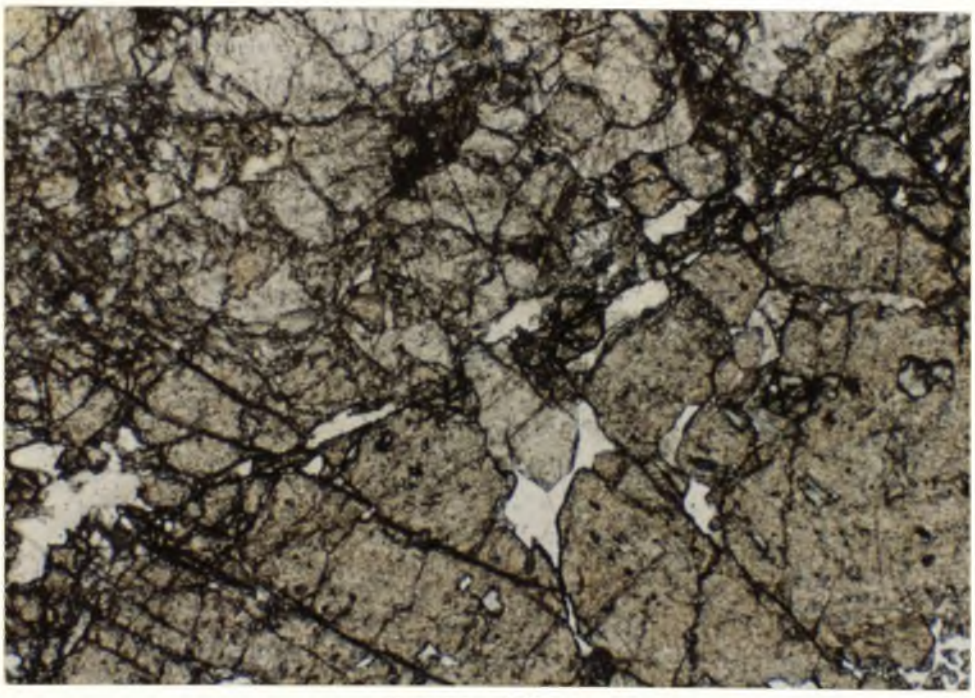

Figure 18a.

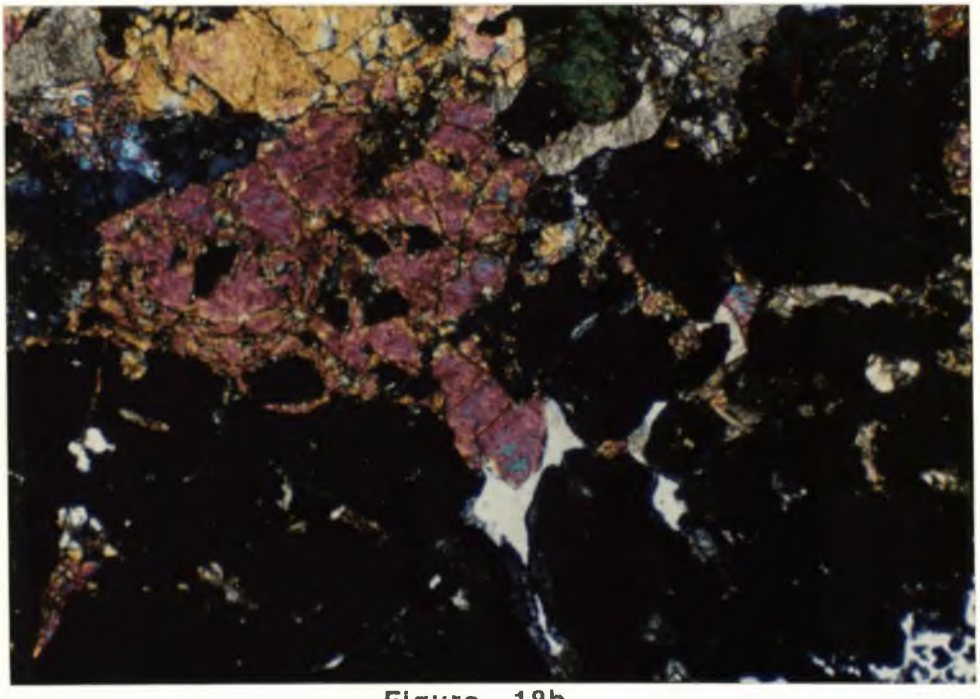

Figure 18b.

Very little compositional zoning resulting in growth rims or anomalous extinction is observed in early prograde garnet. Electron microprobe analyses of garnets from the lower skarn are comparable to garnets of typical Cu-skarns (Fig. 19). Lower skarn garnet compositions lie near the andradite ($Ca_3Fe_2Si_3O_{12}$) end member of the grossularite-andradite series and show low Mn enrichments, with compositions between $Ad_{58}Gr_{36}Sp_6$ and $Ad_{71}Gr_{26}Sp_3$.

Early pyroxene in the lower skarn occurs as subhedral to euhedral, elongate prismatic grains, sometimes with a radiating habit (Fig. 18). Crystals range from 0.1 to 0.5 mm in length. Electron microprobe analyses of lower skarn pyroxenes are within the typical Cu-skarn field (Fig. 19). Lower skarn pyroxenes display a compositional range of $Di_{95}Hd_5$ to $Di_{63}Hd_{33}Jo_4$. The enrichment of Mg in lower skarn pyroxenes relative to upper skarn pyroxenes reflects the higher dolomite abundance in the lower skarn protolith (Srm). Manganese content increases with increasing hedenbergite (Fe^{2+}) composition in lower skarn pyroxenes, but the increase is less than that observed for the upper skarn pyroxenes.

The relative abundance of diopside and garnet varies within the lower skarn. Some areas are nearly pure garnet; others lack garnet. Variations in composition of the protolith may determine the predominance of either garnet or diopside. Sharp parallel boundaries between garnetite areas and diopsidic areas may represent compositional variations controlled by bedding in the pre-skarn carbonate rock (Fig. 20). Other areas dominated by either garnet or diopside show irregular patchy boundaries. In the early anhydrous skarn, garnet and diopside are relatively coarse-grained (0.5-1.2 mm) and make up 95% of the rock. Interstitial areas of garnet and pyroxene are occupied by calcite (2-3%) and quartz (1-2%). Minor alteration of garnet to chlorite is observed. Significant sulfide and hydrous phases are not associated with early anhydrous skarn.

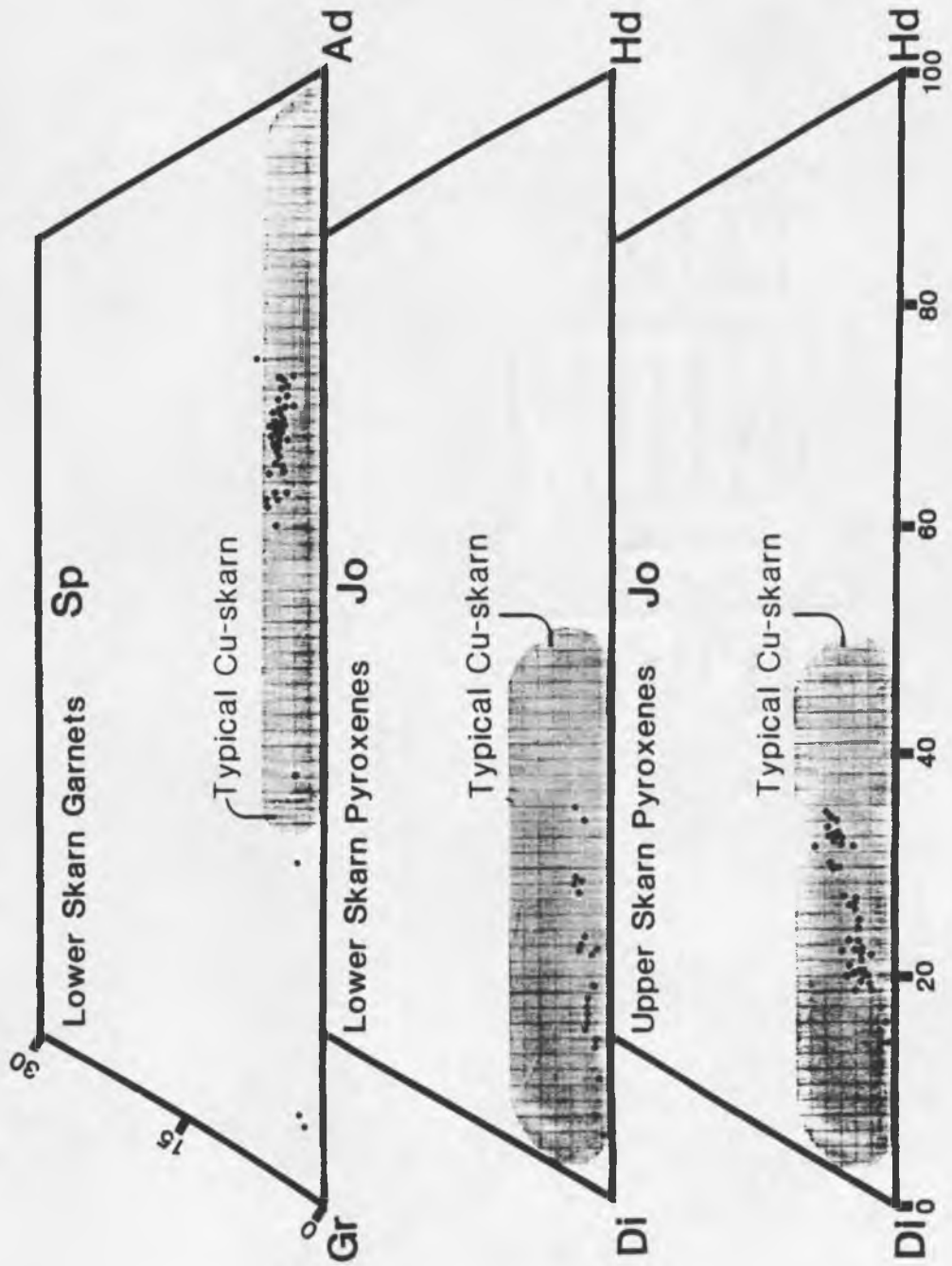

Figure 19. Electron microprobe analyses of garnet and pyroxene from Gold Acres skarn. Shaded areas show typical compositional range of copper skarns (from Einaudi and Burt, 1982). End member components: grossular (Gr), andradite (Ad), pyralspite (Sp), diopside (Di), hedenbergite (Hd), and johannsenite (Jo).

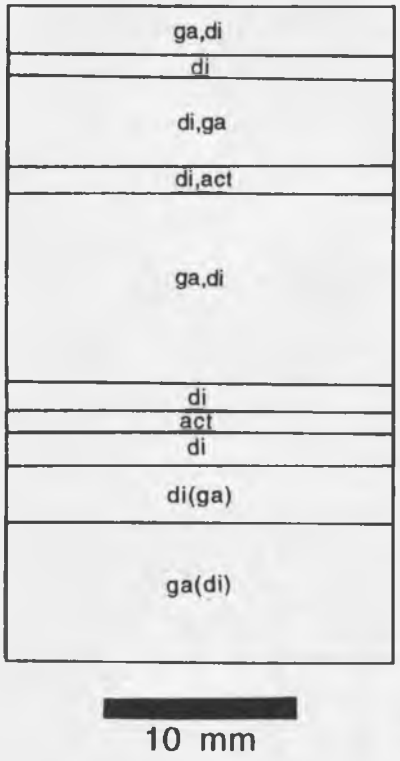

Figure 20. Relict bedding in lower skarn indicated by calc-silicate distribution. Garnet, diopside, and actinolite (ga, di, and act, respectively) listed in order of decreasing abundance. Parentheses indicate minor abundance of that mineral.

Continued hydrothermal alteration fractured the garnet-diopside assemblage, as evidenced by numerous veinlets of quartz cutting the early anhydrous skarn. Wall-rock alteration during this early stage of fracturing and veining was minimal. The observed chlorite alteration of garnet and the infilling of interstices by calcite and quartz may be related to this stage.

As hydrothermal alteration of the skarn progressed, garnet and pyroxene were broken down and replaced by hydrous calc-silicate minerals and sulfides. Zonation in quartz-calcite-pyrite vein assemblages is shown in Fig. 21. These veins cut earlier quartz veinlets. Coarse-grained garnet-diopside skarn is first recrystallized to smaller

Figure 21. Hydrous calc-silicate mineralization in the lower skarn, (a) plane light, (b) crossed polars, field of view is 2.5 mm long. Actinolite (left) grades into tremolite (center) away from quartz-pyrite-calcite vein (just out of view to the left). Tremolite grades into fine-grained garnet-pyroxene skarn (right). Epidote and chlorite are also present.

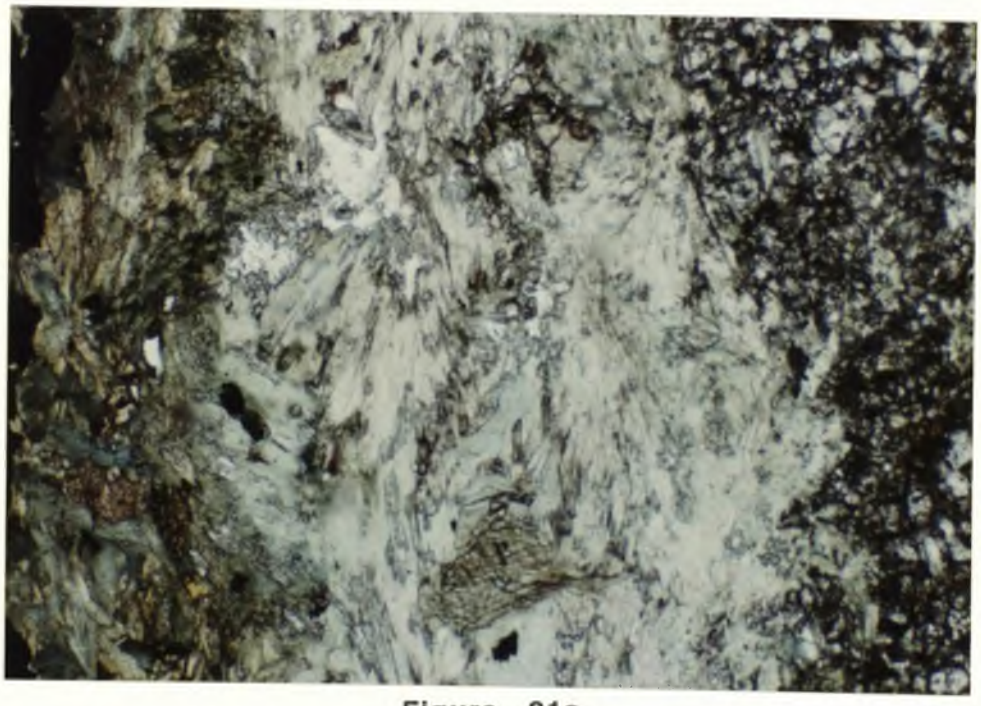

Figure 21a.

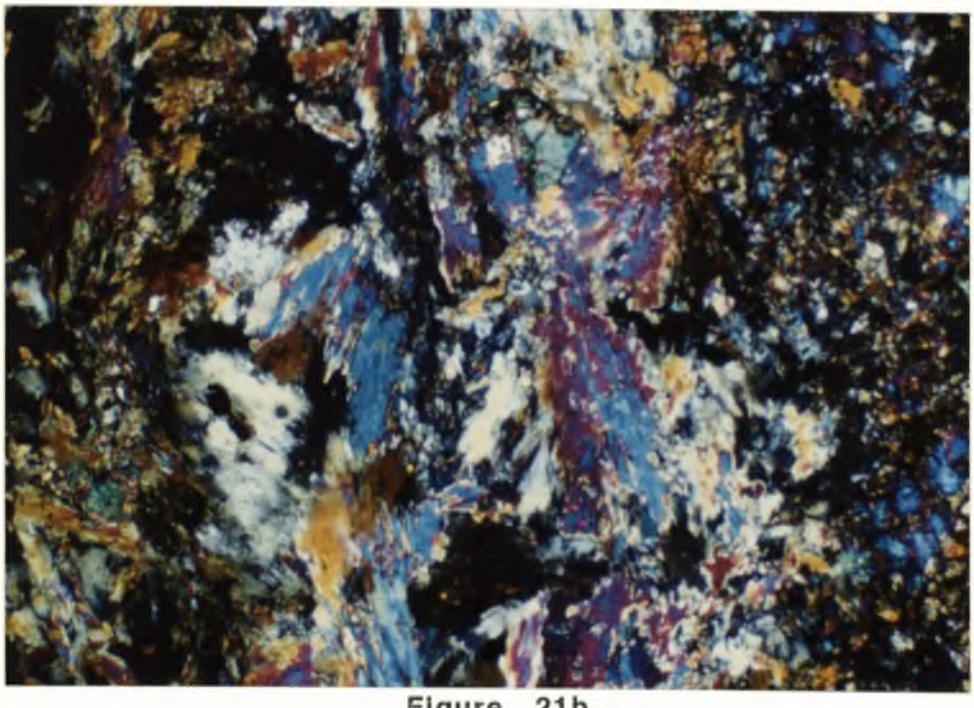

Figure 21b.

grain sizes (<0.1 mm). The fine-grained skarn comprises dominantly diopside with more calcite, quartz, pyrite, and chlorite than was observed in the prograde skarn. Garnet is less abundant in the recrystallized skarn, having been replaced by calcite, quartz, and chlorite. Pyrite is disseminated throughout this zone of altered skarn. The next zone approaching the vein center is dominated by amphibole with lesser chlorite. From the altered skarn to the quartz vein, the amphibole zone grades from pale tremolite ($Ca_5Mg_2Si_8O_{22}(OH)_2$) to green actinolite ($Ca_5(Fe,Mg)_2Si_8O_{22}(OH)_2$). The amphibole zone is successively followed by an earlier quartz stage, pyrite with epidote, calcite, and a later quartz stage in the vein center. Within the central open space of some of the latest calcite veins, aragonite (identified by X-ray diffraction) was crystallized. Mineralogical zoning of the vein assemblage displays sharp boundaries which are symmetrical on either side of the vein. Where quartz-calcite-pyrite veins cut earlier quartz veinlets, the zoned vein assemblage extends along the earlier-formed veinlets away from the later veins.

The reactions involved in the alteration of garnet-diopside skarn by veins of quartz-calcite-pyrite are easily deduced. The initial recrystallization results from breakdown of high-temperature phases as fluids migrate along fractures. The addition of SiO_2 and Ca^{2+} to skarn (concurrent with quartz and calcite vein deposition) results in the replacement of diopside by tremolite:

(1) $2Di + 4SiO_2 + 3Ca^{2+} + 4H_2O \rightarrow Trem + 6H^+$

Tremolite may also be produced by the reaction of diopside with water, Mg^{2+}, and H^+ :

(2) $4Di + Mg^{2+} + 2H^+ \rightarrow Trem + 3Ca^{2+}$

Subsequent addition of Fe^{2+} (accompanied by pyrite mineralization in the quartz/calcite vein) resulted in substitution for Mg^{2+} in tremolite to produce actinolite:

(3) $2Trem + Fe^{2+} \rightarrow 2Act + Mg^{2+}$ $\quad (K=a_{Mg^{2+}}/a_{Fe^{2+}})$

Phase relations between diopside and tremolite for reactions (1) and (2) are shown in Figure 22. These diagrams provide two possibilities for Ca ion activity ratio ($a_{Ca^{2+}}/a^2_{H^+}$). In the first reaction, the saturation limit of quartz provides an upper limit: $(a_{Ca^{2+}}/a^2_{H^+}) \approx 6.0$. For the second reaction, the Mg ion activity ratio (4.5-5.0) of the evolved fluid leaving the Gold Acres stock constrains the Ca ion activity ratio: $(a_{Ca^{2+}}/a^2_{H^+}) \approx 8.0$. To determine which value is accurate, a further constraint is required. In Figure 23, phase relations of garnet, epidote, and calcite as a function of temperature and $(a_{Ca^{2+}}/a^2_{H^+})$, indicate that calcite is only stable with epidote above $(a_{Ca^{2+}}/a^2_{H^+}) \approx 9$. This suggests that reaction (2) was more important in forming tremolite in the lower skarn, and that $(a_{Ca^{2+}}/a^2_{H^+}) \approx 8 - 9$.

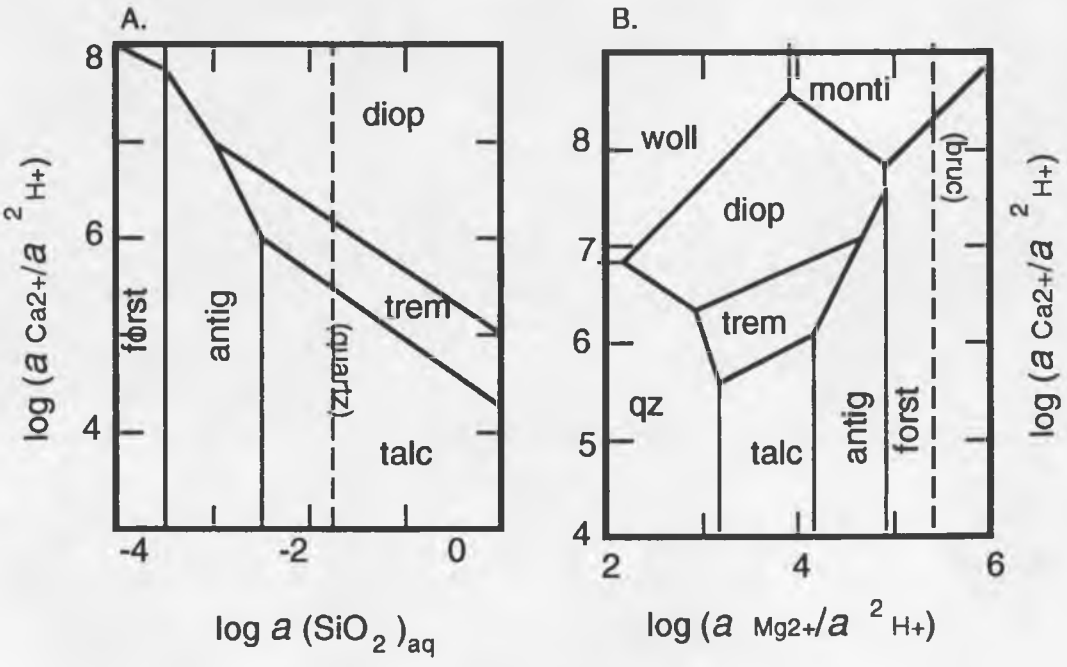

Figure 22. Activity diagrams for the system CaO-MgO-SiO_2-H_2O-HCl at 400°C, 0.5 kbar, showing phase relations between pure compositions of diopside and tremolite according to (a) reaction (1) and (b) reaction (2). See text for reactions. Mineral abbreviations in Appendix A. Phase diagrams modified from Bowers and others, 1984.

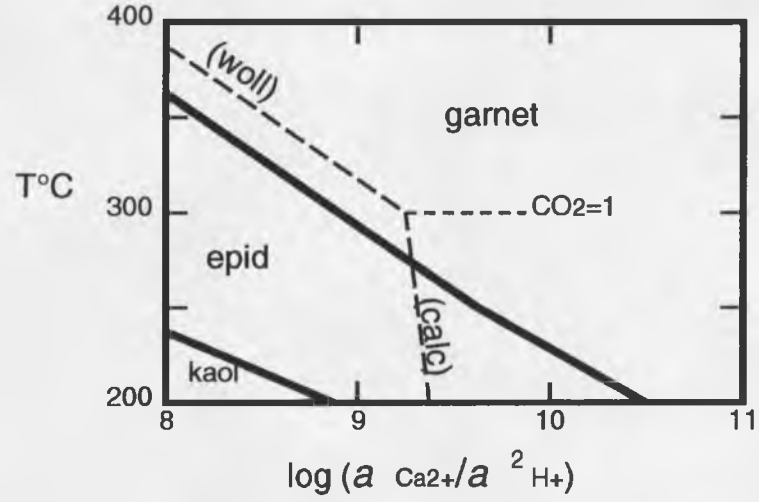

Figure 23. Temperature and Ca-activity phase diagram showing stability relations of garnet, epidote, and kaolinite with wollastonite and calcite at 350°C, 0.5 kbar, and XCO_2=1. Garnet and epidote fields calculated using mineral compositions typically found in porphyry copper plutons ($Ca_3(Al_{0.3},Fe_{0.7})_2Si_3O_{12}$ and $Ca_2Al_2(Al_{0.1},Fe_{0.9})Si_3O_{12}$, respectively). Phase diagram is modified from Beane and Titley, 1981.

Combined phase relations of garnet, pyroxene, epidote, and amphibole compositions typical of porphyry copper systems (Figure 24) indicate the path of the evolving fluid as it interacted with the lower skarn assemblage. Garnet-pyroxene skarn formed in equilibrium with a fluid of composition (A): $(a_{Ca^{2+}}/a^2_{H^+}) \approx$ 8.0-9.0 and $(a_{Mg^{2+}}/a^2_{H^+}) \approx$ 4.5-5.0. As a_{H^+} increased, the fluid evolved down a line of slope=1, to the quartz/pyroxene boundary (B). Further reaction destroyed garnet and pyroxene while epidote and amphibole became stable with quartz (C).

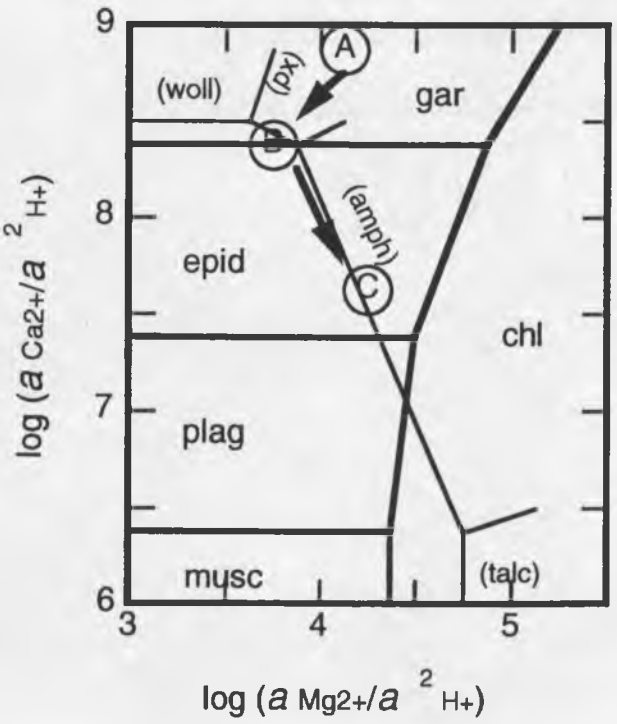

Figure 24. Ca and Mg activity phase diagram for typical porphyry copper minerals, at 350°C, 0.5 kbar, and $a_{K^+}/a_{Na^+} = 3.25$. Circled letters and arrows indicate the path of the evolving fluid during alteration of the lower skarn (see text for discussion). Plagioclase: An_{15}. Pyroxene: $Ca(Mg_{0.8},Fe_{0.2})Si_2O_6$. Amphibole: $Ca_2(Mg_{0.5},Fe_{0.5})_5Si_8O_{22}(OH)_2$. Garnet, epidote, and chlorite compositions are the same as was described in Figures 17 and 23. Modified from Beane and Titley (1981).

Sulfide mineralization accompanied or immediately followed anhydrous calc-silicate mineralization. Pyrite occurs widely disseminated with calc-silicate minerals, in veins, and massive pods. Pyrrhotite mainly occurs in pods associated with pyrite or

sphalerite. Chalcopyrite is present as disseminations in calc-silicate skarn, in small (1-5 cm) pods with pyrite, and as "exsolutions" in sphalerite. Molybdenite is locally abundant in pods and streaks up to 5 cm in length. Sphalerite is associated with pyrite and pyrrhotite in massive pods.

Petrographic study of polished sections reveals details of sulfide mineralogy and paragenesis. The fractured and dissolved appearance of pyrrhotite relative to pyrite (Fig. 25a) suggests it formed early in the retrograde stage and was unstable with the later sulfide minerals. The relative stability of pyrite over pyrrhotite indicates an increase in activity of sulfur species, sulfur fugacity, or oxygen fugacity. Where chalcopyrite is associated with pyrite, the chalcopyrite appears to be younger (Fig. 25b) or contemporaneous. The spotty occurrence of chalcopyrite in sphalerite indicates their contemporaneity (Fig. 25c). Spots of pyrite also occur in sphalerite. Sphalerite is dark brown to black in hand specimen and deep red in thin section, indicating significant Fe^{2+} content in the sphalerite. Comparing textures of associated pyrite and sphalerite suggests sphalerite is younger than pyrite (Fig. 25d). Cross-cutting relationships of molybdenite and pyrite clearly indicate molybdenite is younger (Fig. 25e). Sulfide assemblages are cut by later pyrite-bearing veins, suggesting multiple stages of pyrite mineralization.

Hydrous calc-silicate mineralization and sulfide mineralization coincide with veining stages. Large veins often show multiple stages of mineralization which includes quartz, calcite, pyrite, amphibole, chlorite, and lesser epidote, garnet, pyroxene, and wollastonite. Epidote mineralization is nearly always associated with pyrite, both in veins and in hydrous skarn. Sulfide mineralization took place before or concurrently

Figure 25. Photomicrographs of sulfide phases in the lower skarn (reflected light, field of view is 2.5 mm long). (a) Pyrite replacing pyrrhotite. (b) Chalcopyrite replacing pyrite.

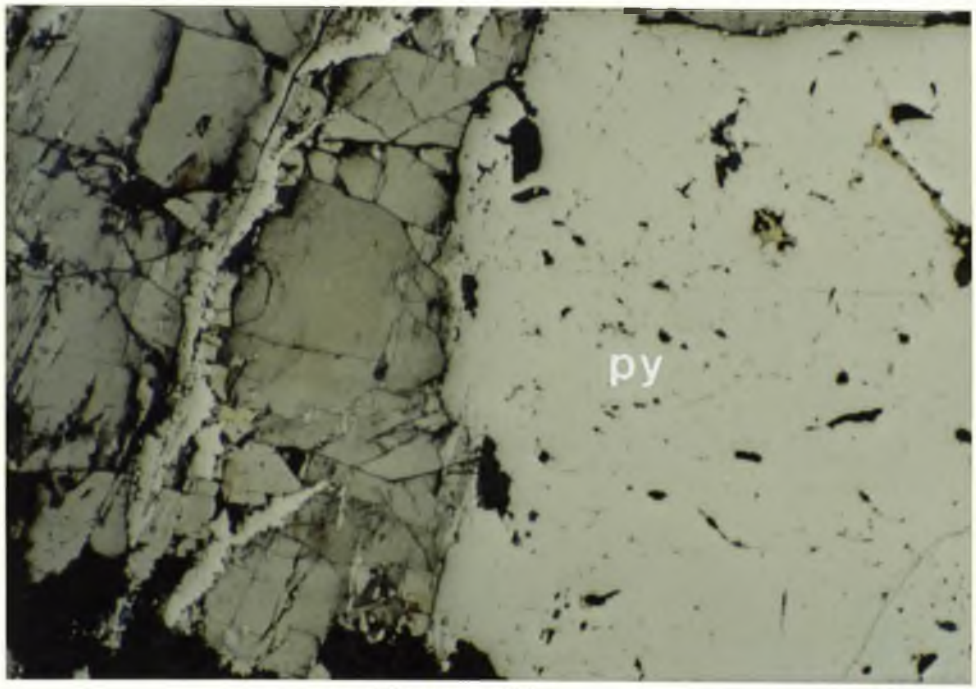

Figure 25a.

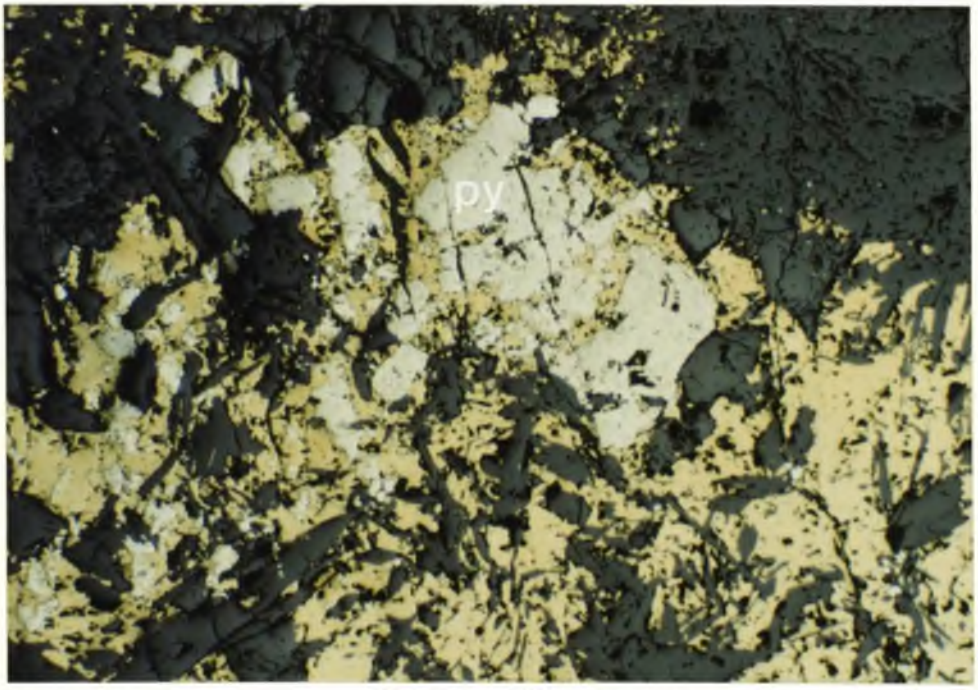

Figure 25b.

Figure 25. Photomicrographs of sulfide phases in the lower skarn, continued (reflected light, field of view is 2.5 mm long). (c) Spotty pyrite and chalcopyrite in sphalerite. (d) Sphalerite replacing pyrite.

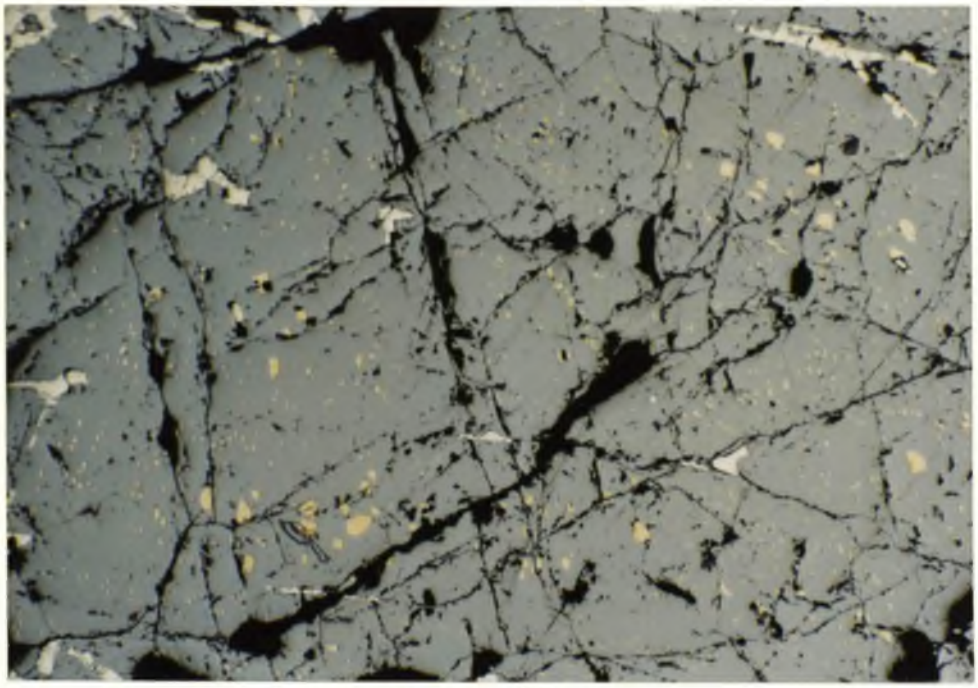

Figure 25c.

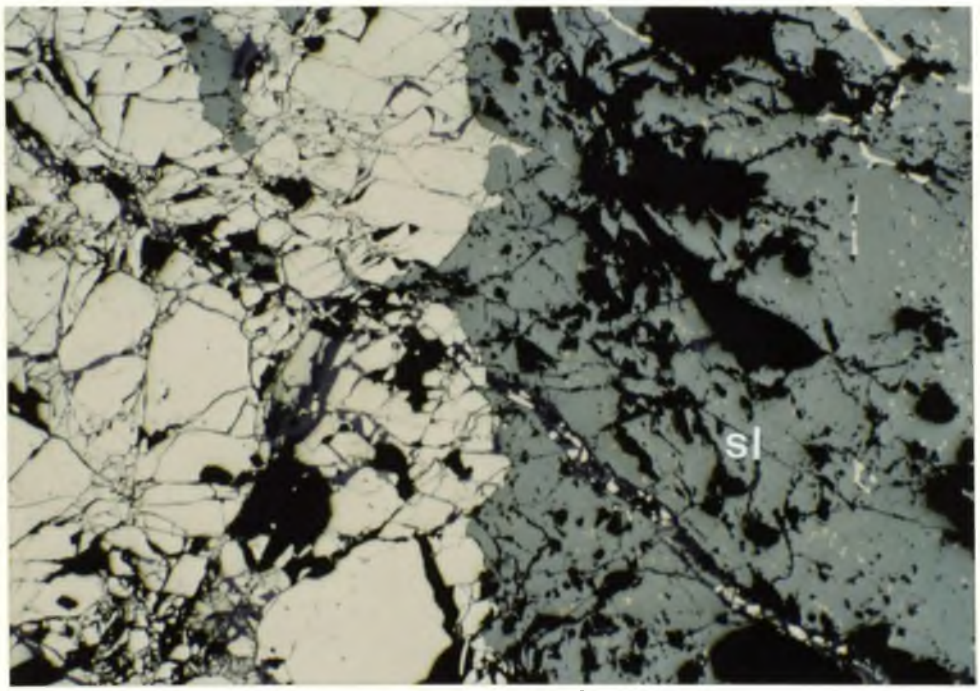

Figure 25d.

Figure 25. Photomicrographs of sulfide phases in the lower skarn, continued (reflected light, field of view is 2.5 mm long). (e) Molybdenite cross-cutting pyrite.

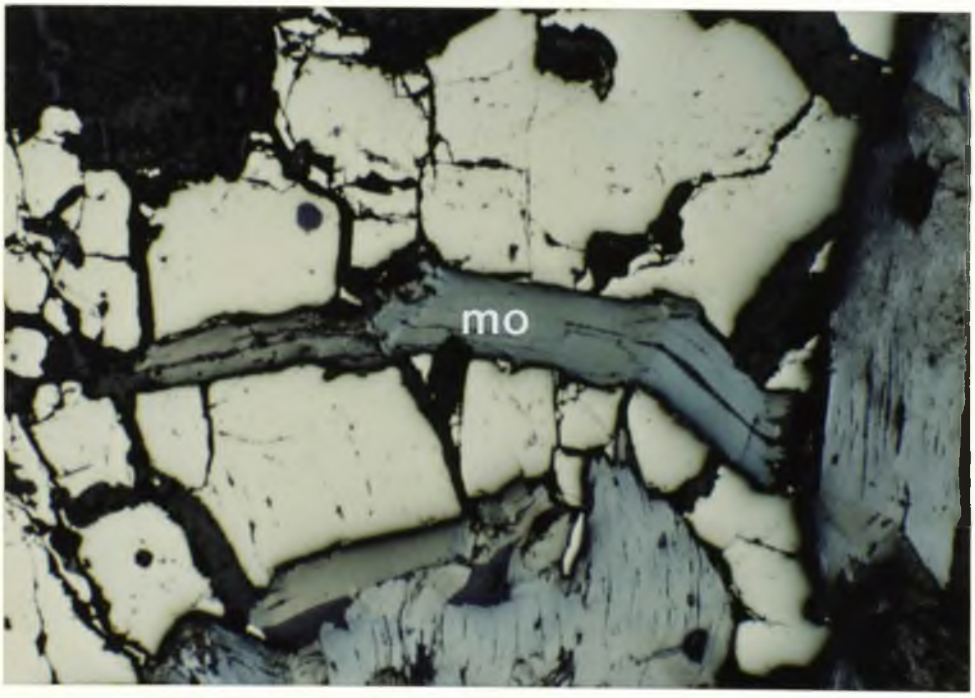

Figure 25e.

with most of the veining events, suggesting high flow of metaliferous fluid through the skarn, causing replacement of anhydrous skarn by pyrrhotite, pyrite, sphalerite, and chalcopyrite. Quartz veins generally are not replaced by sulfides.

A second stage of skarn mineralization is indicated by the occurrence of garnet and pyroxene in late veins which cut the sulfide assemblages. A late stage of garnet veining contains large euhedral zoned anisotropic garnets up to four millimeters across. Quartz, calcite, and diopside typically replace the garnet growth zones. Overgrowths of quartz and calcite on garnet were also observed. Electron microprobe analysis of one of the zoned garnets from a late garnetite vein displayed compositional zoning from an andraditic core (Ad_{68}) to a rim of nearly pure grossularite (Ad_5) (Fig. 26). This rim composition is more grossularite-enriched than indicated for garnets in typical copper,

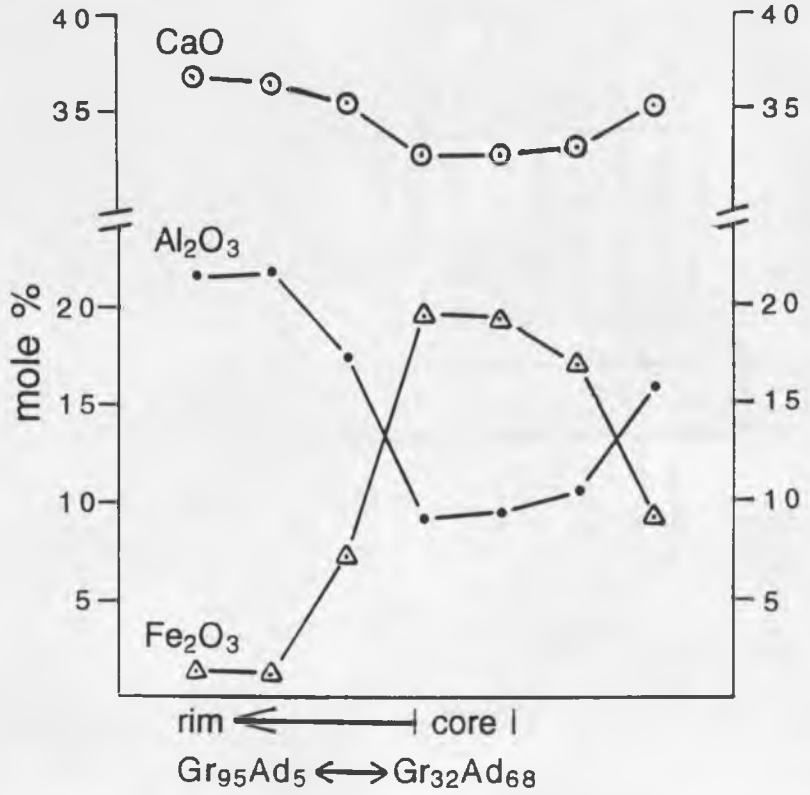

Figure 26. Zonation in banded garnet of late garnetite stage in the lower skarn. Electron microprobe analyses indicate an andraditic core (Ad_{68}) and a grossular rim (Ad_5).

lead-zinc, iron, or gold skarns (Einaudi and others, 1981; Einaudi and Burt, 1982; Meinert, 1989). Compositional zoning of garnets from andraditic to grossular indicates evolution of the hydrothermal system to higher activities of Al^{3+} or lower activities of Fe^{3+} during the second stage of calc-silicate mineralization. Relatively reduced conditions (evidenced by decreased activity of oxidized iron) during this stage may be inferred from the grossular rims.

Coarse-grained pyroxene also occurs in late veins through fine-grained altered skarn, though it is not common. Pyroxene veins probably represent renewed mineralization of pyroxene by the second skarn-forming event (correlative with the development of the garnetite veins discussed above), though cross-cutting vein relationships were not observed.

Deformational textures observed in the lower skarn help constrain the relative timing of alteration events. Molybdenite associated with the anhydrous skarn assemblage shows marked anisotropy (Figure 27), indicating post-mineral deformation. The same inference can be made regarding strained quartz veins associated with anhydrous calc-silicates (Figure 28a). In contrast, a later quartz vein which cuts the anhydrous calc-silicate/sulfide assemblage is relatively fresh and unstrained (Figure 28b). This quartz is also associated with sericite, suggesting post-deformation hydrothermal activity in the lower skarn.

The latest stage of veining seen in all samples of the lower skarn, both in the pit exposures and in thin section, consists of iron oxides. Wherever they occur, iron oxide veins are steep and cut all previous textures. They probably formed at the same time as other supergene minerals mentioned above. Joints and fractures which host iron oxides may be related to Tertiary extension associated with Basin and Range faulting.

The paragenetic sequence for the lower skarn is summarized in Figure 29. Early prograde skarn is characterized by replacement of carbonate by andraditic garnet and

Figure 27. Photomicrograph of deformed molybdenite, lower skarn (reflected light, field of view is 2.5 mm long).

Figure 27.

Figure 28. Photomicrographs of lower skarn quartz veins (crossed polarizers). (a) Strained extinction in quartz indicates post-skarn deformation (field of view is 1.2 mm long). (b) Undeformed quartz vein with associated sericite indicates hydrothermal activity came after skarn mineralization and deformation (field of view is 2.5 mm long).

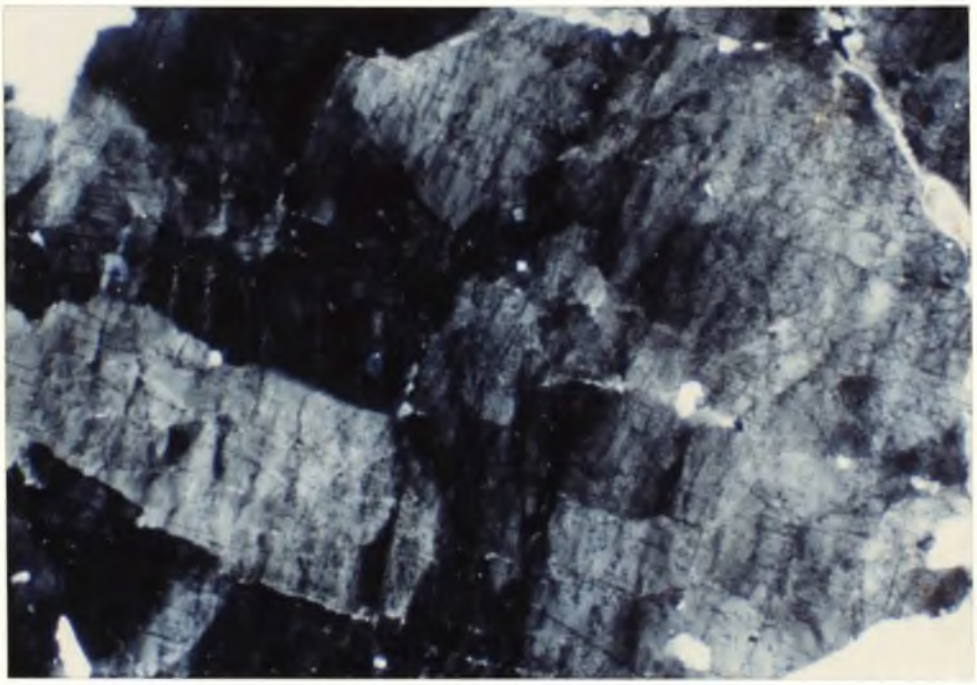

Figure 28a.

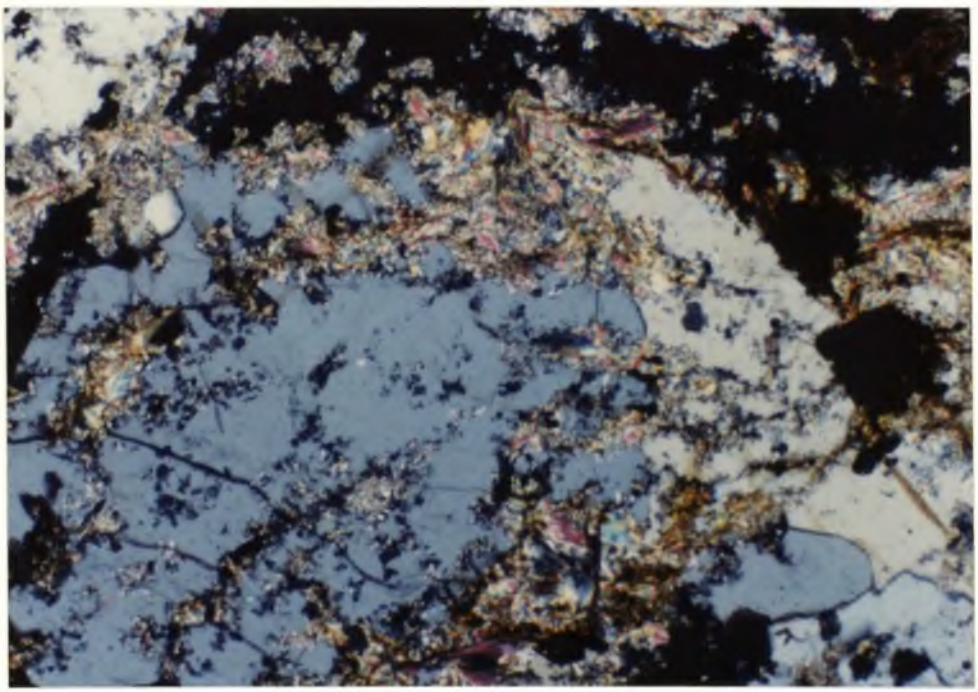

Figure 28b.

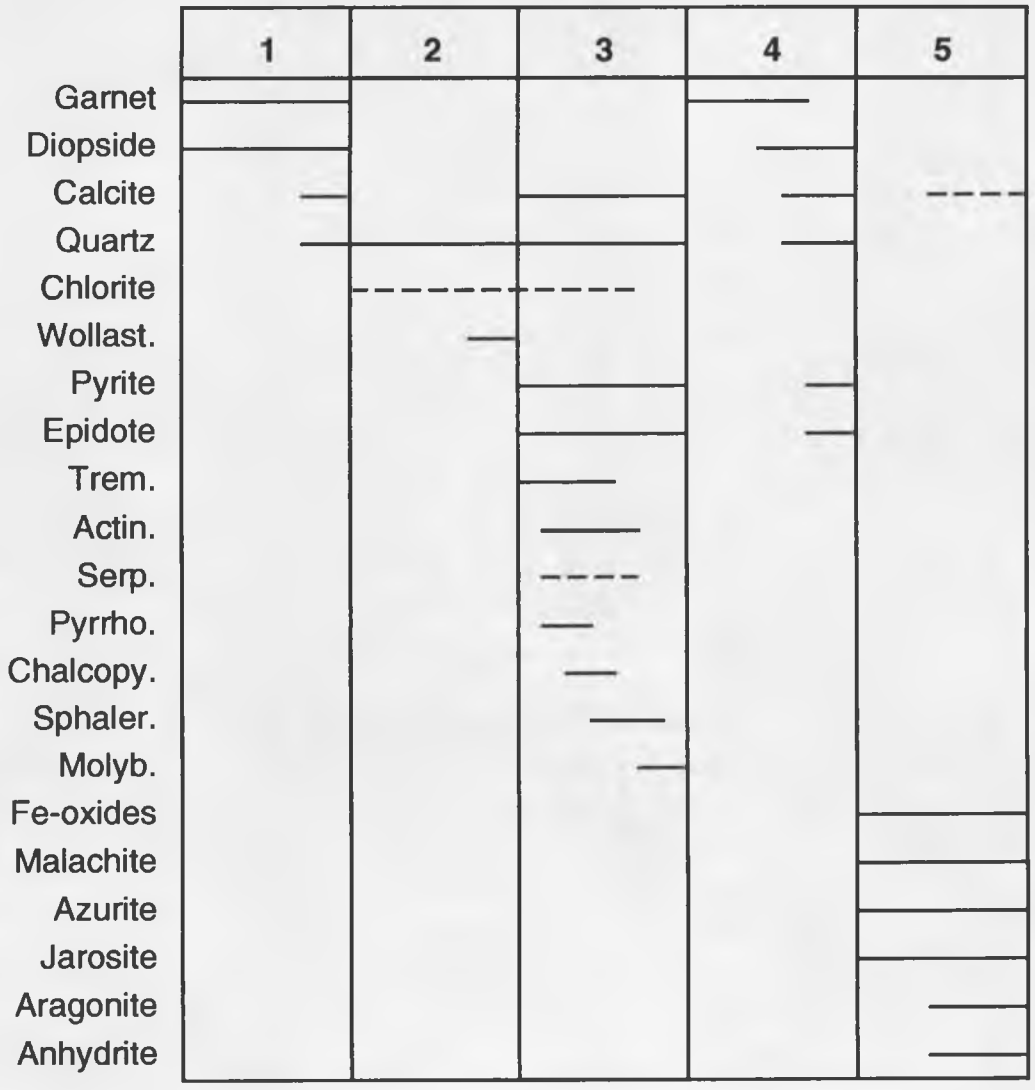

Figure 29. Paragenesis of the lower skarn unit at Gold Acres.

diopsidic pyroxene with interstitial calcite and quartz. An early quartz vein stage followed the prograde stage. Retrograde alteration of the skarn comprised quartz-calcite-pyrite veins and concurrent tremolite, actinolite, epidote, chlorite, and locally significant serpentine. Sulfide minerals (in the sequence po -> py/ccp/sph -> mo) were introduced during retrograde alteration. A deformational event followed the anhydrous skarn mineralization. Evidence for post-deformational hydrothermal activity was observed. Garnet and pyroxene veins cutting the hydrous skarn indicate a late skarn stage, which may have been a precursor to the quartz-sericite veins. Supergene processes produced the latest stage comprising oxide minerals.

IMBRICATE THRUST ZONE

The imbricate thrust zone (ITZ) is of special interest because it hosts the refractory gold mineralization. The objectives of this study did not include gold occurrence, but a summary of the mineralogy and textures observed in the ITZ is relevant to the overall paragenetic history at Gold Acres. The unusual position of the ITZ between the two skarn units makes the origins of the skarns and any relationship between them difficult to determine. Macroscopically, the calcareous rocks in the ITZ are composed almost entirely of calcite and quartz with carbonaceous matter, disseminated pyrite, and minor iron-oxides. Carbonaceous matter occurs within the sheared rock and along fracture surfaces, hence the sooty, black color throughout most of the ITZ (Fig. 30a). Shearing and deformation in the ITZ is extreme. The scale of shearing in the ITZ ranges from microscopic, as displayed by mylonitic fabric in thin section (Fig. 30b), to thrust slices tens of meters long (Figure 30a). Individual slices in the imbricate structure are variably altered. Most slices are silicified Srm (Hays and Foo, 1991), but a few pods of chert from the Roberts Mountains allochthon and slices of adjacent skarn are present in the ITZ. Some limestone slices are relatively

Figure 30. Macroscopic and microscopic textures in the imbricate thrust zone (ITZ). (a) Southwest highwall of Gold Acres pit showing exposure of ITZ (catch benches are 60 feet high). (b) Mylonitic fabric of ITZ in thin section (crossed polars, field of view is 2.5 mm long).

Figure 30a.

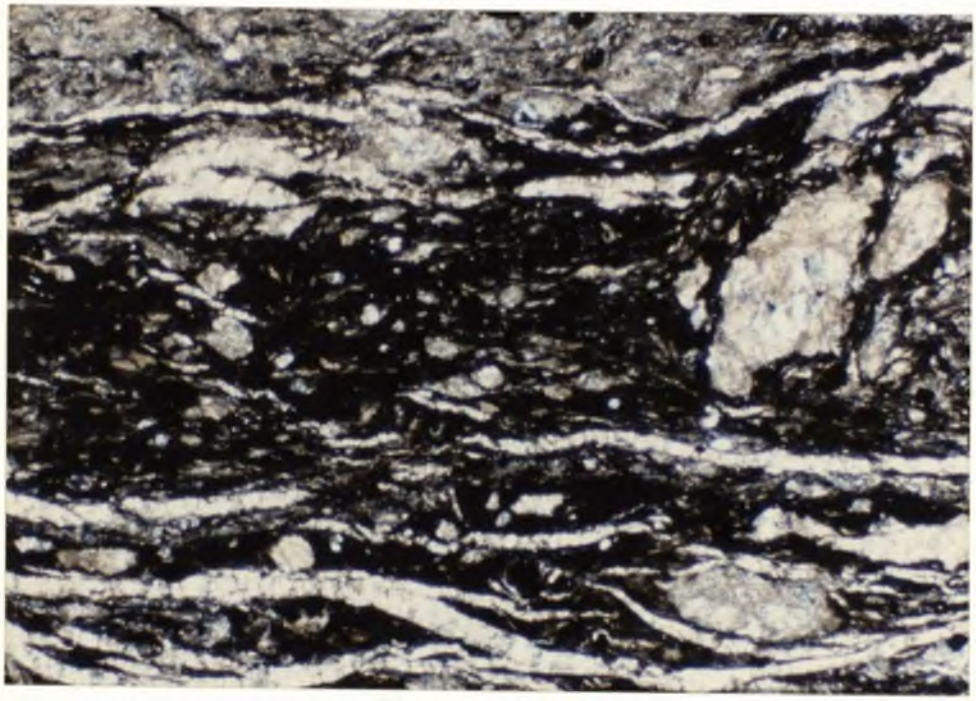

Figure 30b.

fresh, with little alteration, whereas others are almost completely replaced by silica. Degree of silicification varies from moderate to intense throughout the ITZ. Disseminated pyrite is commonly associated with silicification.

Calcite and quartz in the ITZ are very fine-grained, averaging 0.05 mm but ranging up to 0.2 mm. Calcite is generally more abundant than quartz, though relative amounts vary with degree of silicification. Petrographic textures show calcite is replaced by quartz. Increased replacement of calcite by quartz is accompanied by increase in disseminated pyrite and quartz veins. The size range of pyrite is 0.04 - 2.5 mm. Secondary growth of pyrite during silicification of calcite is inferred. Except for slices of skarn which were mechanically incorporated into the ITZ near the contacts with adjacent skarn units, no evidence of calc-silicate or skarn-related sulfide mineralization was seen in the ITZ.

The mylonitic fabric characteristic of the ITZ rocks was caused by low-angle shearing related to the emplacement of the ITZ against the skarn units. A vein of pyrite with quartz and magnetite experienced shortening and compression during the deformation (Fig. 31), suggesting that shearing in the ITZ represents thrusting and not a detachment. Interleaving of small (tens of centimeters thick) skarn slices near the ITZ contacts with upper and lower skarns was observed in drill core. This indicates that thrusting post-dates skarn mineralization. Silicification was probably controlled by enhanced permeability of the ITZ following compressional deformation. Late calcite veins with pyrite cut the sheared and silicified textures of the ITZ. This last stage was accompanied by patches of intense calcite recrystallization.

The paragenesis of the ITZ is summarized in Figure 32. The host rock was Srm. An early pyrite stage preceded imbricate thrusting. Silicification with disseminated pyrite followed deformation. Late calcite-pyrite veins cut deformational textures and silicification. Gold was probably introduced during one of the latter two events.

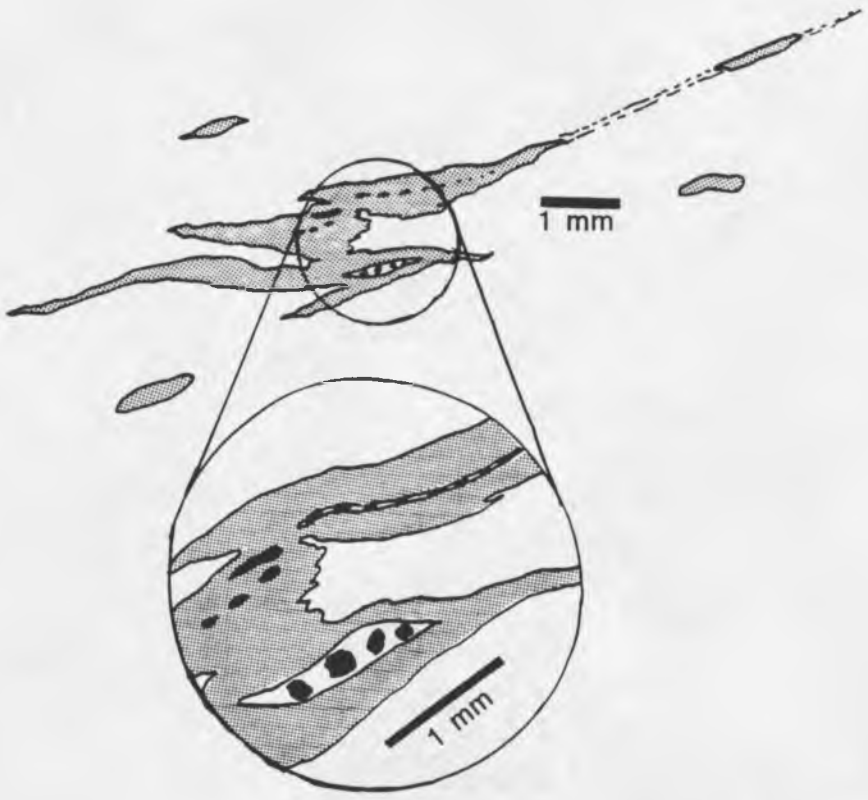

Figure 31. Compressional deformation of a pyrite vein in the ITZ. Note the extreme shortening of the pyrite (shaded). Hematite (black) and quartz (white) are associated with this pre-deformation pyrite stage.

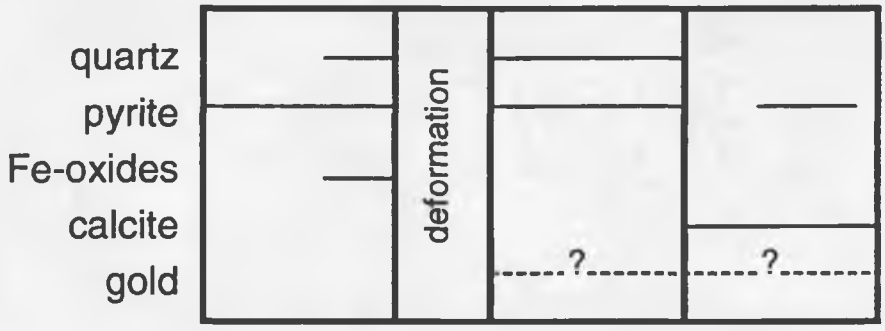

Figure 32. Paragenesis in the imbricate thrust zone (ITZ). Gold mineralization is probably associated with pyrite of one of the latter two stages.

UPPER SKARN

The upper skarn differs in appearance, occurrence, and composition from the lower skarn. The upper skarn is thought to have altered from Dw, which is less silty and dolomitic than the Srm host of the lower skarn mineralization. Mineral assemblages and geochemical signatures of the lower and upper skarns suggest they are part of one zonation pattern related to the stock. Thus, variation in protolith composition as well as relative distance from the stock may account for the mineralogic and geochemical differences between the upper and lower skarns.

The lower contact of the upper skarn with the ITZ is distinct (Fig. 30a). The upper skarn is intensely argillized and bleached, so it appears nearly white, in sharp contrast to the black carbonaceous ITZ. Alteration in the upper skarn is more intense than in the lower skarn. Major minerals are quartz, calcite, tremolite, diopside, clays, and chlorite, with very minor garnet and epidote. Sulfide minerals include pyrite, sphalerite, chalcopyrite, and galena, with minor pyrrhotite and arsenopyrite.

The occurrence of highly altered igneous minerals in the upper skarn near the contact with the ITZ provides evidence for the felsic sill reported by Ketner (1965) and Silberman and McKee (1971) but contested by mine geologists. The intense alteration of the felsic sill makes it difficult to distinguish macroscopically from the upper skarn mineralization. The sill apparently contributed to the alteration of the upper skarn and obscured much of the early texture. Altered K-feldspar (Fig. 33a) and muscovite from biotite (Fig. 33b) indicate the composition of the sill was comparable to that of the Gold Acres stock. Other alteration products (sericite, leucoxene after sphene) and associated textures are also reminiscent of the altered upper part of the Gold Acres stock. Similar compositions indicate the sill is a late intrusive related to the stock. Secondary sericite from the sill was dated at 94.3±1.9 Ma (Silberman and McKee, 1971), about the same age as secondary sericite from the Gold Acres stock (92.8±1.9 Ma).

Figure 33. Photomicrographs of the highly altered felsic sill in the upper skarn. (a) Sericitic alteration of orthoclase (crossed polars, field of view is 2.5 mm long). (b) Biotite replaced by muscovite and opaque minerals (plane light, field of view is 2.5 mm long).

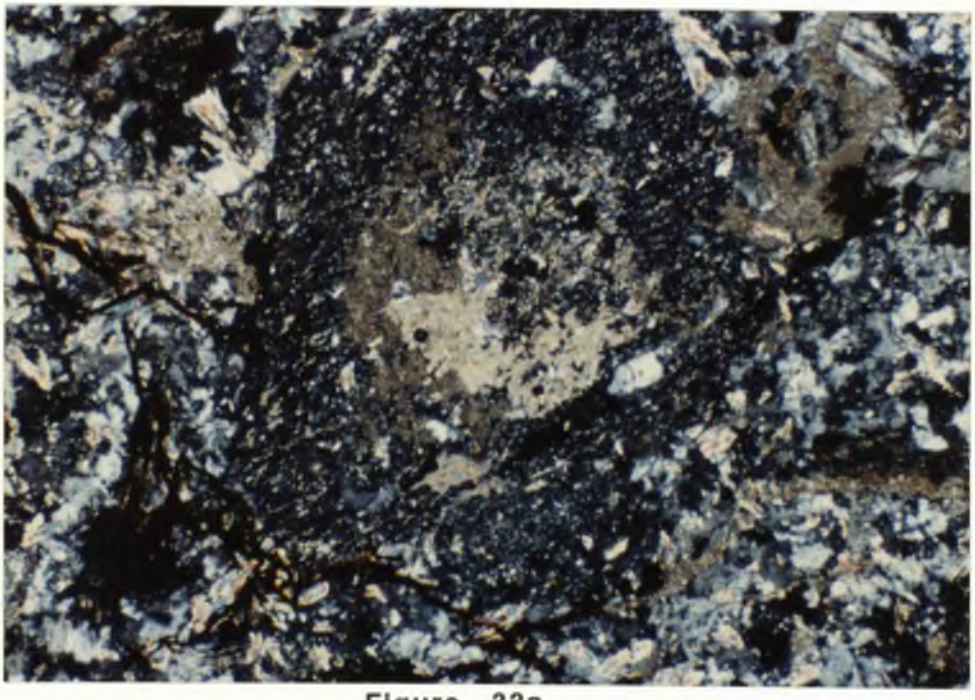

Figure 33a.

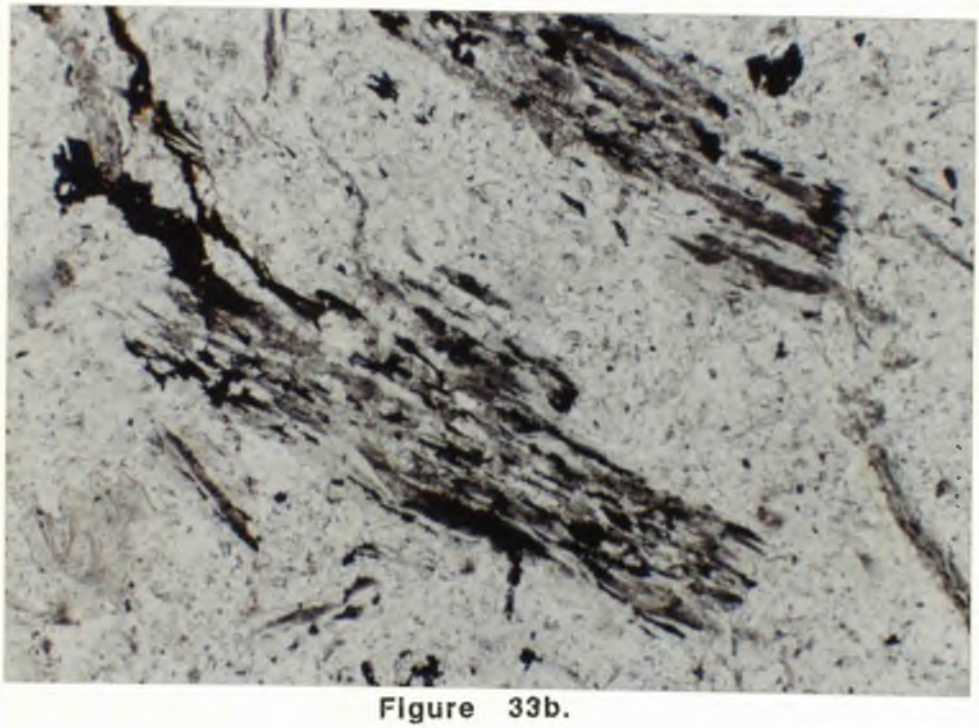

Figure 33b.

The upper skarn contains fewer anhydrous calc-silicate phases and more quartz and calcite than the lower skarn. Very little garnet was observed in the upper skarn, although some quartz and calcite appears pseudomorphous after garnet. Diopside is not abundant, less than 15%. Where present, diopside rims are altered to tremolite. Other regions show replacement of diopside by calcite and quartz (Fig. 34). Tremolite is abundant (20-40%), but its rims are altered as well. Some tremolite appears to be altered to a clay mineral, and some is partly replaced by silica. Silica has flooded the upper skarn such that parts of the unit are up to 80% silicified. Chalcedonic quartz is common in veins and as pervasive alteration (Fig. 34). Sulfide minerals occur as disseminations, veins, and massive replacement pods up to 30 cm across. Pyrite in the upper skarn has a tarnished appearance. Other minerals observed in the upper skarn are Fe- and Cu-oxides, presumably products of oxidation in a supergene environment.

Electron microprobe data on pyroxene compositions of the upper skarn are summarized in Fig. 19. Upper skarn pyroxenes are on the Mg-rich side of the diopside-hedenbergite solid solution series, ranging from Di_{86} to Di_{62}. Upper skarn pyroxenes are less enriched in Mg^{2+} relative to the lower skarn pyroxenes. This may reflect the lower abundance of dolomite in the Wenban limestone protolith. Spessartine enrichment is a function of Fe^{2+} content, ranging from 0.4% in the more Mg^{2+}-enriched pyroxenes to 8.5% in the Fe^{2+}-enriched pyroxenes. The observed range of pyroxene compositions in the upper skarn at Gold Acres falls within the field typically displayed by pyroxenes in Cu-skarns (Einaudi, 1981; Einaudi and Burt, 1982). Mn-enrichment in the upper skarn pyroxenes is more pronounced than in the lower skarn pyroxenes. Distal enrichment of Mn is commonly observed in pyroxenes related to Cu-porphyry systems.

Upper skarn paragenesis is obscured by intense alteration. Early diopside is followed by quartz, calcite, and sulfide minerals with successive tremolite, chlorite, and clays. The felsic sill contributed to the alteration of the upper skarn.

Figure 34. Replacement of upper skarn diopside by (a) quartz and (b) calcite (crossed polars, field of view is 2.5 mm long).

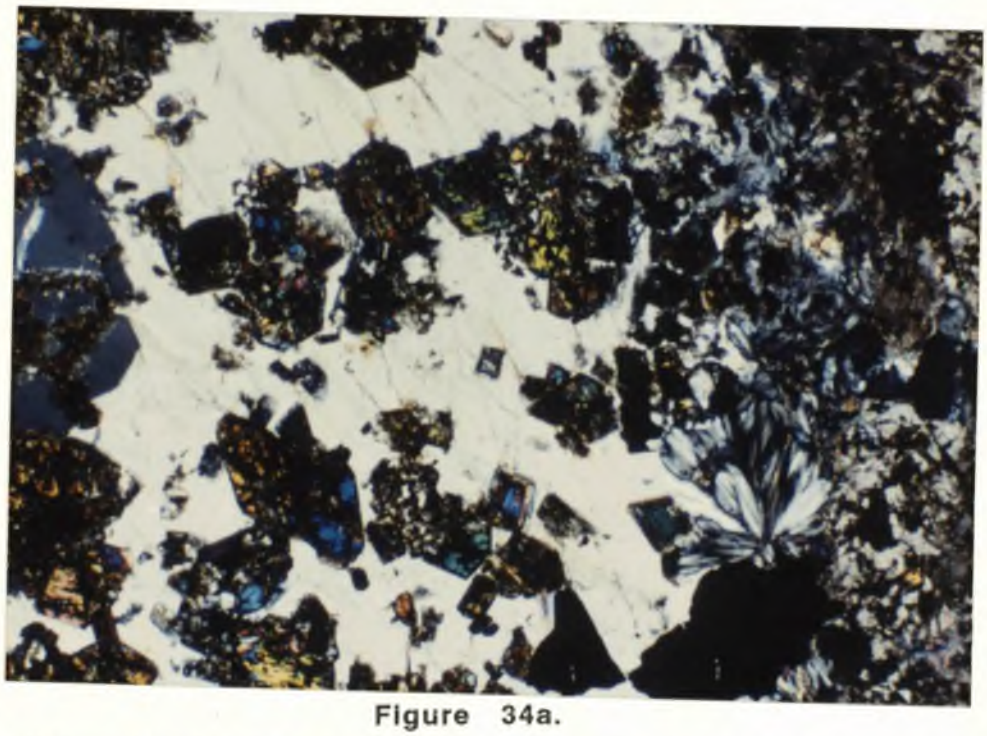

Figure 34a.

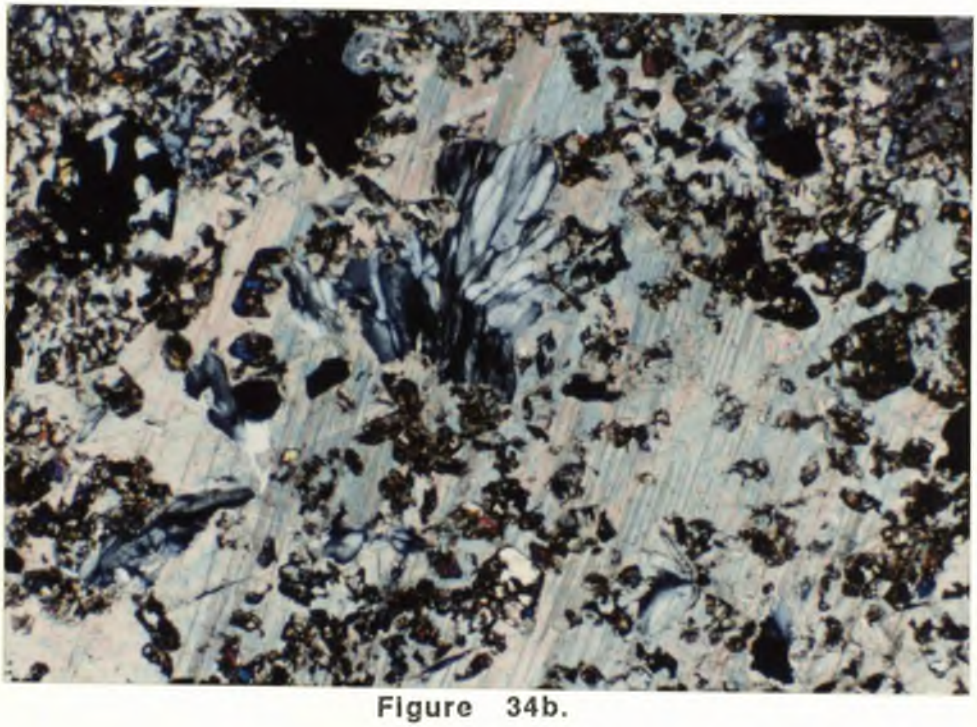

Figure 34b.

DISTAL CALC-SILICATE ALTERATION

Thermal alteration forms a diffuse halo around the Gold Acres mine. Siliceous rocks of the Roberts Mountains allochthon have been heated to hornfels in the area around the pit, and are now bleached and oxidized. Thermal alteration of the carbonate units consists of marble and recrystallized limestone, with accessory mineralization of one or more of tremolite, clinochlore, and scapolite (Fig. 6). Two isolated skarn bodies exist outside the Gold Acres pit. Both are to the east of the pit and are exposed at the surface (Fig. 3). Neither of these separate skarns are known to be associated with gold mineralization, and both appear to be structurally controlled by northwest-trending faults.

Bedrock in the area southeast, east, and northeast of the Gold Acres pits comprises recrystallized Wenban limestone (Dw) with small clusters of a white, radiating, needle-like mineral, identified in the field as tremolite. Hand specimens of the marbleized limestone also contain scapolite and clinochlore, which were identified by X-ray diffraction (John McCormack, personal communication,1990). Tremolite is much more abundant than clinochlore, which is more abundant than scapolite. The marble occurs peripheral to the Gold Acres skarn deposits where the lower plate of the Roberts Mountains Thrust is exposed. The marble grades laterally away from the skarns into unaltered Wenban limestone.

Petrographic study of the altered limestone confirms the recrystallized nature of the calcite which makes up the bulk of the rock (90-95%). The degree of calc-silicate alteration varies. Diopside and garnet are not common. The abundance and alteration of tremolite varies widely.

One thin section contained unaltered needle-shaped tremolite crystals (Fig. 35a), but destruction of tremolite is more commonly observed (Fig. 35b). Quartz has replaced ≈2-3% of the calcite in the marble matrix. Quartz also occurs in veinlets

Figure 35. Distal calc-silicate alteration in Wenban limestone (crossed polars, field of view is 2.5 mm long). (a) Fresh tremolite in marbleized limestone. (b) Altered tremolitic marble.

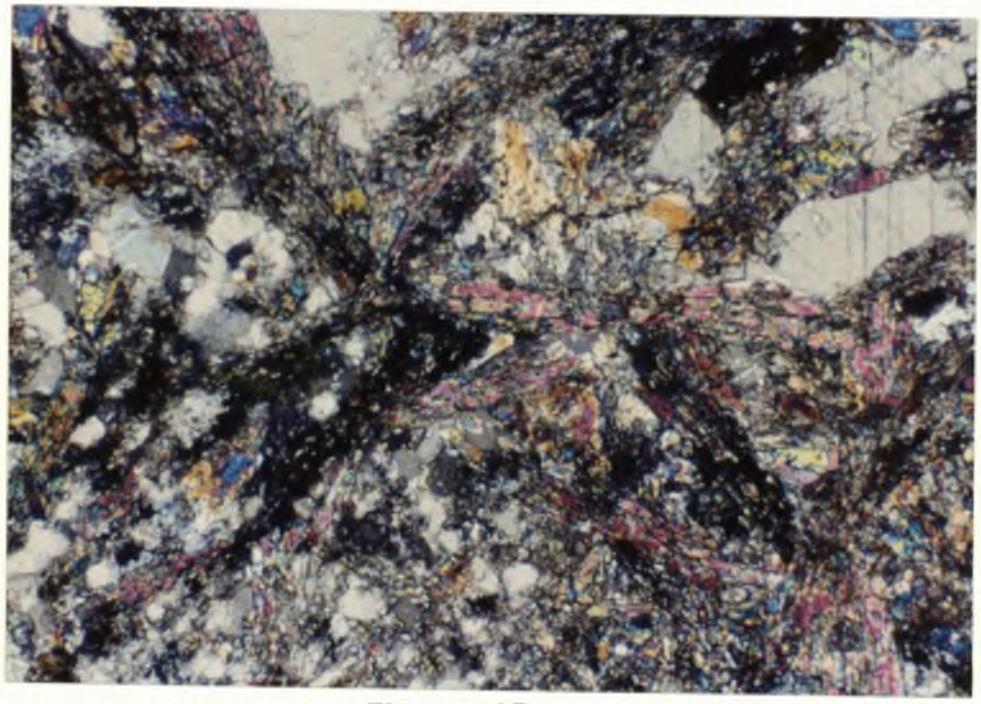

Figure 35a.

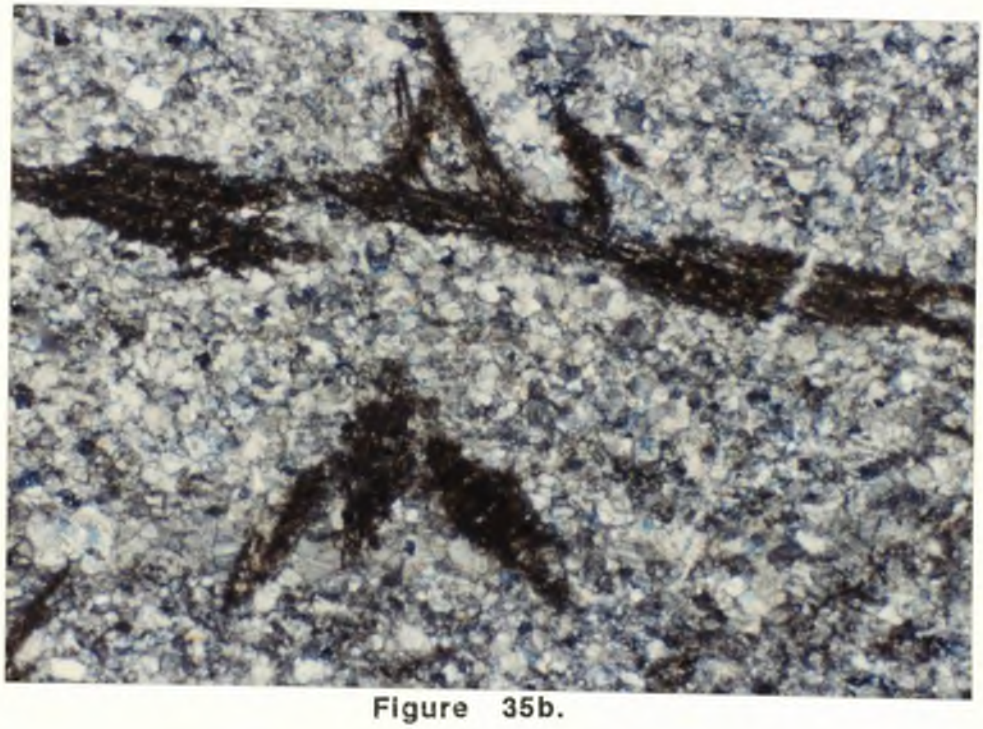

Figure 35b.

cutting the marble and tremolite needles. Pyrite and epidote are present in trace amounts associated with the tremolite needles, and in part replacing tremolite. Late-stage calcite veins also cut tremolite. Elsewhere, tremolite (with pyroxene) is altered to a cloudy brown material which retains the acicular habit of tremolite (Fig. 35b). Replacement of the recrystallized calcite matrix by quartz is slightly more extensive (5%). Quartz has also replaced some of the tremolite. Late-stage calcite veining is more abundant.

In one thin section, calc-silicate alteration of the limestone was slightly more advanced. Recrystallized calcite was 25% replaced by quartz and 4% replaced by garnet with inclusions of epidote. The relict tremolite needles were 80% replaced by quartz, garnet, epidote, and pyrite. A few diopside crystals are also present, showing alteration to quartz and garnet. Even the calcite veinlets are replaced by quartz and garnet. A second stage of calc-silicate mineralization, probably correlative with the later calc-silicate stage of the lower skarn, apparently affected the distal carbonates as well.

The altered limestone of the Billies area represents calc-silicate alteration peripheral to the skarns developed within the Gold Acres pits. The first stage of alteration consisted of recrystallization of the calcite and growth of diopside, tremolite, clinochlore, and scapolite. The second stage involved the breakdown of the tremolite and other calc-silicates accompanied by calcite veinlets and slightly increased silica replacement. The third stage consists of late anhydrous calc-silicate minerals. The paragenesis of calc-silicate mineralization peripheral to the Gold Acres skarns is summarized in Fig. 36.

East of the Gold Acres mine is a small isolated garnetite occurrence within the Wenban limestone which is fault-controlled (Figure 5). It is not known to be associated with gold mineralization. The calc-silicate minerals include quartz, garnet, diopside, tremolite/actinolite, and chlorite. In one section calcite was completely replaced by

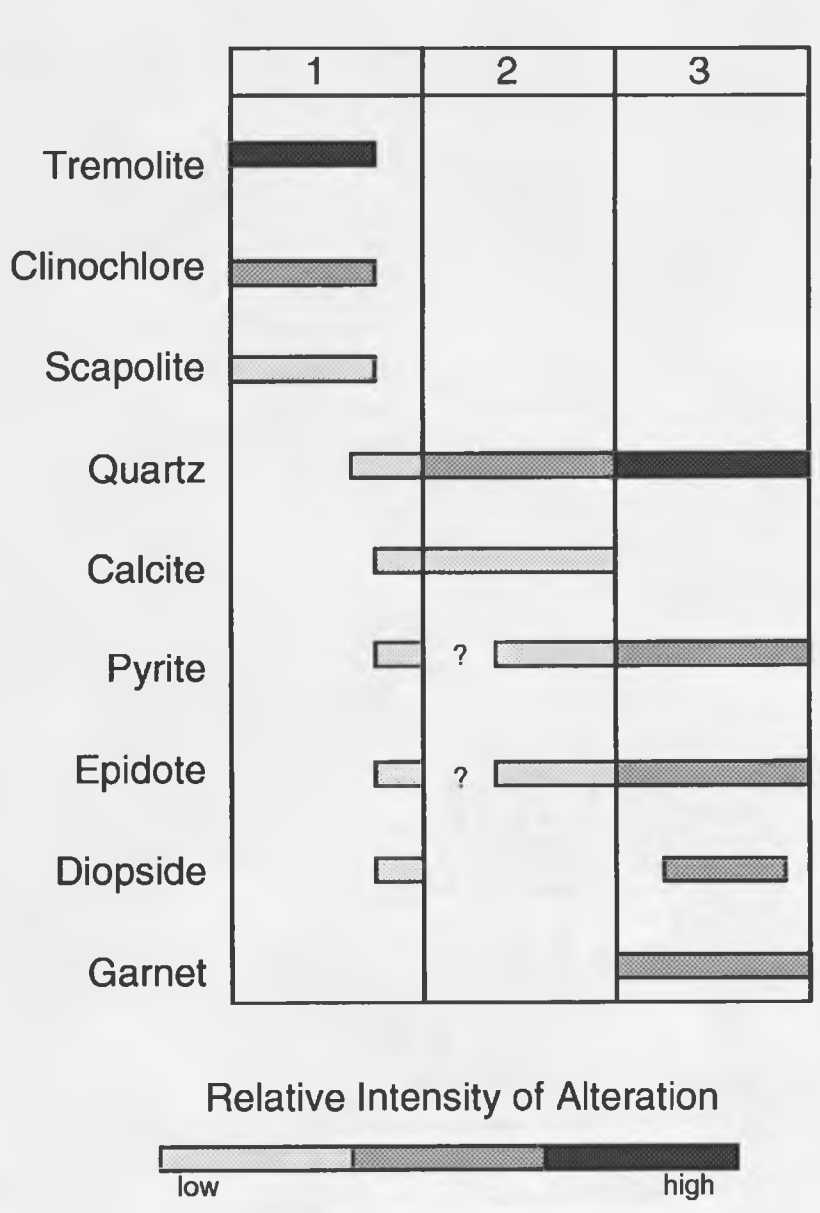

Figure 36. Paragenesis of limestone distal to the Gold Acres mine.

coarse polycrystalline quartz and garnet, with small needles of tremolite/actinolite and diopside. Calcite occurred only as small late-stage veinlets, which were partly replaced by quartz. Tremolite and diopside crystals displayed dog-toothed terminations, indicating incipient resorption by silica. The garnetite consists of brown euhedral andradite crystals (90%), with interstices filled by calcite (3-4%) and quartz (1-2%). The garnets exhibit anisotropy, zoning, and abundant fractures (Fig. 37). The garnet is similar to the late garnet veins described in the lower skarn. The garnets are partially altered by chlorite, biotite, and iron oxides (hematite). The garnets also enclose and partially dissolve prismatic diopside , which is also partly replaced by biotite/chlorite. Late-stage veinlets of calcite and quartz are common. Traces of oxidized pyrite are associated with the calcite veinlets. The abundance of quartz and coarse-grained garnet suggests intense but localized hydrothermal activity along the northwest-trending structure. The hydrothermal fluids were high in silica, low in sulfur, and included Mg and Fe. Calcite was completely replaced by quartz and calc-silicate minerals.

Large quartz veins (up to 20 cm wide) were mapped in the vicinity of the isolated skarn (Figure 5). Green-blue copper stains (malachite and chrysocolla) are present in the quartz veins. Residual fluids rich in silica with copper flooded fractures in the area during the final stages of alteration. Formation of this skarn body may be correlative to the late calc-silicate mineralization described for the peripheral altered limestone and the lower skarn.

TRACE ELEMENT GEOCHEMISTRY

Geochemical analysis for trace elements is a useful way to characterize rock chemistry. Often, economic grades of a desirable metal are accompanied by anomalous values of other metals or elements (geochemical indicators). A typical indicator suite

Figure 37. Banded, zoned garnet from isolated skarn occurrence east of the Gold Acres mine (crossed polars, field of view is 2.5 mm long).

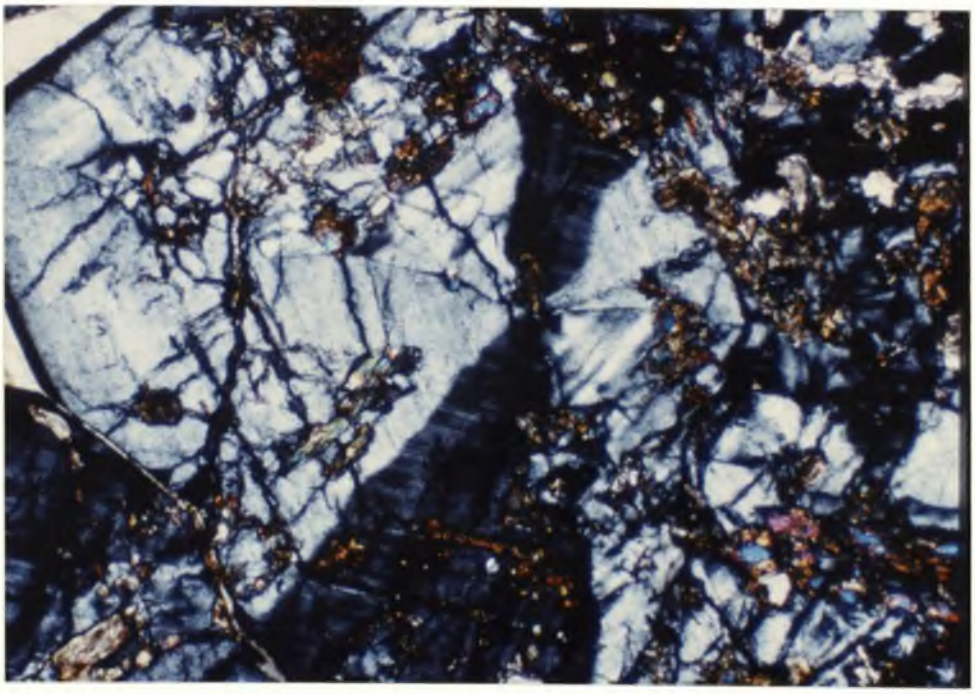

Figure 37.

for disseminated gold deposits in Nevada includes As, Sb, Hg, Tl, and sometimes Bi. Common associations among base metals are Pb-Zn (Ag, Cu) and Cu-Mo-W. Two rotary drill holes at Gold Acres were analyzed for trace element concentrations (89916 and 90816 on Figure 38). Hand samples collected from the Gold Acres pits and vicinity were also analyzed. The Gold Acres rocks were analyzed for As, Sb, Hg, Tl, Bi, Ag, Pb, Zn, Mo, Cu, W, Mn, and Fe. Accuracy was checked by including a standard after every 36 samples. Results of trace element analyses are tabulated in Appendix B. Where trace elements are stated in the summary paragraphs below, they represent typical values. The few very high values, which skew the mean values in the tables, were ignored for the purposes of characterizing the trace element signatures of the different rock units at Gold Acres.

The Gold Acres stock contains relatively high concentrations of molybdenum (average 70 ppm) and moderate copper (average 50 ppm). Concentrations of Pb (12 ppm), Zn (68 ppm), Ag (0.16 ppm), and the gold suite (As, Sb, Hg, Tl, Bi: <5 ppm) were low in the stock relative to the other lithologic units at the Gold Acres mine.

The lower skarn has high abundances of molybdenum and copper relative to other Gold Acres units (average >200 ppm each). Tungsten and manganese are correlated with the occurrence of Mo. Moderate concentration of silver (0.9 ppm) was also seen in the lower skarn. Relatively low concentrations of Pb (<30 ppm), Zn (250 ppm) and the gold suite (As≤200 ppm, Sb≤10 ppm, Hg≤400 ppm, Tl≤2 ppm, and Bi≤10 ppm) are characteristic of the lower skarn.

Significant gold grades were not encountered in the two drillholes analyzed, but the ITZ still contained the highest concentration of elements in the gold suite (As=800 ppm, Sb≤20 ppm, Hg≤8500 ppm, Tl≤4 ppm, and Bi≤9 ppm). The ITZ contained low values for Mo (<15 ppm) and Cu (<100 ppm) and moderate values for Zn (≤1850 ppm) and Pb (≤100 ppm).

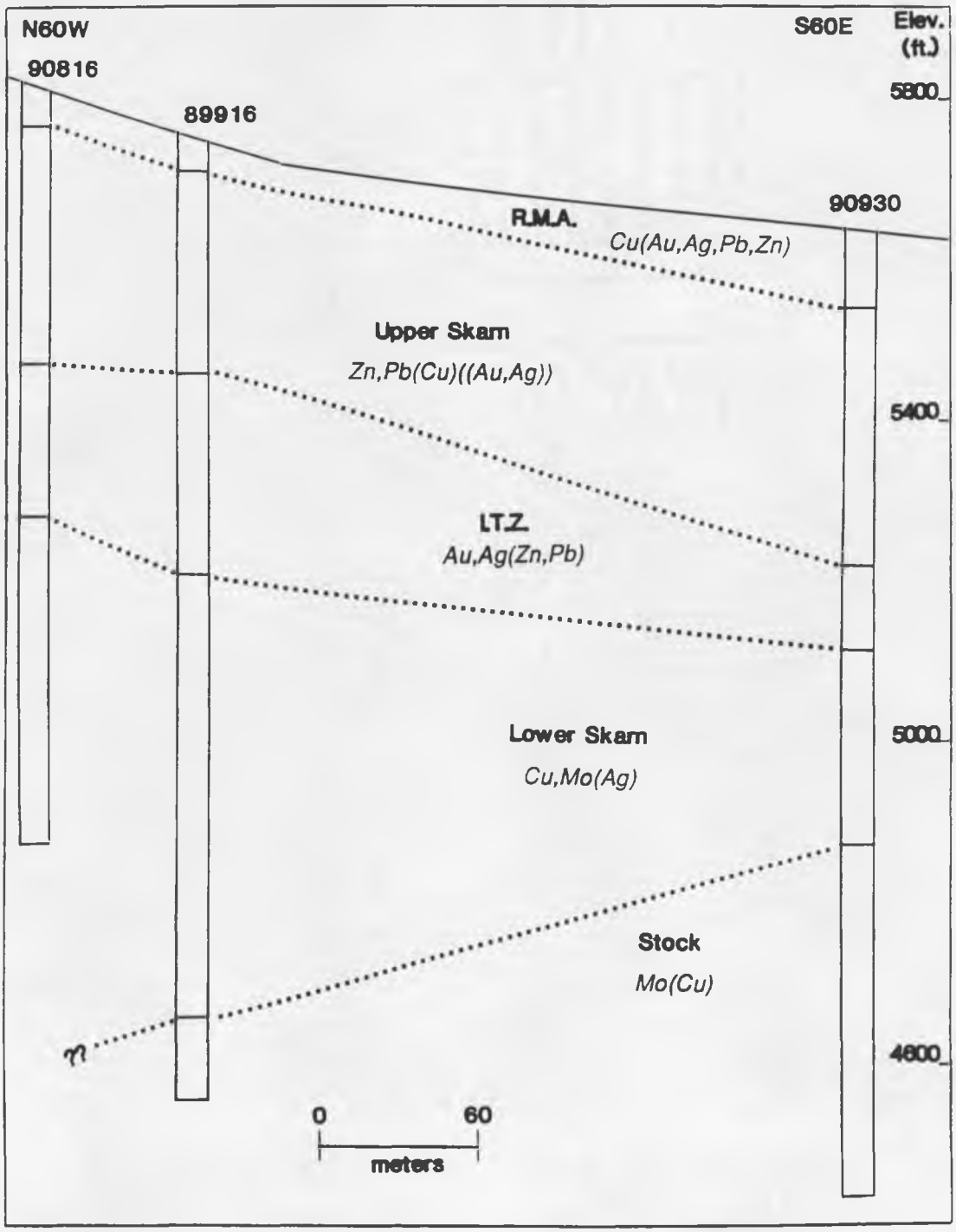

Figure 38. Cross-section of geology and trace-element geochemistry from drillholes. The location of the cross-section is shown on Figure 8.

The upper skarn contained the highest values of lead and zinc (>100 ppm and >4000 ppm, respectively) compared to the other rock units. Moderately anomalous values for Cu (<200 ppm) and some of the elements in the gold suite (Hg >1000 ppm, and As >200 ppm) were observed in the upper skarn. Values for Sb, Tl, and Bi were low (<12 ppm), while values for Mo (<10 ppm) and W were very low in the upper skarn.

In the RMA, copper was the only element with unusual concentration (>300 ppm). Moderate concentrations of Pb, Zn, Ag, (<50, <700, and <1 ppm, respectively) and elements in the gold suite (As≤200 ppm, Sb≤10 ppm, Hg≤200 ppm, Bi≤5 ppm) were detected. Values of Mo (<10 ppm), W, and Hg (<200 ppm) within the RMA were low. The anomalous copper is consistent with field observations. Numerous turquoise prospects with associated chrysocolla, malachite, and azurite exist in the RMA southwest and west of Gold Acres. The copper mineralization is probably related to the late-stage quartz veins with blue copper staining mapped near the isolated skarn occurrences east of the Gold Acres pits (Fig 5). The anomalous values for the gold suite in the RMA probably result from hydrothermal activity associated with the RMT. Trace element geochemical signature of the siliceous RMA is very similar to that of the upper skarn. The major difference geochemically is that the RMA contains high Cu values and moderate Pb-Zn values, whereas the upper skarn has high Pb-Zn values and moderate Cu.

The trace element geochemistry and zonation of rock units at Gold Acres is summarized in Figures 38 and 39. Certain elements are grouped together according to their occurrence and behavior associated with the different rock units. In general, the stock and skarns are enriched in base metals, and the ITZ is enriched in gold and its associated elements. The observed pattern of proximal Cu-Mo and distal Zn-Pb is also reported for Bingham, Utah (Atkinson and Einaudi, 1976) and Copper Canyon, Nevada (Wotruba and others, 1988). The presence of Pb and Zn in the ITZ and Roberts Mountains allochthon may represent "leakage" from the upper skarn.

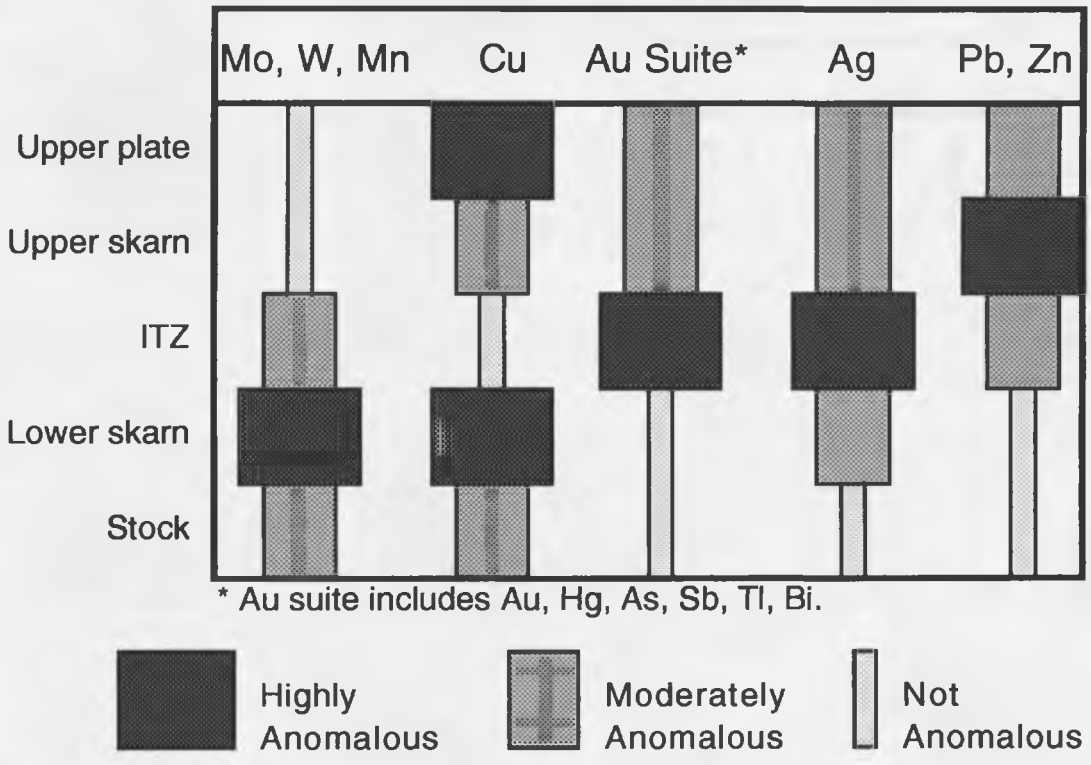

Figure 39. Summary of trace element geochemistry in Gold Acres rock units.

Elements in the gold suite are dominantly in the ITZ, but are also present in relatively high concentration in the upper skarn and RMA. The RMT and the NE-tending normal faults are also mineralized with respect to gold. Auriferous hydrothermal fluids were apparently guided by higher permeabilities in the normal faults and thrusts (ITZ and RMT). The distribution of silver in the Gold Acres rock units correlates best with elements of the gold suite. Possible remobilization from the ITZ may account for silver in the lower skarn.

Variations in metal ratios can also be correlated to a metal zoning pattern from the stock upward to the RMA. The trends in base metal ratios are interrupted by the unusual non-skarn geochemical signature of the ITZ. For the sequence of stock, lower skarn, ITZ, and upper skarn, ratios of Cu:Mo and Zn:Pb increased with distance from the

stock, while Ag:Pb, Ag:Au, and Fe:Cu decreased with distance from the stock. Comparing only the lower and upper skarns, there is a distal increase in Pb:Cu and Au:Cu and a distal decrease in Pb:Zn. Except for the ITZ's anomalous gold suite, the zonation of metal ratios observed for Gold Acres is comparable to other porphyry copper and copper skarn systems (Bingham, Atkinson and Einaudi, 1976; Twin Buttes, Einaudi, 1982).

FLUORESCENCE STUDY

A search for fluorescent minerals in the rocks at Gold Acres brought surprising results. Hand samples and drill cores were illuminated by ultraviolet light to test for fluorescence. The most common fluorescent effect observed was a red-orange glow in calcite. Other types of fluorescence observed included bright blue-white flecks of scheelite, orange-yellow calcite, red-orange quartz, and lime-yellow quartz and calcite.

Red-orange fluorescing calcite is observed in all rock types at Gold Acres, but is most abundant in the skarn units. It commonly occurs as wisps in the central part of quartz-pyrite veins, or constituting late-stage veinlets. In a few veins, fluorescent calcite was followed by a later stage of quartz or non-fluorescent calcite. The red-orange fluorescence of calcite at Franklin, New Jersey, is attributed to the presence of manganese (Klein and Hurlbut, 1985).

Bright blue-white fluorescent flecks of scheelite were also detected by black light. Substitution of Mo for W in scheelite ($CaWO_4$) is thought to account for the pale blue fluorescence (Klein and Hurlbut, 1985). Powellite ($CaMoO_4$) is reported to have a creamy yellow-white fluorescent effect, caused by further substitution of Mo for W, but such was not observed in the Gold Acres rocks. As expected, scheelite was most abundant in the lower skarn, although occurrences in the stock, upper skarn, and distal skarn were also observed. Impurities observed by fluorescent minerals are consistent with trace element geochemical analyses.

DISCUSSION AND CONCLUSIONS

The relative timing of several paragenetic events are critical to unraveling the tectonic and metallogenic history at Gold Acres: (1) high-angle normal faulting, (2) intrusion of the Gold Acres stock, (3) emplacement of the proposed felsic sill, (4) calc-silicate alteration of the lower skarn, (5) calc-silicate alteration of the upper skarn, (6) low-angle faulting which produced the ITZ, and (7) gold deposition in the ITZ.

The relative timing of high-angle faulting is the easiest to establish. The normal faults cut all the units in the Gold Acres mine, but are not cross-cut by other structures in the mine. Therefore, normal faulting was the latest significant structural event to occur at Gold Acres. The normal faults may correlate with Basin and Range extension, but they are probably earlier than the modern range-bounding faults.

The minimum age for the Gold Acres stock is mid-Cretaceous (98.8±2 Ma, Silberman and McKee, 1971). Sericite alteration in the stock (92.8±1.9 Ma) is contemporaneous with sericite alteration in the proposed felsic sill within the upper skarn unit (94.3±1.9 Ma), suggesting the stock and sill formed at the same time. The similarity in composition between the stock and sill further supports their contemporaneity and consanguinity.

Mineralogic and metallogenic zonation observed within the Gold Acres mine indicates the lower skarn is a proximal assemblage and the upper skarn is the distal correlative associated with the same thermal center. Thus the upper and lower skarns are genetically related to one system generated by the Gold Acres stock. Intrusion of the stock and the proposed sill and resultant alteration of the lower skarn and upper skarn are essentially contemporaneous. If the proposed sill is a small localized feature which does not occur throughout the upper skarn, the distribution of the upper skarn may represent a lateral spread of skarn-forming solutions in the carbonates below the RMA.

The disruption of the skarn zonation by the ITZ indicates deformation and thrusting post-dates skarn formation. Textural evidence from the lower skarn also indicates post-mineral deformation. However, the most compelling evidence for post-skarn deformation in the ITZ is the mechanical incorporation of small slices of skarn into the ITZ near its contacts with adjacent skarn units.

The relative timing of gold mineralization is the most ambiguous event to establish. Arehart and others (1993) describe the occurrence of gold in arsenian pyrite overgrowths on pyrite crystals at Gold Acres, but they do not state which stage of pyrite mineralization carries the gold (see Figure 32). Post-deformation paragenesis in the ITZ involves pervasive silicification with disseminated pyrite and late calcite/pyrite veining with calcite recrystallization. The enhanced permeability in the ITZ as a result of thrusting probably favored the flow of gold-bearing hydrothermal solutions, and the abundance of reduced carbon and pyrite in the ITZ may have prompted gold precipitation. In a study of Re-Os geochronometry, McCandless and others (1993) found that molybdenite from the lower skarn carried a hydrothermal overprint. Molybdenite mineralization occurred during retrograde alteration of the lower skarn, so the hydrothermal overprint post-dates skarn formation. Also, the quartz-sericite vein cutting hydrous calc-silicate mineralization of the lower skarn suggests post-skarn and post-deformation hydrothermal activity. Gold mineralization may have accompanied this hydrothermal event.

The best evidence for timing of gold is the occurrence of gold mineralization along the high-angle normal faults. The high-angle faults cut the entire section at the Gold Acres mine. Therefore, if the faults served as conduits for gold mineralizing fluids, then gold mineralization clearly post-dates both skarn formation and compressional deformation in the ITZ.

The most likely sequence of events leading to the current geologic situation at Gold Acres is summarized in Fig. 40. In the mid-Cretaceous (≈100 Ma) a granitic stock intruded into the carbonate section. Roberts Mountains Formation was altered to the assemblage seen in the lower skarn, and Wenban Limestone was altered to the assemblage of the upper skarn (Fig. 40a). Recrystallization produced a marble front between skarn and carbonate protolith. Associated with the stock is a felsic sill which intruded into the upper skarn causing further alteration in that unit (Fig. 40b). A remnant of unaltered Srm remained below the upper skarn, probably to the west. Post-mid-Cretaceous compression, probably correlative with the Late Cretaceous Central Nevada thrust belt, resulted in severe thrusting and deformation of the remnant carbonate rock and produced the ITZ (Fig. 40c). The upper skarn and altered sill were transported (eastward?) above the ITZ as imbricate thrusting occurred. The thrusting event produced the general stratigraphic sequence seen at the Gold Acres mine today. Sometime after formation of the ITZ, regional extension resulted in northeast-trending normal faults which cut the section at Gold Acres. The normal faults served as conduits for gold mineralizing fluids which flowed up the structures and out along permeable zones, mainly in the ITZ and, to a lesser extent, along the RMT (Fig 40d). Timing of normal-faulting, and therefore timing of gold mineralization, may range from Late Cretaceous to Tertiary. Tertiary volcanism and hydrothermal activity is widespread in the Gold Acres area and elsewhere in Nevada, suggesting gold mineralization at Gold Acres is tentatively Tertiary.

FURTHER WORK

Further research to solve details of the tectonic and metallogenic history at Gold Acres may be proposed. Ore microscopy, microprobe, and SEM study will provide a better understanding of how gold occurs in the ore body. Detailed mapping and structural analysis of the low-angle faults, the ITZ, and the high-angle normal faults should help

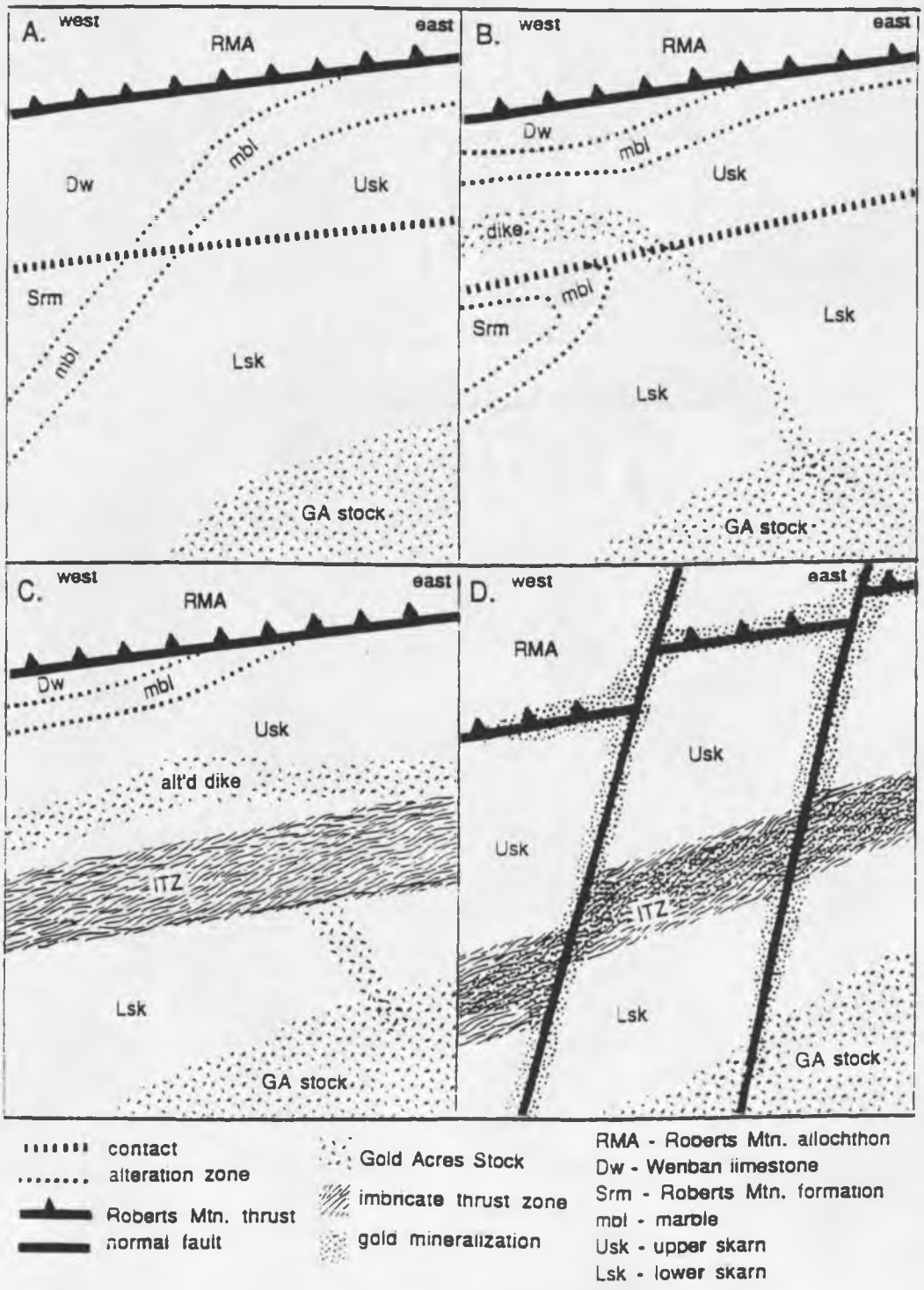

Figure 40. Schematic summary of sequence of geologic events at Gold Acres. See text for explanation.

clarify the relative timing of these events and their correlation to regional tectonics. More extensive fluid inclusion studies would help determine pressure and temperature conditions during mineralization of skarn phases and vein phases, and provide constraints on the composition of the metasomatic and hydrothermal fluids. Stable isotope studies of skarn sulfides and other calc-silicate and hydrothermal gangue minerals will help establish (or disprove) any genetic relations between the skarn units, stock, and gold ore. Further work will contribute to a better understanding of mineralization events at the Gold Acres mine and of relationships among base metal porphyries, skarns, and precious metal deposits.

APPENDIX A. MINERAL ABBREVIATIONS

Ab=albite

Act=actinolite

Ad=andradite

Amph=amphibole

An=anorthite

Antig=antigorite

Biot=biotite

Bruc=brucite

Calc=calcite

Carb=carbonaceous, carbon

Chalcopy=chalcopyrite

Chl=chlorite

Cl=clinochlore

Di=diopside

Diop=diopside

Epid=epidote

Forst=forsterite

Ga=garnet, garnetite

Gr=grossular

Hd=hedenbergite

Jo=johannsenite

Kaol=kaolinite

Mbl=marble

Molyb=molybdenite

Monti=monticellite

Musc=muscovite

Orth=orthoclase

Plag=plagioclase

Px=pyroxene

Pyrrho=pyrrhotite

Qz=quartz

Sc=scapolite

Serp=serpentine

Sk=skarn

Sp=Mn-garnet (pyralspite)

Tr=tremolite

Trem=tremolite

Woll=wollastonite

Wollast=wollastonite

Trace Element Analyses in Drillhole 89916

(ND - Not Detected)

Lith.	Footage	Ag (ppm)	As (ppm)	Au (ppm)	Cu (ppm)	Hg (ppb)	Mo (ppm)	Pb (ppm)	Sb (ppm)	Tl (ppm)	Zn (ppm)	Bi (ppm)
Upper	0-20	0.271	15.6	ND	305	0.209	8.94	28.8	ND	ND	12000	37.5
Plate	20-40	0.297	41	0.017	312	ND	6.16	51.9	ND	ND	18300	30.1
	mean	0.284	28.3	0.0085	308.5	0.1045	7.55	40.35			15150	33.8
Upper	40-60	0.192	6.03	ND	178	ND	4.46	100	ND	ND	6558	9.84
Skarn	60-80	0.251	334	0.331	218	1.59	7.16	157	5.32	ND	3160	9.98
	80 -100	0.262	65.1	0.014	163	0.135	4.13	57.4	0.913	ND	5247	22.1
	100-120	0.537	38.6	ND	131	ND	3.02	107	0.591	ND	2857	22.4
	120-140	0.563	17.9	ND	167	ND	1.33	152	ND	ND	8202	23.2
	140-160	0.224	23.2	0.001	251	ND	4.3	81.8	ND	ND	11200	9.93
	160-180	1.03	321	0.019	242	0.141	2.76	144	6.86	ND	9338	8.8
	180-200	1.15	360	0.016	219	0.335	2.77	123	7.66	ND	4626	6.9
	200-220	0.466	150	0.001	251	0.13	2.17	71	1.71	ND	2319	6.29
	220-240	0.103	141	0.008	107	0.348	0.953	32.8	3.73	ND	136	3.46
	240-260	1.19	426	0.1	120	1.2	3.88	118	15.3	1.45	244	6.82
	260-280	0.162	128	ND	89.6	2.53	5.11	69.9	2.62	1.02	78.1	1.95
	mean	0.61786	221.314	0.04083	182.8	0.66914	3.13471	91.5	5.41143	0.35286	3991.59	6.3071
I.T.Z.	280-300	5	709	0.833	68.5	2.64	4.13	145	28.4	2.08	514	6.54
	300-320	0.768	439	0.757	37.9	1.72	16.9	65.2	14.4	1.31	282	1.99
	320-340	0.287	313	0.315	51.8	1.48	14.1	50	7.13	1.48	264	2.17
	340-360	0.393	182	0.288	45.9	1.22	9.91	101	7.28	0.825	222	1.57
	360-380	0.214	107	0.321	27.4	1.12	14.6	13.5	4.05	ND	224	0.891
	380-400	0.135	128	0.019	33.6	0.706	15.5	15.9	2.86	0.636	217	1.38
	400-420	0.234	251	0.246	52.6	0.892	11.7	23.1	6.38	0.823	218	2.21
	420-440	0.996	315	0.314	65.1	1.08	11.1	21.8	11.8	ND	267	2.71
	440-460	0.8	483	0.547	81.8	2.3	5.88	21.2	17.3	1.54	932	2.8
	460-480	0.62	676	0.309	46.9	0.988	5.75	29.7	15	0.571	335	1.76
	480-500	3.12	458	0.136	67.8	1.14	7.57	192	42.3	0.578	959	5.4
	mean	1.14245	369.182	0.37136	52.6636	1.38964	10.6491	61.6727	14.2636	0.89482	403.091	2.6746

Trace Element Analyses in Drillhole 89916 (ND - Not Detected)

Lith.	Footage	Ag (ppm)	As (ppm)	Au (ppm)	Cu (ppm)	Hg (ppb)	Mo (ppm)	Pb (ppm)	Sb (ppm)	Tl (ppm)	Zn (ppm)	Bi (ppm)
Lower	500-520	0.716	51.6	0.011	56.2	0.334	7.4	69.4	5.65	ND	306	1.98
Skarn	520-540	1.09	56.2	0.015	174	0.515	18.6	115	8.35	ND	442	3.17
	540-560	1.32	72.2	0.021	240	0.79	8.22	84.5	9.7	1.13	575	5.67
	560-580	1.78	17.4	0.006	619	1.41	6.46	129	2.2	ND	1084	14.7
	580-600	2	12.1	0.001	613	1.12	19.9	31.9	1.26	ND	228	16.4
	600-620	0.997	12.6	0.01	746	0.953	23.6	23.4	1.75	ND	132	3.84
	620-640	0.594	5.65	0.003	286	0.252	41.9	7.33	0.768	ND	122	3.42
	640-660	1.16	7.8	0.008	547	0.297	26.6	13.1	0.957	ND	116	1.96
	660-680	0.604	5.77	0.006	417	0.208	50.3	15.9	0.765	ND	41.8	3.17
	680-700	0.393	3.99	0.005	325	0.169	45.7	13.6	0.695	ND	34	4.53
	700-720	0.515	3.66	0.005	602	0.713	58.9	23.4	0.764	ND	39.2	3.11
	720-740	1.74	15.1	0.009	399	0.226	73	41.6	5.05	ND	68.4	2.96
	740-760	0.513	6.16	0.004	215	ND	32.6	24.3	2.52	ND	41.3	1.78
	760-780	0.23	4.25	0.002	145	ND	61.5	34.8	1.02	ND	51	1.81
	780-800	0.295	2.59	0.004	174	ND	47.2	9.04	0.625	ND	49	2.2
	800-820	0.796	3.97	0.002	170	0.108	166	18.7	0.881	ND	402	9.41
	820-840	0.177	2.79	0.002	115	ND	96.4	3.53	0.675	ND	38	3.15
	840-860	0.203	2.59	0.002	104	ND	66.9	6.14	0.668	ND	33.2	1.01
	860-880	0.204	1.31	0.003	89.8	ND	88.3	22.3	0.504	ND	26.1	79.6
	880-900	0.379	3.04	0.003	128	ND	60	5.77	0.693	ND	70.5	4.14
	900-920	0.666	1.82	0.003	293	ND	59.4	7.26	0.805	ND	74.6	3.67
	920-940	0.8	7.86	0.003	179	ND	24	4.69	0.729	ND	317	2.37
	940-960	4.28	11.2	0.004	506	ND	45.3	28.3	1.15	ND	823	37.2
	960-980	2.59	29.1	0.022	252	ND	55.6	51.8	3.98	ND	475	3.45
	980-1000	0.841	4.73	0.003	144	ND	75	23.8	1.36	ND	886	3.24
	1000-1020	0.443	1.86	0.004	174	ND	28.3	9.43	0.874	ND	1343	4.08
	1020-1040	0.097	2.84	0.002	25.8	ND	188	5.15	1.05	ND	211	2.15
	1040-1060	0.2	3.69	0.005	29	ND	92.9	4.86	2.2	ND	42	1.67
	1060-1080	0.929	38.3	0.023	53.6	ND	23.2	19.4	2.46	ND	54.5	3.6
	1080-1100	0.354	4.46	0.003	270	ND	38.5	3.52	1.41	ND	46.7	3.84
	mean	0.89687	13.221	0.00647	269.713	0.2365	54.3227	28.364	2.05043	0.03767	272.41	7.776
Stock	1100-1120	0.39	15.6	0.002	210	0.133	53.1	20.1	2.28	ND	73.2	2.87
	1120-1140	0.085	1.99	0.002	14.8	ND	83.1	7.42	0.935	ND	32.5	0.828
	1140-1160	0.094	2.58	0.002	12.7	ND	138	8.73	2.12	ND	38.7	0.964
	1160-1180	0.134	2.93	0.002	15.7	0.119	50.9	12.2	1.15	ND	87.6	1.03
	1180-1200	0.112	2.17	0.003	13.5	ND	17.7	13.6	0.955	ND	107	0.62
	mean	0.163	5.054	0.0022	53.34	0.0504	68.56	12.41	1.488		67.8	1.2624

Metal Ratios in Drillhole 89916

Lith.	Footage	Pb:Zn	Cu:Mo	Zn:Cu	Pb:Cu	Ag:Cu	Ag:Pb	As:Cu	Ag:Au	Au:Cu
Upper	0-20	0.002	34.12	39.34	0.094	0.0009	0.0094	0.05		
Plate	20-40	0.003	50.65	58.65	0.166	0.0010	0.0057	0.13	17.47	5.4E-05
	mean	0.003	40.86	49.11	0.131	0.0009	0.0070	0.09	33.41	2.8E-05
Upper	40-60	0.015	39.91	36.84	0.562	0.0011	0.0019	0.03		
Skarn	60-80	0.050	30.45	14.50	0.720	0.0012	0.0016	1.53	0.76	0.00152
	80 -100	0.011	39.47	32.19	0.352	0.0016	0.0046	0.40	18.71	8.6E-05
	100-120	0.037	43.38	21.81	0.817	0.0041	0.0050	0.29		
	120-140	0.019	125.56	49.11	0.910	0.0034	0.0037	0.11		
	140-160	0.007	58.37	44.62	0.326	0.0009	0.0027	0.09	224.00	4E-06
	160-180	0.015	87.68	38.59	0.595	0.0043	0.0072	1.33	54.21	7.9E-05
	180-200	0.027	79.06	21.12	0.562	0.0053	0.0093	1.64	71.88	7.3E-05
	200-220	0.031	115.67	9.24	0.283	0.0019	0.0066	0.60	466.00	4E-06
	220-240	0.241	112.28	1.27	0.307	0.0010	0.0031	1.32	12.88	7.5E-05
	240-260	0.484	30.93	2.03	0.983	0.0099	0.0101	3.55	11.90	0.00083
	260-280	0.895	17.53	0.87	0.780	0.0018	0.0023	1.43		
	mean	0.023	58.31	21.84	0.501	0.0034	0.0068	1.21	15.13	0.00022
I.T.Z.	280-300	0.282	16.59	7.50	2.117	0.0730	0.0345	10.35	6.00	0.01216
	300-320	0.231	2.24	7.44	1.720	0.0203	0.0118	11.58	1.01	0.01997
	320-340	0.189	3.67	5.10	0.965	0.0055	0.0057	6.04	0.91	0.00608
	340-360	0.455	4.63	4.84	2.200	0.0086	0.0039	3.97	1.36	0.00627
	360-380	0.060	1.88	8.18	0.493	0.0078	0.0159	3.91	0.67	0.01172
	380-400	0.073	2.17	6.46	0.473	0.0040	0.0085	3.81	7.11	0.00057
	400-420	0.106	4.50	4.14	0.439	0.0044	0.0101	4.77	0.95	0.00468
	420-440	0.082	5.86	4.10	0.335	0.0153	0.0457	4.84	3.17	0.00482
	440-460	0.023	13.91	11.39	0.259	0.0098	0.0377	5.90	1.46	0.00669
	460-480	0.089	8.16	7.14	0.633	0.0132	0.0209	14.41	2.01	0.00659
	480-500	0.200	8.96	14.14	2.832	0.0460	0.0163	6.76	22.94	0.00201
	mean	0.153	4.95	7.65	1.171	0.0217	0.0185	7.01	3.08	0.00705

Metal Ratios in Drillhole 89916

Lith.	Footage	Pb:Zn	Cu:Mo	Zn:Cu	Pb:Cu	Ag:Cu	Ag:Pb	As:Cu	Ag:Au	Au:Cu
Lower	500-520	0.227	7.59	5.44	1.235	0.0127	0.0103	0.92	65.09	0.0002
Skarn	520-540	0.260	9.35	2.54	0.661	0.0063	0.0095	0.32	72.67	8.6E-05
	540-560	0.147	29.20	2.40	0.352	0.0055	0.0156	0.30	62.86	8.8E-05
	560-580	0.119	95.82	1.75	0.208	0.0029	0.0138	0.03	296.67	9.7E-06
	580-600	0.140	30.80	0.37	0.052	0.0033	0.0627	0.02	2,000.00	1.6E-06
	600-620	0.177	31.61	0.18	0.031	0.0013	0.0426	0.02	99.70	1.3E-05
	620-640	0.060	6.83	0.43	0.026	0.0021	0.0810	0.02	198.00	1E-05
	640-660	0.113	20.56	0.21	0.024	0.0021	0.0885	0.01	145.00	1.5E-05
	660-680	0.380	8.29	0.10	0.038	0.0014	0.0380	0.01	100.67	1.4E-05
	680-700	0.400	7.11	0.10	0.042	0.0012	0.0289	0.01	78.60	1.5E-05
	700-720	0.597	10.22	0.07	0.039	0.0009	0.0220	0.01	103.00	8.3E-06
	720-740	0.608	5.47	0.17	0.104	0.0044	0.0418	0.04	193.33	2.3E-05
	740-760	0.588	6.60	0.19	0.113	0.0024	0.0211	0.03	128.25	1.9E-05
	760-780	0.682	2.36	0.35	0.240	0.0016	0.0066	0.03	115.00	1.4E-05
	780-800	0.184	3.69	0.28	0.052	0.0017	0.0326	0.01	73.75	2.3E-05
	800-820	0.047	1.02	2.36	0.110	0.0047	0.0426	0.02	398.00	1.2E-05
	820-840	0.093	1.19	0.33	0.031	0.0015	0.0501	0.02	88.50	1.7E-05
	840-860	0.185	1.55	0.32	0.059	0.0020	0.0331	0.02	101.50	1.9E-05
	860-880	0.854	1.02	0.29	0.248	0.0023	0.0091	0.01	68.00	3.3E-05
	880-900	0.082	2.13	0.55	0.045	0.0030	0.0657	0.02	126.33	2.3E-05
	900-920	0.097	4.93	0.25	0.025	0.0023	0.0917	0.01	222.00	1E-05
	920-940	0.015	7.46	1.77	0.026	0.0045	0.1706	0.04	266.67	1.7E-05
	940-960	0.034	11.17	1.63	0.056	0.0085	0.1512	0.02	1,070.00	7.9E-06
	960-980	0.109	4.53	1.88	0.206	0.0103	0.0500	0.12	117.73	8.7E-05
	980-1000	0.027	1.92	6.15	0.165	0.0058	0.0353	0.03	280.33	2.1E-05
	1000-1020	0.007	6.15	7.72	0.054	0.0025	0.0470	0.01	110.75	2.3E-05
	1020-1040	0.024	0.14	8.18	0.200	0.0038	0.0188	0.11	48.50	7.8E-05
	1040-1060	0.116	0.31	1.45	0.168	0.0069	0.0412	0.13	40.00	0.00017
	1060-1080	0.356	2.31	1.02	0.362	0.0173	0.0479	0.71	40.39	0.00043
	1080-1100	0.075	7.01	0.17	0.013	0.0013	0.1006	0.02	118.00	1.1E-05
	mean	0.104	4.97	1.01	0.105	0.0033	0.0316	0.05	138.69	2.4E-05
Stock	1100-1120	0.275	3.95	0.35	0.096	0.0019	0.0194	0.07	195.00	9.5E-06
	1120-1140	0.228	0.18	2.20	0.501	0.0057	0.0115	0.13	42.50	0.00014
	1140-1160	0.226	0.09	3.05	0.687	0.0074	0.0108	0.20	47.00	0.00016
	1160-1180	0.139	0.31	5.58	0.777	0.0085	0.0110	0.19	67.00	0.00013
	1180-1200	0.127	0.76	7.93	1.007	0.0083	0.0082	0.16	37.33	0.00022
	mean	0.183	0.78	1.27	0.233	0.0031	0.0131	0.09	74.09	4.1E-05

Trace Element Analyses in Drillhole 90816 (ND-Not Detected)

Lith.	Footage	Ag (ppm)	As (ppm)	Au (ppm)	Cu (ppm)	Hg (ppb)	Mo (ppm)	Pb (ppm)	Sb (ppm)	Tl (ppm)	Zn (ppm)	Bi (ppm)	Fe (%)
Upper	0-20	0.5	76	ND	39	190	5	41	4	2	84	2	1.42
Plate	20-40	1	124	ND	144	300	19	68	7	2	111	3	1.78
	40-60	0.8	116	ND	54	390	7	57	12	2	151	2	1.54
	60-80	0.2	380	ND	53	180	2	42	16	2	554	5	2.28
	80 -100	0.2	275	ND	28	90	2	28	11	2	187	2	1.97
	100-120	0.4	102	ND	57	80	1	26	8	2	523	6	1.72
	120-140	0.4	98	ND	53	90	1	14	6	2	476	6	1.69
	140-160	2.1	266	ND	112	460	2	67	14	2	3742	35	2.42
	160-185	1	306	ND	92	1200	2	64	11	2	668	7	1.74
	mean	0.7	190		70	306	5	45	10	2	723	8	1.96
Upper	185-210	0.7	137	ND	311	30	5	41	10	2	8237	13	5.59
Skarn	210-230	0.5	118	ND	98	30	6	26	4	2	863	4	2.23
	230-250	1.2	42	ND	185	10	14	72	3	2	741	5	3.5
	250-270	0.6	28	ND	118	5	13	36	3	2	1143	9	2.17
	270-290	0.8	51	ND	48	5	12	57	2	2	800	18	1.41
	290-310	0.5	149	ND	160	20	4	11	4	2	1027	7	2.49
	310-330	0.4	287	ND	116	30	3	12	5	2	272	3	2.28
	330-345	0.3	58	ND	112	20	7	9	3	2	138	2	2.5
	mean	0.6	110		139	18	8	34	4	2	1,484	8	2.74
I.T.Z.	345-370	0.4	242	ND	44	660	8	11	2	2	178	2	1.56
	370-395	1.3	598	ND	149	350	18	18	12	4	131	17	2.99
	395-415	1	889	ND	94	3400	24	8	17	6	109	4	2.26
	415-435	2	1905	ND	132	14000	15	9	53	12	544	12	4.74
	435-455	1.1	779	ND	74	5400	13	10	23	4	1245	7	1.76
	455-470	13.7	599	ND	94	7800	21	361	28	2	1737	7	1.3
	470-490	1.3	377	ND	41	1900	4	41	11	2	1023	5	0.85
	490-510	1.7	563	ND	59	15000	7	118	10	2	2537	2	1.16
	510-530	1.7	1190	ND	121	28000	19	20	9	2	8016	4	2.16
	530-540	6.5	1621	ND	151	17000	22	885	70	3	5403	2	3.06
	mean	2.5	822		93	8,545	14	98	20	4	1,832	7	2.50

Trace Element Analyses in Drillhole 90816 (ND-Not Detected)

Lith.	Footage	Ag (ppm)	As (ppm)	Au (ppm)	Cu (ppm)	Hg (ppb)	Mo (ppm)	Pb (ppm)	Sb (ppm)	Tl (ppm)	Zn (ppm)	Bi (ppm)	Fe (%)
Lower	540-560	1.4	242	ND	297	1800	371	70	15	4	902	2	8.97
Skarn	560-580	0.5	90	ND	216	540	402	22	5	2	251	2	9.1
	580-600	0.5	52	ND	347	180	266	16	6	3	101	2	10.58
	600-620	0.7	40	ND	526	40	387	10	6	2	82	2	12.04
	620-640	1.3	57	ND	307	30	256	20	9	2	106	2	10.81
	640-660	0.8	14	ND	457	50	103	19	12	3	712	17	8.78
	660-680	2.2	14	ND	160	190	305	67	12	2	331	10	5.3
	680-700	0.3	2	ND	131	40	424	10	2	2	59	4	3.43
	700-720	0.4	9	ND	92	100	554	7	3	2	86	5	3.72
	720-740	0.7	30	ND	309	160	298	19	2	2	93	2	8.2
	740-760	0.6	40	ND	233	360	234	10	3	2	83	2	5.78
	760-780	0.8	25	ND	424	170	256	8	3	2	70	18	7.46
	780-800	1.2	33	ND	103	120	181	35	5	2	180	17	4.42
	800-820	0.5	39	ND	85	180	216	20	4	2	194	5	4.26
	820-840	0.7	28	ND	109	160	99	22	4	2	101	3	3.41
	840-860	0.9	209	ND	189	1800	249	12	7	2	247	2	4.95
	860-880	0.9	70	ND	240	380	44	25	3	2	156	65	5.18
	880-900	0.3	44	ND	154	500	20	14	2	2	249	10	5.98
	900-920	0.2	68	ND	52	550	12	17	2	2	161	9	7.57
	920-940	1.4	26	ND	47	180	14	33	4	2	356	4	6.86
	mean	0.8	57	ND	224	377	235	23	5	2	226	9	6.84

Metal Ratios in Drillhole 90816

Lith.	Footage	Pb:Zn	Cu:Mo	Zn:Cu	Pb:Cu	Ag:Cu	Ag:Pb	As:Cu	Fe:Cu
Upper	0-20	0.488	7.8	2.15	1.05	0.0128	0.0122	1.95	364
Plate	20-40	0.613	7.6	0.77	0.47	0.0069	0.0147	0.86	124
	40-60	0.377	7.7	2.80	1.06	0.0148	0.0140	2.15	285
	60-80	0.076	26.5	10.45	0.79	0.0038	0.0048	7.17	430
	80 -100	0.150	14.0	6.68	1.00	0.0071	0.0071	9.82	704
	100-120	0.050	57.0	9.18	0.46	0.0070	0.0154	1.79	302
	120-140	0.029	53.0	8.98	0.26	0.0075	0.0286	1.85	319
	140-160	0.018	56.0	33.41	0.60	0.0188	0.0313	2.38	216
	160-185	0.096	46.0	7.26	0.70	0.0109	0.0156	3.33	189
	mean	0.214	30.2	9.13	0.71	0.0099	0.0162	2.74	281
Upper	185-210	0.005	62.2	26.49	0.13	0.0023	0.0171	0.44	180
Skarn	210-230	0.030	16.3	8.81	0.27	0.0051	0.0192	1.20	228
	230-250	0.097	13.2	4.01	0.39	0.0065	0.0167	0.23	189
	250-270	0.031	9.1	9.69	0.31	0.0051	0.0167	0.24	184
	270-290	0.071	4.0	16.67	1.19	0.0167	0.0140	1.06	294
	290-310	0.011	40.0	6.42	0.07	0.0031	0.0455	0.93	156
	290-310	0.044	38.7	2.34	0.10	0.0034	0.0333	2.47	197
	330-345	0.065	16.0	1.23	0.08	0.0027	0.0333	0.52	223
	mean	0.045	24.0	9.16	0.33	0.0058	0.0189	0.79	197
I.T.Z.	345-370	0.062	5.5	4.05	0.25	0.0091	0.0364	5.50	355
	370-395	0.137	8.3	0.88	0.12	0.0087	0.0722	4.01	201
	395-415	0.073	3.9	1.16	0.09	0.0106	0.1250	9.46	240
	415-435	0.017	8.8	4.12	0.07	0.0152	0.2222	14.43	359
	435-455	0.008	5.7	16.82	0.14	0.0149	0.1100	10.53	238
	455-470	0.208	4.5	18.48	3.84	0.1457	0.0380	6.37	138
	470-490	0.040	10.3	24.95	1.00	0.0317	0.0317	9.20	207
	490-510	0.047	8.4	43.00	2.00	0.0288	0.0144	9.54	197
	510-530	0.002	6.4	66.25	0.17	0.0140	0.0850	9.83	179
	530-540	0.164	6.9	35.78	5.86	0.0430	0.0073	10.74	203
	mean	0.069	6.9	19.92	1.00	0.0275	0.0256	8.82	269

Metal Ratios in Drillhole 90816

Lith.	Footage	Pb:Zn	Cu:Mo	Zn:Cu	Pb:Cu	Ag:Cu	Ag:Pb	As:Cu	Fe:Cu
Lower	540-560	0.078	0.8	3.04	0.24	0.0047	0.0200	0.81	302
Skarn	560-580	0.088	0.5	1.16	0.10	0.0023	0.0227	0.42	421
	580-600	0.158	1.3	0.29	0.05	0.0014	0.0313	0.15	305
	600-620	0.122	1.4	0.16	0.02	0.0013	0.0700	0.08	229
	620-640	0.189	1.2	0.35	0.07	0.0042	0.0650	0.19	352
	640-660	0.027	4.4	1.56	0.04	0.0018	0.0421	0.03	192
	660-680	0.202	0.5	2.07	0.42	0.0138	0.0328	0.09	331
	680-700	0.169	0.3	0.45	0.08	0.0023	0.0300	0.02	262
	700-720	0.081	0.2	0.93	0.08	0.0043	0.0571	0.10	404
	720-740	0.204	1.0	0.30	0.06	0.0023	0.0368	0.10	265
	740-760	0.120	1.0	0.36	0.04	0.0026	0.0600	0.17	248
	760-780	0.114	1.7	0.17	0.02	0.0019	0.1000	0.06	176
	780-800	0.194	0.6	1.75	0.34	0.0117	0.0343	0.32	429
	800-820	0.103	0.4	2.28	0.24	0.0059	0.0250	0.46	501
	820-840	0.218	1.1	0.93	0.20	0.0064	0.0318	0.26	313
	840-860	0.049	0.8	1.31	0.06	0.0048	0.0750	1.11	262
	860-880	0.160	5.5	0.65	0.10	0.0038	0.0360	0.29	216
	880-900	0.056	7.7	1.62	0.09	0.0019	0.0214	0.29	388
	900-920	0.106	4.3	3.10	0.33	0.0038	0.0118	1.31	1456
	920-940	0.093	3.4	7.57	0.70	0.0298	0.0424	0.55	1460
	mean	0.127	1.9	1.50	0.16	0.0055	0.0357	0.25	305

522000

523000

524000

525000

526000

4457000

4456000

4455000

4454000

4453000

PLATE 1.

Gold Acres Airborne Magnetics - Relative Intensity

Base value: 53380 nT Contour interval: 10 nT

(UTM grid coordinates) Scale 1:12000

Michaela Nicole Young, M.S
University of Arizona, 1993
Department of Geosciences
Characteristics of skarns related
to gold mineralization at
Gold Acres, Nevada

REFERENCES

Arehart, G.B., Chryssoulis, S.L., and Kesler, S.E., 1993, Gold and arsenic in iron sulfides from sediment-hosted gold deposits: Implications for depositional processes: Econ. Geol., v. 88, p. 171-185.

Armstrong, P.A., and Bartley, J.M., 1989, Tear faulting at the lateral tip of a thrust, southern Golden Gate Range, Nevada, [abs.]: Geol. Soc. America Abstracts with Programs, v. 21, p. 51.

Atkinson, W.W., and Einaudi, M.T., 1976, Skarn formation and mineralization in the contact aureole at Carr Fork, Bingham, Utah, Econ. Geol., v. 73, p. 1326-1365.

Bartley, J.M., 1990, Structure of the Eureka thrust belt, Nevada, [abs.]: Geol. Soc. America Abstracts with Programs, v. 22, p. 5.

Bartley, J.M., and Gleason, G., 1988, Tertiary normal faults superimposed on Mesozoic thrusts, northern Quinn Canyon and southern Grant Ranges, Nye County, Nevada, [abs.]: Geol. Soc. America Abstracts with Programs, v. 20, p. 141.

Bartley, J.M., Matulevich, J.B., and Gleason, G.G., 1987, Style and significance of Mesozoic thrusts in the Garden Valley area, Nevada, [abs.]: Geol. Soc. America Abstracts with Programs, v. 19, p. 581.

Barton, M.D., 1990, Cretaceous magmatism, metamorphism, and metallogeny in the east-central Great Basin, Geol. Soc. America Mem. 174, p. 283-302.

Beane, R.E., and Titley, S.R., 1981, Porphyry copper deposits: Part II. Hydrothermal alteration and mineralization, Econ. Geol. 75th Anniv. Volume, p. 235-269.

Bowers, T.S., Jackson, K.J., and Helgeson, H.C., 1984, Equilibrium activity diagrams for coexisting minerals and aqueous solutions at pressures and temperatures to 5kb and 600°C: Berlin, Germany, Springer-Verlag, 297 p.

Burchfiel, B.C., and Davis, G.A., 1972, Structural framework and evolution of the southern part of the Cordilleran orogen, western United States, Amer. Jour. Science, v. 272, p. 97-118.

Burchfiel, B.C., and Davis, G.A., 1975, Nature and controls of Cordilleran orogenesis, western United States: Extensions of an earlier synthesis, Amer. Jour. Science, v. 275-A, p. 363-396.

Burchfiel, B.C., and Royden, L.H., 1991, Antler orogeny: A Mediterranean-type orogeny, Geology v. 19, p. 66-69.

Chamberlain, A.K., and Chamberlain, R.L., 1990, Monte Mountain thrust, additional confirmation of the Central Nevada thrust belt, [abs.]: Geol. Soc. America Abstracts with Programs, v. 22, p. 13.

Churkin, M., Jr., 1974, Paleozoic marginal ocean basin-volcanic arc systems in the Cordilleran foldbelt, Soc. Econ. Paleo. Min. Spec. Pub. 19, p. 174-192.

Dickinson, W.R., 1977, Paleozoic plate tectonics and the evolution of the Cordilleran continental margin, *in* Stewart, J.H., Stevens, C.H., and Fritsche, A.E., eds., Paleozoic paleogeography of the western United States: Los Angeles, CA, Soc. Econ. Paleo. Min., p. 181-215.

Dickinson, W.R., Harbaugh, D.W., Saller, A.H., Heller, P.L., and Snyder, W.S., 1983, Detrital modes of Upper Paleozoic sandstones derived from Antler orogen in Nevada: Implications for nature of Antler orogeny, Amer. Jour. Science, v. 283, p. 481-509.

Einaudi, M.T., 1982a, Description of skarns associated with porphyry copper plutons, southwestern North America, *in* Titley, S.R., ed., Advances in the geology of the porphyry copper deposits, southwestern North America: Tucson, AZ, Univ. of Arizona, p. 139-183

Einaudi, M.T., 1982b, General features and origin of skarns associated with porphyry copper plutons, southwestern North America, *in* Titley, S.R., ed., Advances in the geology of the porphyry copper deposits, southwestern North America: Tucson, AZ, Univ. of Arizona, p. 185-209.

Einaudi, M.T., and Burt, D.M., 1982, Introduction-Terminology, classification, and composition of skarn deposits, Econ. Geol., v. 77, p. 745-754.

Einaudi, M.T., Meinert, L.D., and Newberry, R., 1981, Skarn deposits, Econ. Geol. 75th Anniv. Volume, p. 317-391.

Engebretson , D.C., Cox, A., and Gordon, R.G., 1985, Relative motions between oceanic and continental plates in the Pacific basin, Geol. Soc. America Spec. Paper 206, 59p.

Gilluly, J., and Gates, O., 1965, Tectonic and igneous geology of the northern Shoshone Range, Nevada, U.S. Geol. Survey Prof. Paper 465, 153 p.

Gilluly, J., and Masursky, H., 1965, Geology of the Cortez Quadrangle, U.S. Geol. Survey Bull. 1175, 117 p.

Guth, P.L., 1988, Superposed Mesozoic thrusts and Tertiary extension, northwestern Clark County, Nevada [abs.]: Geol. Soc. America Abstracts with Programs, v. 20, p. 165.

GSA, 1993, Mesozoic (?) contraction in central Nevada: the Central Nevada thrust belt [field trip description]: GSA Today, v.3, p.41.

Hays, R.C., and Foo, S.T., 1991, Geology and mineralization of the Gold Acres deposit, Lander County, Nevada, *in* Raines, G.L., Lisle, R.E., Shafer, R.W., and Wilkinson, W.H., eds., Geology and ore deposits of the Great Basin: Reno, NV, Geol. Soc. Nevada, p. 677-686.

Johnson, J.W., and Norton, D., 1985, Theoretical prediction of hydrothermal conditions and chemical equilibria during skarn formation in porphyry copper systems, Econ. Geol., v. 80, p. 1797-1823.

Johnson, J.G., and Pendergast, A., 1981, Timing and mode of emplacement of the Roberts Mountains allochthon, Antler orogeny, Geol. Soc. America Bull, v. 92, p. 648-658.

Ketner, K.B., 1965, *Section on* Economic Geology, *in* Gilluly, J., and Masursky, Tectonic and igneous geology of the northern Shoshone Range, Nevada, U.S. Geol. Survey Prof. Paper 465, 129-144.

Ketner, K.B., and Smith, J.F., Jr., 1974, Folds and overthrusts of Late Jurassic or Early Cretaceous age in northern Nevada, U.S. Geol. Survey Jour. Research, v. 2, p. 417-419.

Ketner, K.B., and Smith, F.R., Jr., 1982, Mid-Paleozoic age of the Roberts thrust unsettled by new data from northern Nevada, Geology, v.10, p. 298-303.

Klein, C., and Hurlbut, C.S., Jr., 1985, Manual of Mineralogy: New York, NY, John Wiley and Sons, 596 p.

Mabey, D.R., 1965a, *Section on* Gravity and aeromagnetic surveys, *in* Gilluly, J., and Masursky, H., Geology of the Cortez Quadrangle, U.S. Geol. Survey Bull. 1175, p. 105-111.

McCandless, T.E., Ruiz, J., and Campbell, A.R., 1993, Rhenium behavior in molybdenite in hypogene and near-surface environments: Implications for Re-Os geochronometry, Geochim. et Cosmochim. Acta, v. 57, p. 889-905.

Meinert, L.D., 1989, Gold skarn deposits-Geology and exploration criteria, Econ. Geol. Mon. 6, p. 537-552.

Meriam, C.W., and Anderson, C.A.,1942, Reconnaissance survey of the Roberts Mountains, Nevada, Geol. Soc. America Bull., v. 53, p. 1675-1727.

Nash, J.T. , 1972, Fluid inclusion studies of some gold deposits in Nevada, U.S. Geol. Survey Prof. Paper 800-C, p. C15-C19.

Nolan, T.B., 1974, Stratigraphic evidence on the age of the Roberts Mountains thrust, Eureka and White Pine Counties, Nev., U.S. Geol. Survey Jour. Research, v. 2, p. 411-416.

Oldow, J.S., 1984, Spatial variability in the structure of the Roberts Mountains allochthon, western Nevada, Geol. Soc. America Bull., v. 95, p. 174-185.

Roberts, R.J., 1960, Alinement of mining districts in north-central Nevada, U.S. Geol. Survey Prof. Paper 400-B, p. B17-B19.

Schmitt, J.G., 1992, Cretaceous sedimentary basins of the eastern Great Basin, Nevada [abs.]: Geol. Soc. America Abstracts with Programs, v. 24, p.61.

Schmitt, J.G., and Vandervoot, D.S., 1987, Cretaceous through Eocene basin evolution in the hinterland of the Sevier orogenic belt, east-central Nevada [abs.]: Geol. Soc. America Abstracts with Programs, v. 19, p. 833.

Silberman, M.L. and McKee, E.H., 1971, K-Ar ages of granitic plutons in north-central Nevada, Isochron/West, v. 71-1, p. 15-32.

Sillitoe, R.H., and Bonham, H.F., 1990, Sediment-hosted gold deposits: Distal products of magmatic-hydrothermal systems, Geology, v. 18, p. 157-161.

Snyder, W.S., Spinosa, C., and Gallegos, D.M., 1991, Pennsylvanian-Permian tectonism on the western U.S. continental margin, *in* Raines, G.L., Lisle, R.E., Shafer, R.W., and Wilkinson, W.H., eds., Geology and ore deposits of the Great Basin: Reno, NV, Geol. Soc. Nevada, p. 5-20.

Speed, R.C., 1983, Precenozoic tectonic evolution of northeastern Nevada, Geothermal Resources Council Special Report No. 13, p. 11-24.

Speed, R.C., and Sleep, N.H., 1982, Antler orogeny and foreland basin: A model, Geol. Soc. America Bull., v. 93, p. 815-828.

Speed, R., Ellison, M.W., and Heck, F.R., 1988, Phanerozoic tectonic evolution of the Great Basin, *in* Ernst, G.E., ed., Metamorphism and crustal evolution of the western United States: Rubey Volume VII: Prentice Hall, p. 572-605.

Stewart, J.H., 1980, Geology of Nevada, Nevada Bur. Mines Geol. Spec. Pub. 4, 136 p.

Stewart, J.H., 1991, Latest Proterozoic and Cambrian rocks of the western United States, *in* Cooper, J.D., and Stevens, C.H., eds., Paleozoic paleogeography of the western United States-II: Soc. Econ. Paleo. Min. v. 67, p. 13-37.

Stewart, J.H., and Poole, F.G., 1974, Lower Paleozoic and uppermost Precambrian Cordilleran Miogeocline, Great Basin, western United States, Soc. Econ. Paleo. Min. Spec. Pub. 22, p. 28-57.

Stewart, J.H., and Suzcek, C.A., 1977, Cambrian and latest Precambrian paleogeography and tectonics in the western United States, *in* Stewart, J.H., Stevens, C.H., and Fritsche, A.E., eds., Paleozoic paleogeography of the western United States: Los Angeles, CA, Soc. Econ. Paleo. Min., p. 1-17.

Thorman, C.H., Ketner, K.B., Brooks, W.E., Snee, L.W., Zimmerman, R.A., 1991, Late Mesozoic-Cenozoic tectonics in northeastern Nevada, *in* Raines, G.L., Lisle, R.E., Shafer, R.W., and Wilkinson, W.H., eds., Geology and ore deposits of the Great Basin: Reno, NV, Geol. Soc. Nevada, p. 25-46.

Titley, S.R., 1961, Genesis and control of the Linchburg orebody, Socorro County, New Mexico, Econ. Geol., v. 56, p. 695-722.

Wells, J.D., Elliott, J.E., and Obradovich, J.D., 1971, Age of the igneous rocks associated with ore deposits, Cortez-Buckhorn area, Nevada, U.S. Geol. Survey Prof. Paper 750-C, p. C127-C135.

Wotruba, P.R., Benson, R.G., and Schmidt, K.W.,1988, Geology of the Fortitude gold-silver skarn deposit, Copper Canyon, Lander County, Nevada, *in* Shafer, R.W., Cooper, J.J., and Vikre, P.G., eds., Bulk-mineable precious metal deposits of the western United States: Reno, NV, Geol. Soc. Nevada, p. 159-172.

Wrucke, C.T., and Armbrustmacher, T.J., 1975, Geochemical and geologic relation of gold and other elements at the Gold Acres open-pit mine, Lander County, Nevada, U.S. Geol. Survey Prof. Paper 860, 27 p.

Wrucke, C.T., Armbrustmacher, T.J., and Hessin, T.D., 1968, Distribution of gold, silver, and other metals near Gold Acres and Tenabo, Lander County, Nevada, U.S. Geol. Survey Circular 589, 19 p.